

8-1995

A Theoretical Nonlinear Dynamical Model of Coupled Heat and Momentum Transfer in Forced Convection Film Boiling

Jolie Ann Long
Clemson University

Follow this and additional works at: https://tigerprints.clemson.edu/all_theses

 Part of the [Mechanical Engineering Commons](#)

Recommended Citation

Long, Jolie Ann, "A Theoretical Nonlinear Dynamical Model of Coupled Heat and Momentum Transfer in Forced Convection Film Boiling" (1995). *All Theses*. 2315.

https://tigerprints.clemson.edu/all_theses/2315

This Thesis is brought to you for free and open access by the Theses at TigerPrints. It has been accepted for inclusion in All Theses by an authorized administrator of TigerPrints. For more information, please contact kokeefe@clemson.edu.

August 4, 1995

To the Graduate School:

This thesis entitled "A Theoretical Nonlinear Dynamical Model of Coupled Heat and Momentum Transfer in Forced Convection Film Boiling" and written by Jolie Ann Long is presented to the Graduate School of Clemson University. I recommend that it be accepted in partial fulfillment of the requirements for the degree of Master of Science with a major in Mechanical Engineering.

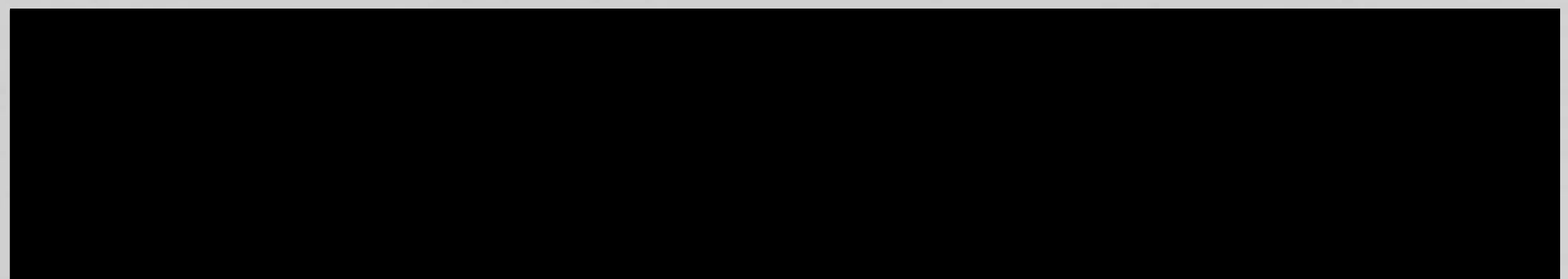


Thesis Advisor

We have reviewed this thesis
and recommend its acceptance:



Accepted for the Graduate School:



22
7153
4254

**A THEORETICAL NONLINEAR DYNAMICAL MODEL
OF COUPLED HEAT AND MOMENTUM TRANSFER
IN FORCED CONVECTION FILM BOILING**

A Thesis

Presented to

the Graduate School of

Clemson University

In Partial Fulfillment

of the Requirements for the Degree

Master of Science

Mechanical Engineering

by

Jolie Ann Long

August 1995

S.C.

TJ153

.L654

1995

A THEORETICAL AND EXPERIMENTAL MODEL
OF COUPLED HEAT AND MOMENTUM TRANSFER

IN FORCED CONVECTION FILM BOILING

A Thesis

Presented to

the Graduate School of

Clemson University

In Partial Fulfillment

of the Requirements for the Degree

Master of Science

Mechanical Engineering

by

John Am Long

August 1995

ABSTRACT

In film boiling, a layer of vapor completely blankets the heated surface and prevents liquid contact with the surface. Film boiling is usually considered undesirable because it is an inefficient mode of heat transfer and can lead to temperatures in excess of those allowed for many materials. Because film boiling may inhibit desired heat transfer in several processes including metals manufacturing, cryogenic engineering, and electronic cooling, it is useful to consider how the film boiling vapor layer may be destabilized or altered such that time-averaged heat transfer is improved.

The purpose of this investigation is to develop a mathematical model of the nonlinear dynamics of a liquid-vapor interface in film boiling arising in the vicinity of a planar stagnation flow. The model applies to stagnation regions beneath jets, to stagnation regions within internal flows where the flow is incident on a wall, and to frontal stagnation regions on cylinders in cross-flows. The influences of flow pulsation, interfacial tension, radiation heat transfer, and surface motion are included in the formulation.

Time-dependent conservation equations for mass, momentum, and energy are solved by the integral method for film boiling in forced convection boundary layer flow in the vicinity of a stagnation region on a flat isothermal plate in motion perpendicular to the incident flow. Conservation of mass, momentum, and energy are applied to the boundary layers in the liquid and the vapor as well as across the liquid-vapor interface in order to model the coupled heat and momentum transfer which arise in film boiling. The result is a system of nonlinear partial differential equations which govern transient and spatial

boundary layer response. Symmetry in the dividing flow about the stagnation streamline is invoked to produce a set of nonlinear, first-order, ordinary differential equations which governs the temporal boundary layer response in the vicinity of the stagnation line.

Chaotic behavior is a possibility in the system under consideration. The set of differential equations may be characterized with recently established methods developed for chaotic dynamics in discrete mechanical systems.

Numerical solutions to the resulting system of differential equations are obtained by fourth- and fifth-order Runge-Kutta integration techniques for a sinusoidal variation in the flow velocity. Instantaneous boundary layer thicknesses and Nusselt numbers are computed. The boundary layers undergo non-sinusoidal oscillations due to the nonlinear content of the governing equations. Sinusoidal flow pulsation tends to increase the boundary layers above their initial starting values much more than it causes them to fall below their initial starting values. The influence of flow pulsation and interfacial tension as a means to destabilize the vapor layer is considered. The curvature of the liquid-vapor interface in the vicinity of the stagnation line is shown to vary temporally due to flow pulsations. Results suggest that flow pulsation may be a means to destabilize the vapor layer under high radiation conditions in film boiling. Similarly, reducing interfacial tension is shown to increase boundary layer oscillation which may lead to vapor layer instability. For the specific parametric condition considered, flow pulsation is shown to decrease time-averaged heat transfer.

ACKNOWLEDGMENTS

Support for this work was provided by the U.S. National Science Foundation under Grant MSS-9253640 and is gratefully acknowledged.

ABSTRACT	ii
ACKNOWLEDGMENTS	iv
LIST OF FIGURES	vii
NOMENCLATURE	x
CHAPTER	
I. INTRODUCTION	1
Rationale	2
Literature Review	5
Objectives	16
II. ANALYSIS	18
Description of Analytical Method and Assumptions	18
Conservation Equations and Boundary Conditions	21
Model Formulation	33
Forcing Functions for Incident Flow	41
III. SOLUTION METHODOLOGY AND MODEL VERIFICATION	46
Solution Methodology for Stagnation Line Temporal Response	47
Liquid-Vapor Interface Shape in the Vicinity of the Stagnation Line	55
Liquid Layer Model Verification	55
Vapor Layer Model Verification	57
IV. RESULTS AND DISCUSSION	62
V. CONCLUSIONS AND RECOMMENDATIONS	86

TABLE OF CONTENTS

	Page
TITLE PAGE	i
ABSTRACT	ii
ACKNOWLEDGMENTS	iv
LIST OF FIGURES	vii
NOMENCLATURE	x
CHAPTER	
I. INTRODUCTION	1
Rationale	2
Literature Review	5
Objectives	16
II. ANALYSIS	18
Description of Analytical Method and Assumptions	18
Conservation Equations and Boundary Conditions	21
Model Formulation	33
Forcing Functions for Incident Flow	41
III. SOLUTION METHODOLOGY AND MODEL VERIFICATION	46
Solution Methodology for Stagnation Line Temporal Response	47
Liquid-Vapor Interface Shape in the Vicinity of the Stagnation Line	55
Liquid Layer Model Verification	55
Vapor Layer Model Verification	57
IV. RESULTS AND DISCUSSION	62
V. CONCLUSIONS AND RECOMMENDATIONS	86

Table of Contents (Continued)

	Page
LIST OF FIGURES	
APPENDIX	90
REFERENCES CITED	96
2.1 Boundary layer development for forced convection film boiling in the vicinity of a planar jet impinging on a moving plate	19
2.2 Differential control volume about a moving interface for the formulation of conservation of mass	26
2.3 Differential control volume about a moving interface for the formulation of balance of momentum normal and tangential to the interface	28
2.4 Normal and tangential velocity components at the liquid-vapor interface	30
2.5 Differential control volume about a moving interface for the formulation of thermal energy conservation	32
3.1 Comparison of predicted Nusselt numbers for film boiling with water with those given by Epstein and Hauser's correlation (equation 3.25) with $Re_d = 1742$, $Re_w = 3.4$, $Pr = 1.9$, $Pr_v = 1.0$, $\rho/\rho_v = 11.5$, $\mu/\mu_v = 2789$, $\beta_1 = 0.5$, $\beta = 0.01$, $Ja = 0.3$, and $wh_0/k_s = 0$	60
4.1 Response for sinusoidal flow pulsations: (a) normalized boundary layer thicknesses, (b) normalized Nusselt number with $Sc_s = 0.1667$, $\alpha = 0.1$, $V_p = 1$, $Re_w = 1700$, $Re_d = 15$, $Pr = 4.0$, $Pr_v = 1.0$, $\rho/\rho_v = 20$, $\mu/\mu_v = 2200$, $\beta_1 = 0.4$, $\beta = 0.03$, $Ja = 0.2$, $wh_0/k_s = 0$, $\bar{X}_s = 0.005500062$, $\bar{X}_v = 0.057736632$, and $\bar{N}_s = 0.051433888$	69
4.2 Response for sinusoidal flow pulsations: (a) normalized boundary layer thicknesses, (b) normalized Nusselt number with $Sc_s = 0.1667$, $\alpha = 0.1$, $V_p = 1$, $Re_w = 1700$, $Re_d = 15$, $Pr = 4.0$, $Pr_v = 1.0$, $\rho/\rho_v = 20$, $\mu/\mu_v = 2200$, $\beta_1 = 0.48$, $\beta = 0.05$, $Ja = 0.2$, $wh_0/k_s = 0$, $\bar{X}_s = 0.006776772$, $\bar{X}_v = 0.056952235$, and $\bar{N}_s = 0.051337164$	72

LIST OF FIGURES

Figure	Page
2.1	Boundary layer development for forced convection film boiling in the vicinity of a planar jet impinging on a moving plate 19
2.2	Differential control volume about a moving interface for the formulation of conservation of mass 26
2.3	Differential control volume about a moving interface for the formulation of balance of momentum normal and tangential to the interface 28
2.4	Normal and tangential velocity components at the liquid-vapor interface 30
2.5	Differential control volume about a moving interface for the formulation of thermal energy conservation 32
3.1	Comparison of predicted Nusselt numbers for film boiling with water with those given by Epstein and Hauser's correlation (equation 3.25) with $Re_{wl} = 1742$, $Re_{ww} = 8.4$, $Pr_l = 1.9$, $Pr_v = 1.0$, $\mu_l/\mu_v = 13.5$, $\rho_l/\rho_v = 2789$, $\bar{\sigma}_s = 0.6$, $\beta = 0.03$, $Ja = 0.5$, and $wh_R/k_v = 0$ 60
4.1	Response for sinusoidal flow pulsations: (a) normalized boundary layer thicknesses, (b) normalized Nusselt number with $Sr_w = 0.1667$, $\varepsilon = 0.1$, $\bar{v}_p = 1$, $Re_{wl} = 1700$, $Re_{ww} = 15$, $Pr_l = 4.0$, $Pr_v = 1.0$, $\mu_l/\mu_v = 20$, $\rho_l/\rho_v = 2200$, $\bar{\sigma}_s = 0.6$, $\beta = 0.03$, $Ja = 0.2$, $wh_R/k_v = 0$, $\bar{\delta}_{v0} = 0.006500068$, $\bar{\delta}_0 = 0.057726632$, and $\bar{\Delta}_0 = 0.051433868$ 69
4.2	Response for sinusoidal flow pulsations: (a) normalized boundary layer thicknesses, (b) normalized Nusselt number with $Sr_w = 0.1667$, $\varepsilon = 0.1$, $\bar{v}_p = 1$, $Re_{wl} = 1700$, $Re_{ww} = 15$, $Pr_l = 4.0$, $Pr_v = 1.0$, $\mu_l/\mu_v = 20$, $\rho_l/\rho_v = 2200$, $\bar{\sigma}_s = 0.48$, $\beta = 0.03$, $Ja = 0.2$, $wh_R/k_v = 0$, $\bar{\delta}_{v0} = 0.006776778$, $\bar{\delta}_0 = 0.086052238$, and $\bar{\Delta}_0 = 0.081337101$ 72

List of Figures (Continued)

	Page
4.3 Response for sinusoidal flow pulsations: (a) normalized boundary layer thicknesses, (b) normalized Nusselt number with $Sr_w = 0.1667$, $\varepsilon = 0.2$, $\bar{v}_p = 1$, $Re_{wl} = 1700$, $Re_{ww} = 15$, $Pr_l = 4.0$, $Pr_v = 1.0$, $\mu_l/\mu_v = 20$, $\rho_l/\rho_v = 2200$, $\bar{\sigma}_s = 0.6$, $\beta = 0.03$, $Ja = 0.2$, $wh_R/k_v = 0$, $\bar{\delta}_{v0} = 0.006500068$, $\bar{\delta}_0 = 0.057726632$, and $\bar{\Delta}_0 = 0.051433868$	73
4.4 Response for sinusoidal flow pulsations: (a) normalized boundary layer thicknesses, (b) normalized Nusselt number with $Sr_w = 0.1667$, $\varepsilon = 0.3$, $\bar{v}_p = 1$, $Re_{wl} = 1700$, $Re_{ww} = 15$, $Pr_l = 4.0$, $Pr_v = 1.0$, $\mu_l/\mu_v = 20$, $\rho_l/\rho_v = 2200$, $\bar{\sigma}_s = 0.6$, $\beta = 0.03$, $Ja = 0.2$, $wh_R/k_v = 0$, $\bar{\delta}_{v0} = 0.006500068$, $\bar{\delta}_0 = 0.057726632$, and $\bar{\Delta}_0 = 0.051433868$	74
4.5 Response for sinusoidal flow pulsations: (a) normalized boundary layer thicknesses, (b) normalized Nusselt number with $Sr_w = 0.1667$, $\varepsilon = 0.1$, $\bar{v}_p = 1$, $Re_{wl} = 1700$, $Re_{ww} = 15$, $Pr_l = 4.0$, $Pr_v = 1.0$, $\mu_l/\mu_v = 20$, $\rho_l/\rho_v = 2200$, $\bar{\sigma}_s = 0.6$, $\beta = 0.03$, $Ja = 0.2$, $wh_R/k_v = 10$, $\bar{\delta}_{v0} = 0.006561428$, $\bar{\delta}_0 = 0.063421017$, and $\bar{\Delta}_0 = 0.057488483$	77
4.6 Response for sinusoidal flow pulsations: (a) normalized boundary layer thicknesses, (b) normalized Nusselt number with $Sr_w = 0.1667$, $\varepsilon = 0.2$, $\bar{v}_p = 1$, $Re_{wl} = 1700$, $Re_{ww} = 15$, $Pr_l = 4.0$, $Pr_v = 1.0$, $\mu_l/\mu_v = 20$, $\rho_l/\rho_v = 2200$, $\bar{\sigma}_s = 0.6$, $\beta = 0.03$, $Ja = 0.2$, $wh_R/k_v = 10$, $\bar{\delta}_{v0} = 0.006561428$, $\bar{\delta}_0 = 0.063421017$, and $\bar{\Delta}_0 = 0.057488483$	79
4.7 Response for sinusoidal flow pulsations: (a) normalized boundary layer thicknesses, (b) normalized Nusselt number with $Sr_w = 0.1667$, $\varepsilon = 0.3$, $\bar{v}_p = 1$, $Re_{wl} = 1700$, $Re_{ww} = 15$, $Pr_l = 4.0$, $Pr_v = 1.0$, $\mu_l/\mu_v = 20$, $\rho_l/\rho_v = 2200$, $\bar{\sigma}_s = 0.6$, $\beta = 0.03$, $Ja = 0.2$, $wh_R/k_v = 10$, $\bar{\delta}_{v0} = 0.006561428$, $\bar{\delta}_0 = 0.063421017$, and $\bar{\Delta}_0 = 0.057488483$	80

List of Figures (Continued)

	Page
4.8 Response for sinusoidal flow pulsations: (a) normalized boundary layer thicknesses, (b) normalized Nusselt number with $Sr_w = 0.1667$, $\varepsilon = 0.3$, $\bar{v}_p = 1$, $Re_{wl} = 1700$, $Re_{ww} = 15$, $Pr_l = 4.0$, $Pr_v = 1.0$, $\mu_l/\mu_v = 20$, $\rho_l/\rho_v = 2200$, $\bar{\sigma}_s = 0.6$, $\beta = 0.03$, $Ja = 0.02$, $wh_R/k_v = 10$, $\bar{\delta}_{v0} = 0.006206590$, $\bar{\delta}_0 = 0.034341779$, and $\bar{\Delta}_0 = 0.027005552$	83
4.9 Dimensionless liquid-vapor interface shape in the vicinity of the stagnation line for sinusoidal flow pulsations with $Sr_w = 0.1667$, $\varepsilon = 0.1$, $\bar{v}_p = 1$, $Re_{wl} = 1700$, $Re_{ww} = 15$, $Pr_l = 4.0$, $Pr_v = 1.0$, $\mu_l/\mu_v = 20$, $\rho_l/\rho_v = 2200$, $\bar{\sigma}_s = 0.6$, $\beta = 0.03$, $Ja = 0.2$, $wh_R/k_v = 0$, $\bar{\delta}_{v0} = 0.006500068$, $\bar{\delta}_0 = 0.057726632$, and $\bar{\Delta}_0 = 0.051433868$	85
A-1. Unit tangent vector \mathbf{T} and angle ϕ for the determination of curvature κ at point P	91
A-2. Circle of curvature at $P(x,y)$ for the determination of radius of curvature	91
A-3. A differential of arc length ds for the formulation of the relationship between ds , dx , and dy	93
A-4. The liquid-vapor interface modeled as the plane curve $\delta_v(x)$ at an instant in time	93

NOMENCLATURE

- C = steady state free stream velocity gradient
 \bar{C} = dimensionless steady state free stream velocity gradient = Cw/v_j
 c_p = specific heat at constant pressure
 f = pulsation frequency
 \bar{f} = dimensionless pulsation frequency = $f\tau$
 g = acceleration due to gravity ($g = 9.81 \text{ m/s}^2$)
 \bar{g} = dimensionless acceleration due to gravity = wg/v_j^2
 H = fluid depth
 \bar{H} = dimensionless fluid depth = H/w ($\bar{H} = 0.5$)
 h_{lv} = latent heat of vaporization
 h_R = radiation heat transfer coefficient
 Ja = Jakob number = $c_{pv}(T_p - T_s)/h_{lv}$
 k = thermal conductivity
 n = normal to the interface
 Nu_v = Nusselt number = hw/k_v
 Nu_* = normalized Nusselt number = Nu_v/Nu_{v0}
 p = pressure
 \bar{p}_l = dimensionless liquid pressure = $(p_l - p_\infty)/(1/2 \rho_l v_j^2)$
 \bar{p}_v = dimensionless vapor pressure = $(p_v - p_\infty)/(1/2 \rho_v v_j^2)$
 Pr = Prandtl number = $\mu c_p/k$

- q_y = heat flux ($q_y = -k \partial T / \partial y$)
- r_c = radius of curvature of liquid-vapor interface
- Re_{wl} = Reynolds number for liquid = $\rho_l v_j w / \mu_l$
- Re_{wv} = Reynolds number for vapor = $\rho_v v_j w / \mu_v$
- Sr_w = Strouhal number = $w / \tau v_j$
- t = time
- \bar{t} = dimensionless time = t / τ
- T = temperature
- \bar{T}_{ll} = dimensionless interface temperature used in liquid layer equations = $(T_{ll} - T_\infty) / (T_s - T_\infty)$
- \bar{T}_{vl} = dimensionless interface temperature used in vapor layer equations = $(T_{vl} - T_p) / (T_p - T_s)$
- T_s = constant saturation temperature
- T^* = reference temperature
- u = x component of velocity
- \bar{u}_{ll} = dimensionless x component of velocity in the liquid at the interface = u_{ll} / v_j
- \bar{u}_{vl} = dimensionless x component of velocity in the vapor at the interface = u_{vl} / v_j
- \bar{u}_∞ = dimensionless freestream velocity = u_∞ / v_j
- u_l = x component of velocity for liquid-vapor interface
- \bar{u}_l = dimensionless x component of velocity for liquid-vapor interface = u_l / v_j
- v = y component of velocity
- v_i = incident flow velocity
- v_j = time averaged jet impingement velocity along jet centerline

- v_p = plate velocity
 \bar{v}_{ll} = dimensionless y component of velocity in the liquid at the interface = v_{ll}/v_j
 \bar{v}_{vl} = dimensionless y component of velocity in the vapor at the interface = v_{vl}/v_j
 \bar{v}_p = dimensionless plate velocity = v_p/v_j
 V = velocity
 \bar{V} = velocity vector
 w = incident jet width
 w_I = mass vaporization rate of liquid per unit plate width
 x = streamwise coordinate (Figure 2.1)
 \bar{x} = dimensionless streamwise coordinate = x/w
 x^* = value for \bar{x} where $\bar{p}_1 = 0$ (equation 2.45)
 y = vertical position above plate (Figure 2.1)
 \bar{y} = dimensionless vertical position above plate = y/w
 y_1 = vertical position above vapor layer ($y_1 = y - \delta_v$)
 β = subcooling parameter = $Pr_v c_{pl}(T_s - T_\infty) / Pr_l c_{pv}(T_p - T_s)$
 δ = velocity boundary layer thickness in the liquid
 $\bar{\delta}$ = dimensionless velocity boundary layer thickness in the liquid = δ/w
 δ_* = normalized velocity boundary layer thickness in the liquid = $\bar{\delta}/\bar{\delta}_0$
 δ_v = vapor layer thickness
 $\bar{\delta}_v$ = dimensionless vapor layer thickness = δ_v/w
 δ_{v*} = normalized vapor layer thickness = $\bar{\delta}_v/\bar{\delta}_{v0}$
 Δ = thermal boundary layer thickness in liquid

- $\bar{\Delta}$ = dimensionless thermal boundary layer thickness in liquid = Δ/w
- Δ_* = normalized thermal boundary layer thickness in liquid = $\bar{\Delta}/\bar{\Delta}_0$
- ε = dimensionless peak to mean amplitude
- ϵ = emissivity
- μ = dynamic viscosity
- ρ = mass density
- σ = Stefan-Boltzman constant ($\sigma = 5.670 \times 10^{-8} \text{ W/m}^2\text{K}^4$)
- σ_s = interfacial tension
- $\bar{\sigma}_s$ = dimensionless interfacial tension = $\sigma_s/(v_j^2 w \rho_l)$
- τ = pulsation period
- τ_{yx} = shear stress ($\tau_{yx} = \mu \partial u / \partial y$)

Subscripts:

- I = liquid-vapor interface
- l = liquid
- p = plate
- ss = steady state
- v = vapor
- ∞ = liquid free stream
- 0 = initial value
- (n) = normal
- (s) = tangential

CHAPTER I

INTRODUCTION

Film boiling occurs when a surface is hot enough to sustain a vapor film. A heated surface may be blanketed with a nearly continuous film of vapor that separates the surface from the liquid. In general, heat is transported across the vapor film from the wall to the interface between the liquid and vapor phases by convection, conduction, and radiation. However, film boiling is an inefficient mode of heat transfer and is therefore often considered a very undesirable boiling regime.

Instability associated with liquid-vapor interfaces, such as in film boiling, have a strong impact on the heat and mass transfer at the interface (Carey, 1992). Kelvin-Helmholtz and Rayleigh-Taylor instabilities have been identified in some commonly encountered vaporization processes. Kelvin-Helmholtz instability refers to interface instability which occurs due to an arbitrary perturbation of the interface between a moving vapor phase overlaying a moving liquid phase in a gravitational field that exerts a downward body force on the fluids. Rayleigh-Taylor instability refers to the interface instability of a motionless liquid overlaying a motionless vapor region in a gravitational field. It is conventional to refer to interface instabilities occurring without relative velocity effects as Taylor instability. When relative velocity is important, the phenomenon is called a Helmholtz instability (Berenson, 1961). An investigation of means to activate interface instabilities will be useful in several processes in which film boiling may potentially occur.

Rationale

In metals manufacturing, forced convection film boiling has been observed in several cooling methods, such as those involving metallic strips or plates cooled by water jet impingement. A good example is the hot rolling process in which a series of rollers reduces a steel strip to its final thickness (McGannon, 1971). After rolling, the strip is typically cooled along a runout table by jets of water. Temperatures in this process are high enough for film boiling to occur (Collier, 1981). Although film boiling is very undesirable in metals cooling, it is currently an unfortunate reality of the process. The vapor layer acts to inhibit heat transfer and poses difficulty for accurately predicting the thermal response of materials to cooling methods used in their manufacture.

The ability to destabilize film boiling could potentially improve cooling methods used in metals manufacturing. For example, it may be possible to destabilize the vapor layer by pulsing the flow from impinging water jets used in cooling. The pulsing flow may induce waviness at the liquid-vapor interface which may cause the vapor film to eventually become unstable and collapse. It is also possible that surface motion, which significantly influences heat transfer in film boiling, may affect vapor layer stability. Radiative heat transfer may also influence vapor layer stability. High radiation heat transfer may tend to stabilize the vapor layer in film boiling because liquid is vaporized as it approaches the heated surface.

In the event of loss of cooling accidents, stable film boiling may also occur in certain types of water cooled nuclear reactors. If the coolant flow to the core of these reactors is interrupted due to some malfunction, the fuel elements will overheat. When emergency

cooling water is incident on the surfaces of hot fuel elements, stable film boiling may occur. In some locations, stagnation flow patterns can develop where the cooling water is directed normally to a surface. Film boiling is very undesirable in such instances since heat generation may continue due to fission or the decay of radionuclides. Therefore, there exists a need to know how to destabilize the vapor film as efficiently as possible. In this application, techniques to destabilize the vapor film, such as by pulsing the flow of emergency cooling water which may form local stagnation flows, are critical for quickly establishing a stable quenching front.

Forced convection film boiling also arises in the field of cryogenic engineering. Although film boiling is not desired, it must be dealt with as superconductors are initially cooled from environmental temperatures to normal operating temperatures. Efficiently destabilizing the vapor layer during this process, such as by pulsing the flow of the cryogenic fluid used in cooling, would allow superconductors to be brought down to normal operating temperatures more quickly. Similarly, destabilization methods could be used to restore the desired heat transfer condition if film boiling happens to occur or is at risk of occurring during operation due to some fault in the system. Therefore, being able to consistently destabilize the vapor film which occurs in film boiling would allow superconductors to be used more reliably.

Film boiling can also be encountered in electronic cooling where circuits are immersed in refrigerants which can easily flash to vapor. Therefore, when using refrigerants susceptible to film boiling, methods to destabilize the vapor film are important for maintaining adequate cooling. Methods of destabilization in this application may include

pulsing the flow of refrigerant as well as altering the interfacial tension between the liquid and the vapor by means of surfactants. The model of this study can be used to assess the influence of interfacial tension on stability.

Film boiling may potentially occur when metallic parts are solidified. When molten metals are cooled rapidly by water jets, such as in the manufacture of some alloys, the high temperatures involved result in stable film boiling. Film boiling and the associated poor heat transfer condition are very undesirable since it facilitates the formation of undesirably large grain structures. Methods to efficiently destabilize the vapor film could significantly accelerate solidification processes.

Resulting model equations for the dynamical response of the vapor layer and the boundary layers in the liquid are nonlinear and chaotic responses are possible. Chaos (Moon, 1992) is a term assigned to that class of motions in deterministic physical and mathematical systems whose time history has a sensitive dependence on initial conditions. For chaotic behavior to occur, a governing system of coupled ordinary differential equations must consist of at least two equations for the nonautonomous case (i.e., behavior influenced by applied forcing functions) and of at least three equations for the autonomous case (i.e., no external forcing). In addition, the system of equations must include nonlinear terms in at least one dependent variable (Parker and Chua, 1989). Because the system under consideration meets these criteria, it is a candidate for chaotic behavior. The possibility of chaotic behavior points out a need to formulate a model which is consistent with approaches used in recent studies of nonlinear dynamics and chaos of thermal systems. Most prior models are based on linearizations, so the nonlinear

dynamical responses cannot be predicted. The model which has been developed in this study retains nonlinear terms allowing the nonlinear dynamical responses to be investigated.

Literature Review

Numerous studies of forced convection film boiling have been performed. Stevens and Witte (1973) studied energy transfer and vapor destabilization processes experimentally by quenching a sphere traveling with constant velocity in distilled water. Data were obtained for the instantaneous heat flux and the transient vapor film behavior over a range of sphere temperatures and water subcoolings. Very thick, smooth vapor films were established at higher water temperatures with a correspondingly large decrease in instantaneous heat transfer rate. However, the destabilization mechanism for the thick vapor film was not determined in this study. Thin smooth vapor films and films with bubble-like irregularities were observed at lower water temperatures and were subject to two types of vapor film destabilization mechanisms. In the first mechanism, the vapor shell around the sphere suddenly appeared to "explode" causing the spherical vapor shell to become unstable in less than 0.25 ms. This appeared to be a function of heat flux rather than the surface temperature of the sphere. The second method of vapor film destabilization was a comparatively gradual phenomenon, requiring on the order of from 50 to 100 ms, in which bubble-like irregularities triggered oscillations in the vapor shell. This study suggests a need to investigate the influence of heat flux on vapor film stability.

Ruch and Holman (1975) experimentally measured heat transfer and heat flux for a jet impinging upward on a flat heated test surface in the nucleate and film boiling regimes.

Test variables were jet nozzle inside diameter, test surface orientation, and test surface temperature. All of the stable film boiling runs had the same characteristic flow pattern on the surface, with the liquid leaving the surface as a conical spray. As jet velocity was increased, the angle that the conical spray formed with the test surface decreased, as did the size of the droplets in the spray. Nozzle diameter, test surface temperature, and test surface orientation did not influence the angle. Increasing jet velocity, nozzle diameter, and test surface temperature each served to increase the heat transfer, while increasing the test surface orientation angle served to decrease the heat transfer. The film boiling heat flux was independent of nozzle diameter and test surface orientation, although the heat transfer and contact area were dependent on these variables. The jet velocity had only a minor effect on the contact area during film boiling for the range of velocities studied. Dimensional correlations of the heat transfer and heat flux data for stable film boiling were obtained for Freon-113. The dimensional film boiling heat transfer correlation represented the test data within 24%. The film boiling heat flux correlation represented test data within 35%.

Piggott et al. (1976) experimentally investigated the wetting delay due to film boiling by impinging a jet of water onto electrically heated circular rods in air. Constant power was supplied to the rods to maintain the initial steady temperature in air as the jet was applied. A stable region of film boiling, in which the surface was unwetted due to a blanket of vapor, was observed visually when a jet of hot water was applied to a heated rod. The stable film boiling was maintained, with the liquid forming a sheet, for times ranging from less than a second to several minutes, depending on test conditions. The

time to achieve wetting was found to be strong functions of water subcooling, jet velocity, thermal conductivity of the rod material, heat generation rate, jet impact angle, and surface temperature. At high water subcooling, wetting delay was negligible, tending to infinity at low subcooling. As wall temperature was increased, the delay time increased for a given subcooling. As thermal conductivity was increased, the delay time increased for a given subcooling. For delay times of less than 10 seconds the heat generation rate had no effect, but for longer delays increasing heat generation rate increased delay time. As the normal component of jet velocity was increased, film boiling heat transfer coefficient was increased for a given subcooling. A theoretical model was developed which treats the rate of cooling of the region under the liquid sheet by considering forced convection film boiling, heat generation rate, and heat conduction from the surrounding regions. The model showed good agreement with experimental results.

Orozco and Dix (1988) studied the effects of liquid subcooling, velocity, and wall superheat on the waviness of the liquid-vapor interface in film boiling from a sphere in Freon-113. Photographs taken in the film boiling regime showed that the wavy nature of the liquid-vapor interface is a function of the above-mentioned parameters. For low liquid subcooling, ripples were present on the liquid-vapor interface. At greater subcooling, ripples disappeared. For very large wall superheat and liquid velocity, ripples were always present on the liquid-vapor interface. A smooth interface was observed to become wavy with increasing wall superheat for a given velocity and liquid subcooling. The study proposed that the increase in wall superheat, which must be accompanied by an increase in vapor production, could possibly lead to an early transition to turbulent flow in the vapor

layer. The study concluded, that during stable film boiling, the wavy nature of the liquid-vapor interface should be attributed to the transition to turbulent vapor flow in the vapor film.

Chang and Witte (1990) experimentally investigated the nature of the vapor layer in film boiling from a 6.35 mm diameter cylindrical heater in cross-flow. Experiments were performed with liquid R-11 flowing upward in the regime of film and transition boiling. Photographs revealed the details of wake formation and behavior near the minimum heat flux condition. For film boiling just above the minimum point on the boiling curve, the vapor film over the front of the heater was smooth. A separation line could be clearly seen that indicated where a wake was formed on the cylinder. The wake collected the vapor produced by the smooth thin film that existed over the forward portion of the heater. The wake was characterized as a vapor region with condensation occurring at its liquid-vapor interface when the liquid was subcooled. Vapor was torn away intermittently from the wake along the separation line. Kelvin-Helmholtz instability was investigated in a linear analysis. The Kelvin-Helmholtz analysis predicted that the growth rate of an interfacial wave increases with liquid subcooling and velocity. This suggests that increased velocity and subcooling cause the breakdown of the vapor film at angles closer to the 90-degree point. If separation angle is interpreted as an indicator of vapor film stability, then the experimentally observed movement of the separation point toward 90-degrees as subcooling and velocity were increased supports the Kelvin-Helmholtz analysis.

Cess and Sparrow (1961) used a boundary layer similarity transformation to analyze the heat transfer and friction characteristics in forced convection film boiling on a flat

plate. It was shown that the resulting two-phase flow problem can be formulated exactly within the framework of laminar boundary layer theory. Relative to the case of single phase, liquid flow, skin friction was substantially reduced due to film boiling. Results also showed that the heat transfer coefficient decreased as the temperature difference between wall temperature and free stream temperature increased. This decrease was related to the increased thickness of the vapor film. However, the investigation omitted interfacial waviness and film instability which are likely to occur in film boiling. Based on the experimental observations of Orozco and Dix (1988), the liquid-vapor interface may remain smooth under certain parametric conditions. For example, a wavy interface was observed to become smooth as average surface temperature dropped. However, at high wall superheat and high liquid velocity, interfacial waviness was likely to occur. Therefore, the applicability of Cess and Sparrow's (1961) model may be limited to the parametric range where instabilities at the interface are small.

Berenson (1961) analyzed film pool boiling heat transfer from a horizontal surface considering Taylor-Helmholtz hydrodynamic instability. A physical model was used in the analysis to approximate the actual shape of the liquid-vapor interface. The physical model consisted of a semicircular vapor bubble on top of a vapor film of constant thickness. A first-order perturbation analysis assuming potential flow was used to apply Taylor-Helmholtz instability to film boiling from a horizontal surface. The effects of relative velocity parallel to the interface and surface tension were included in the analysis. Near the minimum film boiling heat flux, bubble spacing and growth rate were determined by Taylor instability, upon neglecting the effect of fluid depth and viscosity. In other words,

bubble spacing and growth rate were determined, independent of heat transfer effects, by hydrodynamic considerations above. The study concluded that it is quantitatively reasonable to neglect the effect of vapor velocity and film thickness on the liquid-vapor interface behavior in film pool boiling near the minimum temperature difference.

Analytical expressions were derived to predict the heat transfer coefficient and minimum temperature difference for film pool boiling from a horizontal surface and these expressions agreed with experimental results to within about ten percent.

Walsh and Wilson (1979) theoretically investigated forced convection film boiling on a wedge by performing a similarity transformation within the framework of two-phase boundary layer theory. The boundary layer equations were developed for a smooth liquid-vapor interface and neglected surface tension and radiation. The study showed that the effect of pressure gradient in the liquid dominates the dynamics of the flow in the vapor layer. This is in contrast to flow past a flat plate where no appreciable pressure gradient exists. The study showed that within the two regimes of small and large subcooling, values for the skin friction and heat transfer coefficients may be obtained by an analytical procedure using similarity transformations. The analytical solutions for these two limiting cases were found to compare with numerical solutions to within a few percent over the greater portion of the parametric range for a water-steam system. The study concluded that to a good approximation potential flow may be assumed in the liquid phase since for small subcooling it is not necessary to determine the liquid boundary flow and for large subcooling the tangential stress exerted on the liquid at the interface by the vapor is small.

Epstein and Hauser (1980) theoretically analyzed subcooled forced convection film boiling in the forward stagnation region of a sphere. A similarity solution to boundary layer momentum and energy conservation equations was implemented. Their analysis assumed that the vapor flow is laminar around the sphere with a smooth liquid-vapor interface. A continuous vapor film of uniform thickness equal to that in the forward stagnation region was assumed over the lower surface of the sphere and radiation heat transfer was neglected. The heat transfer relation derived for the stagnation region was assumed to approximate heat transfer over most of the surface of the sphere not covered by the thick vapor wake. Therefore, the heat transfer coefficient was averaged over the total surface area of the sphere. A semi-theoretical correlation for subcooled forced convection film boiling heat transfer was obtained by modifying the analytical solution to provide a reasonable correlation of experimental data for forced convection film boiling from spheres or cylinders. Experimental data was based on forced convection film boiling with water from a sphere and with ethyl alcohol, hexane, carbon tetrachloride, and benzene from cylinders of 0.983, 1.26, and 1.62 cm diameter. The resulting correlating expression based on the notion of a uniform vapor film for forced convection film boiling heat transfer incorporates the effects of both wall superheat and liquid subcooling for cylinders and spheres.

Fodemski (1985) theoretically modeled forced convection film boiling in the stagnation region of sphere based on a dimensionless fluid flow stream function. The analysis treated a steady flow problem with a smooth liquid-vapor interface. The effect of vapor velocity, which includes a component directed from the interface towards the hot surface, and the

influence of system pressure were taken into account by the model. Although the influence of system pressure was taken into account by the model, the difference in pressure gradient between the liquid and vapor layers was ignored. Therefore, the analysis is limited to cases in which the effect of interfacial tension is small. The model was used to calculate vapor layer thickness at the stagnation point of the sphere as well as heat fluxes at the interface and at the hot surface. The results of the analysis gave values of heat flux and vapor thickness for water which differed from experimental data for atmospheric pressure by about 25-30%.

Orozco et al. (1987) presented a boundary layer analysis of the vapor film in stagnation point flow film boiling on a sphere immersed in a subcooled liquid. The analysis included the effects of liquid subcooling, liquid velocity, and vapor superheat on the wavy nature of the liquid-vapor interface but assumed surface tension effects were negligible. A viscous dominant equation of motion for the liquid-vapor interface was derived based on a balance of forces in the vicinity of the lower stagnation point of the sphere. The effect of system parameters on the dynamic behavior of the liquid-vapor interface as well as the response to step changes in the temperature and velocity fields were investigated. Results showed that changes in the liquid velocity or the vapor superheat initiated large oscillations in the vapor film thickness and the heat transfer coefficient. This provides good evidence that vapor film destabilization may result from flow pulsations.

Orozco and Stellman (1988) theoretically studied stagnation point flow film boiling on a sphere and on a cylinder immersed in a subcooled liquid. The analysis treated stagnation point flow film boiling under the assumption that the behavior of the vapor film is inertially

dominant. Comparisons were made to the viscous dominant solution for the oscillation of the vapor film presented by Orozco et al. (1987). The effects of system parameters on the dynamic behavior as well as the response of a liquid-vapor interface to changes in the temperature and velocity fields were investigated. Large changes in free stream velocity produced unsymmetric oscillations of the interface. The study showed that interface oscillations become very small as the liquid subcooling increases. However, Piggott et al. (1976) experimentally observed a negligible wetting delay for high liquid subcooling. In order to produce liquid contact with the surface as experimentally observed for high subcooling, interface oscillations are expected to become large as liquid subcooling increases. This contradicts the model prediction. Comparison to Orozco et al. (1987) showed that the viscous solution gives a higher frequency of oscillation than the inertial solution. The study concluded that the inertial dominated solution better predicts the motion of the liquid-vapor interface in forced convection film boiling.

Zumbrunnen et al. (1989) examined the effect of plate motion and radiative heat transfer across the vapor on heat transfer in the film boiling regime. Conservation equations for mass, momentum, and energy were solved by the integral method for film boiling in forced convection boundary layer flow on a flat isothermal plate in motion parallel to the flow direction. Heat transfer was shown to depend on plate velocity as well as plate and liquid temperatures. Radiation heat transfer across the vapor layer was shown to increase with vapor thickness, decrease convective heat transfer, and decrease in importance with increasing plate velocity. However, the analysis neglected the waviness of the liquid-vapor interface, which was modeled as a smooth boundary.

Chappidi et al. (1990) proposed a simple approach to analyze steady laminar forced convection film boiling flow over a horizontal flat plate. Analytical results for a moving surface in a flowing single-phased fluid are used to describe the liquid boundary layer characteristics at the liquid-vapor interface. The vapor flow was decoupled from the liquid flow by using expressions of skin friction and heat transfer for a moving surface in a flowing fluid. Approximate closed-form expressions to estimate the wall heat transfer and skin friction for the corresponding wall superheat were obtained. Comparisons with other numerical simulations indicated that the model was accurate for subcooled conditions. However, the relative accuracy of the model degenerated as wall temperature was increased and as the liquid approached saturation temperature.

Chappidi et al. (1991) analyzed stable laminar film boiling flow along a vertical flat plate theoretically for a water-steam system at atmospheric pressure. A local similarity concept was applied to the governing partial differential equations developed within the framework of boundary layer theory to reduce them to ordinary differential form. This steady state study neglected radiation and modeled the liquid-vapor interface as smooth. Surface tension effects were assumed negligible. Numerical results indicated that skin friction drag on the plate in a film-boiling flow may increase or decrease relative to single-phase all liquid flow level and that the wall heat transfer coefficient always deteriorates in film boiling flow. Changes in skin friction drag were found to be dependent on the surface temperature, liquid subcooling, velocity, and local streamwise position. Subcooling was determined to promote wall heat transfer but could increase or decrease the wall skin friction beyond the single-phase flow level. Cess and Sparrow (1961) demonstrated that a

stable film boiling flow along a horizontal flat surface can reduce skin friction drag on the plate to a very low value, beyond the single-phase liquid flow level. Chappidi et al. (1991) showed that such drag reduction results when the streamwise component of buoyancy force driving the vapor film in film boiling is negligible.

Liu et al. (1992) developed a correlation for forced convection film boiling heat transfer from a cylinder under subcooled conditions. Forced convection film boiling heat transfer from a horizontal cylinder in water or Freon-113 flowing upward perpendicular to the cylinder under saturated and subcooled conditions was measured for the flow rates ranging from 0 to 1 m/s at system pressures ranging from 100 to 500 kPa. The cylinders made of platinum with diameters ranging from 0.7 to 5 mm were used as the test heaters and the cylinder surface superheats in film boiling were raised up to 800 K for water and 400 K for Freon-113. The film boiling heat transfer coefficients obtained show marked improvement with the increase in flow rate and in liquid subcooling, and they are higher for higher system pressures and for smaller cylinder diameters. It was confirmed that the correlation can express the forced convection film boiling heat transfer coefficients from a horizontal cylinder including the effects of radiation in various kinds of subcooled liquids for wide ranges of cylinder surface superheats, system pressures, and cylinder diameters. The correlation was confirmed to describe the experimental data obtained in this work within $\pm 20\%$ for the flow rates below 0.7 m/s, and within -30% to $+20\%$ for the higher flow rates.

Many of the prior studies on film boiling have considered the effects of surface temperature (wall superheat), liquid subcooling, and liquid velocities. The consideration

of transient effects has primarily focused on experimentally observing the wetting delay caused by the vapor film. Several studies neglect the waviness of the liquid-vapor interface while earlier studies impose an assumed shape on the interface. There are also possible contradictions between theoretical and experimental findings regarding the behavior of the liquid-vapor interface. Although Orozco and Stellman (1988) theoretically showed that interface oscillations become very small as the liquid subcooling increases, Piggott et al. (1976) experimentally observed a negligible wetting delay for high subcooling. A contradiction arises because interface oscillations are expected to become large for high subcooling in order to produce liquid contact with the surface as observed experimentally. Because the ability to effectively destabilize the vapor film arising in film boiling could potentially enhance heat transfer in many processes, a theoretical model for the actual behavior of the vapor film is potentially very useful. Prior studies also point to a need to further investigate the effects of heat flux and incident liquid velocity changes on vapor film stability.

Objectives

The purpose of this study is to develop a nonlinear dynamical model of a liquid-vapor interface in film boiling arising in the vicinity of a planar stagnation flow. Of particular interest is a realistic coupling between heat and momentum transfers. Motivation is derived from the possibility that flow pulsations may induce oscillations in the interface which will destabilize the vapor layer. High heat transfer rates suggest that waves in the liquid interface may be preferentially vaporized as they approach the hot surface and a stable vapor film will be promoted as a consequence. The effect of interfacial tension on

interface instability will also be considered. It is possible that altering interfacial tension, such as by using surfactants, in combination with flow pulsations could induce vapor film destabilization.

The objectives of this study are to:

1. Develop a mathematical model of the nonlinear dynamics of a liquid-vapor interface and heat transfer in film boiling in the vicinity of a planar stagnation flow on an isothermal moving surface. The mathematical model will consist of transient heat transfer and momentum conservation models coupled with equations governing force and energy balances at the liquid-vapor interface.
2. Propose a methodology for solving the model equations to determine local, instantaneous convective heat transfer rates.
3. Utilize the model in selected cases to assess the influence of flow pulsations and interfacial tension on vapor and liquid layer dynamics and on instantaneous heat transfer.
4. Compare model predictions with those of other theoretical models and to available experimental data where possible.

Figure 2.1

Description of Analytical Method and Assumptions

An analytical method was chosen which would allow characteristics due to nonlinearities in the equations governing the transient responses to be revealed. Unlike many earlier studies, the method accounts for interfacial wavyness without imposing an assumed shape on the interface. Although prior studies have also decoupled the vapor flow from the liquid flow, coupling of the vapor flow to the liquid flow is an important aspect in realistically modeling the liquid-vapor interface in film boiling because the velocity of the liquid-vapor interface depends on the vaporization rate. The vapor flow is coupled to the liquid flow in this study.

CHAPTER II

ANALYSIS

The stagnation region which is considered in this study is depicted in Figure 2.1. Such flows may arise beneath impinging planar jets, on a cylinder in cross-flow, or in the front stagnation region of any bluff body where the frontal surface can be effectively represented by a tangent plane. Due to film boiling, a thin layer of vapor insulates the surface from the impinging liquid flow. The vapor layer δ_v is thin enough to be modeled as a boundary layer. Thermal and velocity boundary layers, Δ and δ , develop in the liquid layer. The goal of this study is to develop a model to investigate the boundary layer dynamics and heat transfer characteristics which arise in stagnation regions represented by Figure 2.1.

Description of Analytical Method and Assumptions

An analytical method was chosen which would allow characteristics due to nonlinearities in the equations governing the transient responses to be revealed. Unlike many earlier studies, the method accounts for interfacial waviness without imposing an assumed shape on the interface. Although prior studies have also decoupled the vapor flow from the liquid flow, coupling of the vapor flow to the liquid flow is an important aspect in realistically modeling the liquid-vapor interface in film boiling because the velocity of the liquid-vapor interface depends on the vaporization rate. The vapor flow is coupled to the liquid flow in this study.

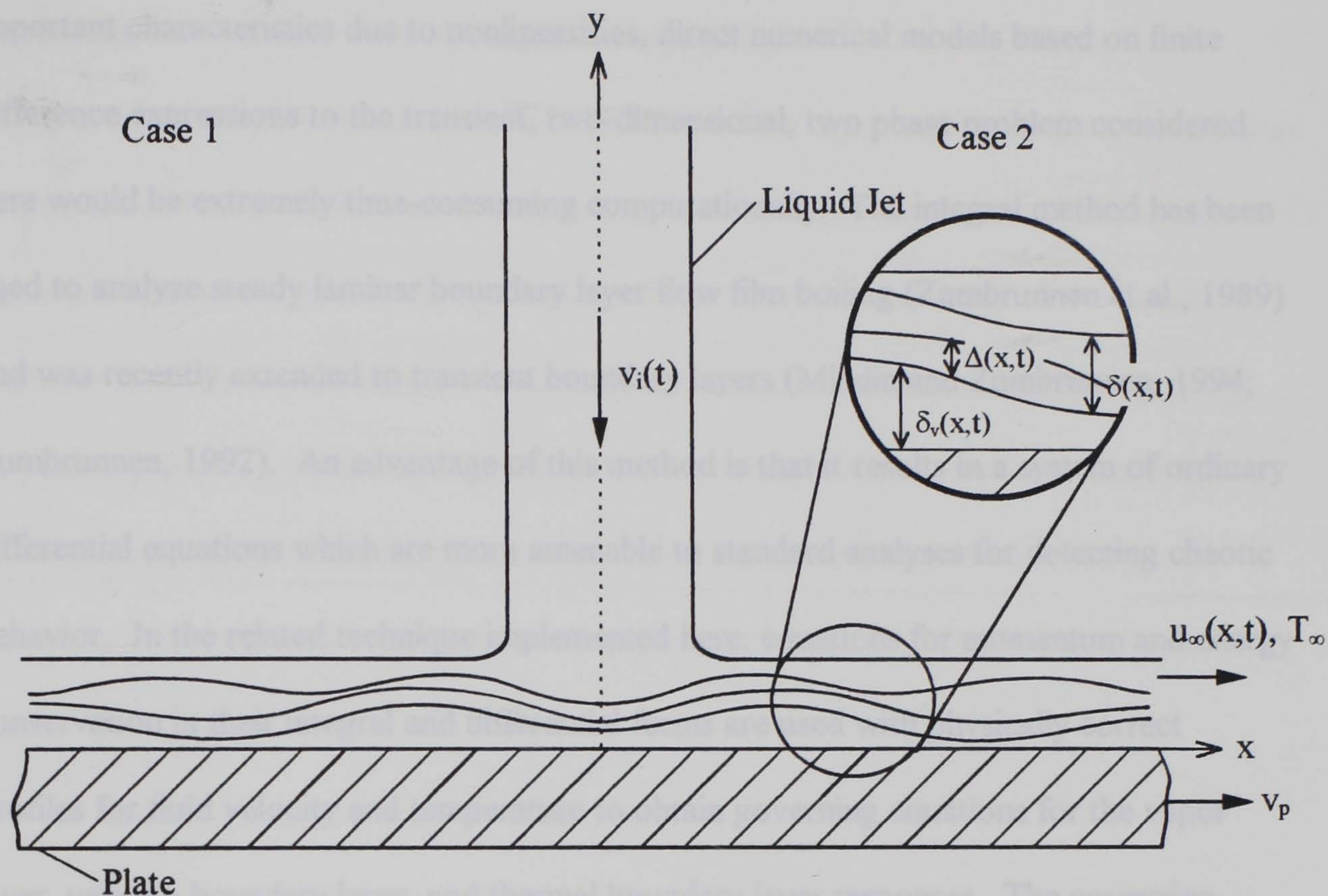


Figure 2.1. Boundary layer development for forced convection film boiling in the vicinity of a planar jet impinging on a moving plate. (Boundary layer waviness and thicknesses are exaggerated for clarity.)

Because calculations in this study must be performed over large time intervals to reveal important characteristics due to nonlinearities, direct numerical models based on finite difference expressions to the transient, two-dimensional, two phase problem considered here would be extremely time-consuming computationally. The integral method has been used to analyze steady laminar boundary layer flow film boiling (Zumbrunnen et al., 1989) and was recently extended to transient boundary layers (Mladin and Zumbrunnen, 1994; Zumbrunnen, 1992). An advantage of this method is that it results in a system of ordinary differential equations which are more amenable to standard analyses for detecting chaotic behavior. In the related technique implemented here, equations for momentum and energy conservation in their integral and differential forms are used with physically correct profiles for fluid velocity and temperature to obtain governing equations for the vapor layer, velocity boundary layer, and thermal boundary layer responses. The governing equations enforce momentum and energy conservation in the liquid and vapor layers as well as across the liquid-vapor interface.

The integral method applied in this study is a generalization of one described by Arpaci and Larsen (1984) and Zumbrunnen et al. (1989). The analysis is applied to boundary layers in the vapor and liquid adjacent to a jet impinging on a moving plate (Figure 2.1). The stagnation line or plane of symmetry, which is fixed, serves as the origin to the coordinate system. In case 1, the plate velocity is opposite to that of the liquid, while in case 2, the plate and liquid travel in the same direction. The bulk of the vapor and liquid flows can be oppositely directed in case 1 if the plate speed approaches or exceeds the jet impingement velocity. The model that follows pertains to case 1 only when the

plate speed is sufficiently small to preclude reversal of the bulk vapor flow. Under these conditions the boundary layer equations are applicable.

In order to simplify the analysis, only the case where vapor and liquid flows are laminar is considered and a constant plate temperature is prescribed. Thus the analysis applies to locations prior to the point where turbulence begins in either the vapor or the liquid. Laminar flow is assumed in order to simplify the model and also in recognition that the favorable pressure gradient in the stagnation zone tends to laminarize turbulent flows (Schlichting, 1979). The analysis assumes that the plate temperature exceeds the saturation temperature of the liquid by an amount sufficient to establish a continuous vapor film.

The specific assumptions of the analysis are:

- (i) incompressible, laminar boundary layer flow,
- (ii) constant thermophysical properties,
- (iii) negligible viscous heating,
- (iv) constant free stream temperature T_∞ in the liquid layer,
- (v) $Pr_l \geq 1$,
- (vi) negligible vapor loss from the vapor layer,
- (vii) a radiatively nonparticipating vapor layer,
- (viii) opaque, diffuse/gray interface and plate surface.

Conservation Equations and Boundary Conditions

Conservation equations for mass, momentum, and energy conservation are presented by Arpaci and Larsen (1984). The transient boundary layer equation for conservation of

mass in differential form for the vapor layer, which corresponds to the aforementioned assumptions and the stagnation flow in Figure 2.1, is

$$\frac{\partial u_v}{\partial x} + \frac{\partial v_v}{\partial y} = 0. \quad (2.1)$$

The integral form of conservation of mass for the vapor layer relates the mass vaporization rate of liquid per unit plate width w_I to the mass flow in the vapor by the expression

$$w_I = \frac{\partial}{\partial t} \int_0^{\delta_v} \rho_v dy + \frac{\partial}{\partial x} \int_0^{\delta_v} \rho_v u_v dy. \quad (2.2)$$

Transient boundary layer equations for momentum conservation in differential and integral forms for the vapor layer are given by equations 2.3 and 2.4.

$$\frac{\partial u_v}{\partial t} + u_v \frac{\partial u_v}{\partial x} + v_v \frac{\partial u_v}{\partial y} = -\frac{1}{\rho_v} \frac{\partial p_v}{\partial x} + \frac{\mu_v}{\rho_v} \frac{\partial^2 u_v}{\partial y^2} \quad (2.3)$$

$$\frac{\partial}{\partial t} \int_0^{\delta_v} \rho_v u_v dy + \frac{\partial}{\partial x} \int_0^{\delta_v} \rho_v u_v u_v dy - w_I u_I = -\int_0^{\delta_v} \frac{\partial p_v}{\partial x} dy - \tau_{yx} \Big|_{y=0} + \tau_{yx} \Big|_{y=\delta_v}. \quad (2.4)$$

The associated transient boundary layer equations for energy conservation, in differential and integral forms, for the vapor layer are

$$\rho_v c_{pv} \left(\frac{\partial T_v}{\partial t} + u_v \frac{\partial T_v}{\partial x} + v_v \frac{\partial T_v}{\partial y} \right) = k_v \frac{\partial^2 T_v}{\partial y^2} \quad (2.5)$$

and

$$-c_{pv} (T_I - T_*) \frac{\partial}{\partial t} \int_0^{\delta_v} \rho_v dy - c_{pv} (T_I - T_*) \frac{\partial}{\partial x} \int_0^{\delta_v} \rho_v u_v dy + \quad (2.6)$$

$$\frac{\partial}{\partial t} \int_0^{\delta_v} \rho_v c_{pv} (T_v - T_*) dy + \frac{\partial}{\partial x} \int_0^{\delta_v} \rho_v c_{pv} (T_v - T_*) u_v dy = q_y \Big|_{y=0} - q_y \Big|_{y=\delta_v}.$$

Transient boundary layer equations for momentum conservation, in differential and integral forms, for the liquid layer in Figure 2.1 are

$$\frac{\partial u_1}{\partial t} + u_1 \frac{\partial u_1}{\partial x} + v_1 \frac{\partial u_1}{\partial y} = -\frac{1}{\rho_1} \frac{\partial p_1}{\partial x} + \frac{\mu_1}{\rho_1} \frac{\partial^2 u_1}{\partial y^2} \quad (2.7)$$

and

$$\frac{\partial}{\partial t} \int_0^\delta \rho_1 u_1 dy_1 + \frac{\partial}{\partial x} \int_0^\delta \rho_1 u_1 u_1 dy_1 - u_\infty \frac{\partial}{\partial t} \int_0^\delta \rho_1 dy_1 - u_\infty \frac{\partial}{\partial x} \int_0^\delta \rho_1 u_1 dy_1 \quad (2.8)$$

$$-w_I u_\infty + w_I u_I = -\int_0^\delta \frac{\partial}{\partial x} p_1 dy_1 - \tau_{yx} \Big|_{y_1=0}.$$

The associated transient boundary layer equations for energy conservation, in differential and integral forms, for the liquid layer are

$$\rho_1 c_{pl} \left(\frac{\partial T_1}{\partial t} + u_1 \frac{\partial T_1}{\partial x} + v_1 \frac{\partial T_1}{\partial y} \right) = k_1 \frac{\partial^2 T_1}{\partial y^2} \quad (2.9)$$

and

$$-c_{pl} (T_\infty - T_*) \frac{\partial}{\partial t} \int_0^\Delta \rho_1 dy_1 - c_{pl} (T_\infty - T_*) \frac{\partial}{\partial x} \int_0^\Delta \rho_1 u_1 dy_1 + \frac{\partial}{\partial t} \int_0^\Delta \rho_1 c_{pl} (T_1 - T_*) dy_1 + \frac{\partial}{\partial x} \int_0^\Delta \rho_1 c_{pl} (T_1 - T_*) u_1 dy_1 + c_{pl} (T_1 - T_\infty) w_I = q_y \Big|_{y_1=0}. \quad (2.10)$$

With reference to the unsteady stagnation flow film boiling in Figure 2.1, $\delta_v = \delta_v(x, t)$,

$$\Delta = \Delta(x, t), \quad \delta = \delta(x, t), \quad u_v = u_v(x, y, t), \quad u_1 = u_1(x, y, t), \quad u_\infty = u_\infty(x, t),$$

$$T_v = T_v(x, y, t), \quad \text{and} \quad T_1 = T_1(x, y, t) \quad \text{in equations 2.1 through 2.10.}$$

The conservation equations are subject to conditions at the plate surface, the liquid-vapor interface, and the extremities of the thermal and velocity boundary layers in the liquid. At the plate surface ($y = 0$),

$$u_v = v_p \quad (2.11a)$$

and

$$T_v = T_p \quad (2.11b)$$

At the liquid-vapor interface ($y = \delta_v$, $y_1 = 0$),

$$u_v = u_{vI} \quad (2.12a)$$

$$T_v = T_{vI} \quad (2.12b)$$

and

$$u_1 = u_{II} \quad (2.13a)$$

$$T_1 = T_{II} \quad (2.13b)$$

With increasing distance y from the interface, the temperature of the liquid decreases until it approaches the liquid free stream value as indicated by equation 2.14a. Therefore, the large temperature gradients which exist in the thermal boundary layer in the liquid become negligible as the outer reaches of the thermal boundary layer are approached. This physical observation is expressed by equation 2.14 which pertains near the edge of the thermal boundary layer in the liquid ($y_1 = \Delta$).

$$T_1 = T_\infty \quad (2.14a)$$

and

$$\frac{\partial T_1}{\partial y_1} = 0 \quad (2.14b)$$

With increasing distance y from the interface, the x component of liquid velocity increases until it approaches the liquid free stream value as indicated by equation 2.15a. Therefore, the large velocity gradients which exist within the velocity boundary layer become negligible as the outer reaches of the boundary layer are approached. This physical

observation is reflected by equation 2.15 which pertains near the edge of the velocity boundary layer in the liquid ($y_1 = \delta$).

$$u_1 = u_\infty(x, t). \quad (2.15a)$$

$$\frac{\partial u_1}{\partial y_1} = 0. \quad (2.15b)$$

Beyond the velocity boundary layer ($y > \delta$), $u_1(x, t) = u_\infty(x, t)$ and the flow is governed by the time-dependent Euler equation below:

$$\frac{\partial u_\infty}{\partial t} + u_\infty \frac{\partial u_\infty}{\partial x} = -\frac{1}{\rho_1} \frac{\partial p_1}{\partial x}. \quad (2.16)$$

Since $\partial p_1 / \partial y \ll \partial p_1 / \partial x$ across the velocity boundary layer in the liquid, equation 2.16 relates pressure gradient $\partial p_1 / \partial x$ to the free stream velocity u_∞ . The pressure distribution $p_1(x, t)$ in the liquid is considered known and will be adapted from distributions for steady and pulsating planar jets given by Zumbrunnen et al. (1992) and Mladin and Zumbrunnen (1994).

As in the liquid and vapor layers, conservation of mass, momentum, and energy must be satisfied at the liquid-vapor interface. These relationships are obtained by considering a differential control volume in Figure 2.2 surrounding the phase boundary at the liquid-vapor interface (Arpaci and Larsen, 1984). The differential control volume moves with the interface and is assumed to be so thin that it accumulates negligible mass.

Conservation of mass at the liquid-vapor interface is given by

$$\rho_l (V_{l(n)} - V_{l(n)}) - \rho_v (V_{v(n)} - V_{l(n)}) = 0 \quad (2.17)$$

where $V_{L(n)}$ and $V_{V(n)}$ denote velocities in the direction normal to the interface and $V_{I(n)}$ is the interface velocity in the normal direction. In the vapor region, mass moves toward the interface with a velocity $V_{V(n)}$, with respect to a stationary observer. However, the interface is also moving with a velocity $V_{I(n)}$, so that the vapor mass flow rate toward the control volume moving with the interface is $\rho_v(V_{V(n)} - V_{I(n)})$. By a similar argument, the

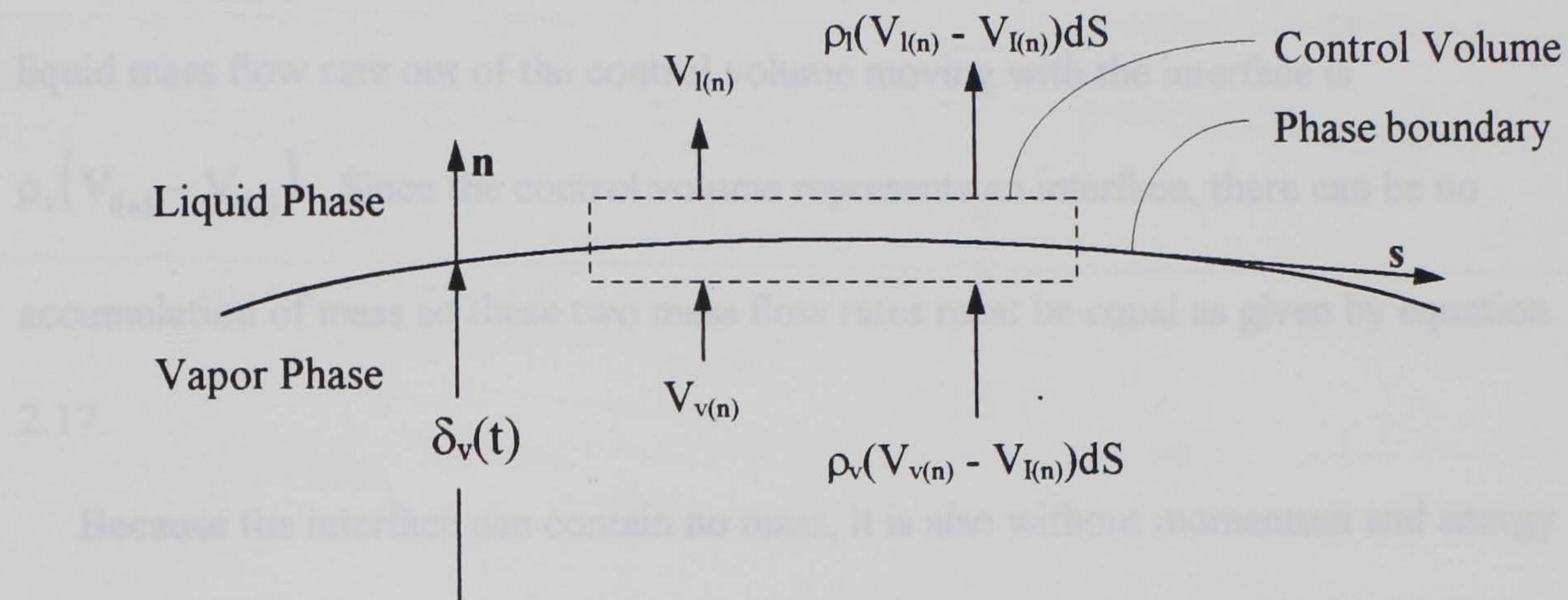


Figure 2.2. Differential control volume about a moving interface for the formulation of conservation of mass.

where the radius of curvature r_c of the interface is assumed that the vapor phase and determines the effects of interfacial tension σ . Radius of curvature is given by

where $V_{l(n)}$ and $V_{v(n)}$ denote velocities in the direction normal to the interface and $V_{I(n)}$ is the interface velocity in the normal direction. In the vapor region, mass moves toward the interface with a velocity $V_{v(n)}$, with respect to a stationary observer. However, the interface is also moving with a velocity $V_{I(n)}$, so that the vapor mass flow rate toward the control volume moving with the interface is $\rho_v (V_{v(n)} - V_{I(n)})$. By a similar argument, the liquid mass flow rate out of the control volume moving with the interface is $\rho_l (V_{I(n)} - V_{l(n)})$. Since the control volume represents an interface, there can be no accumulation of mass so these two mass flow rates must be equal as given by equation 2.17.

Because the interface can contain no mass, it is also without momentum and energy except for free surface energy which is related to the interfacial tension. Ignoring normal viscous stress, the momentum balance in the direction of the normal to the interface can be depicted as in Figure 2.3. Because of the motion of the interface, momentum in the direction of the unit normal vector \hat{n} is convected into the control volume moving with the interface at the relative velocity of the fluid with respect to the interface. Therefore, the momentum balance in the direction of the normal to the interface is given by

$$\rho_l (V_{I(n)} - V_{l(n)}) V_{I(n)} - \rho_v (V_{v(n)} - V_{I(n)}) V_{v(n)} = p_v - p_l - \frac{\sigma_s}{r_c} \quad (2.18)$$

where the radius of curvature r_c of the interface is measured from the vapor phase and determines the effects of interfacial tension σ_s . Radius of curvature is given by

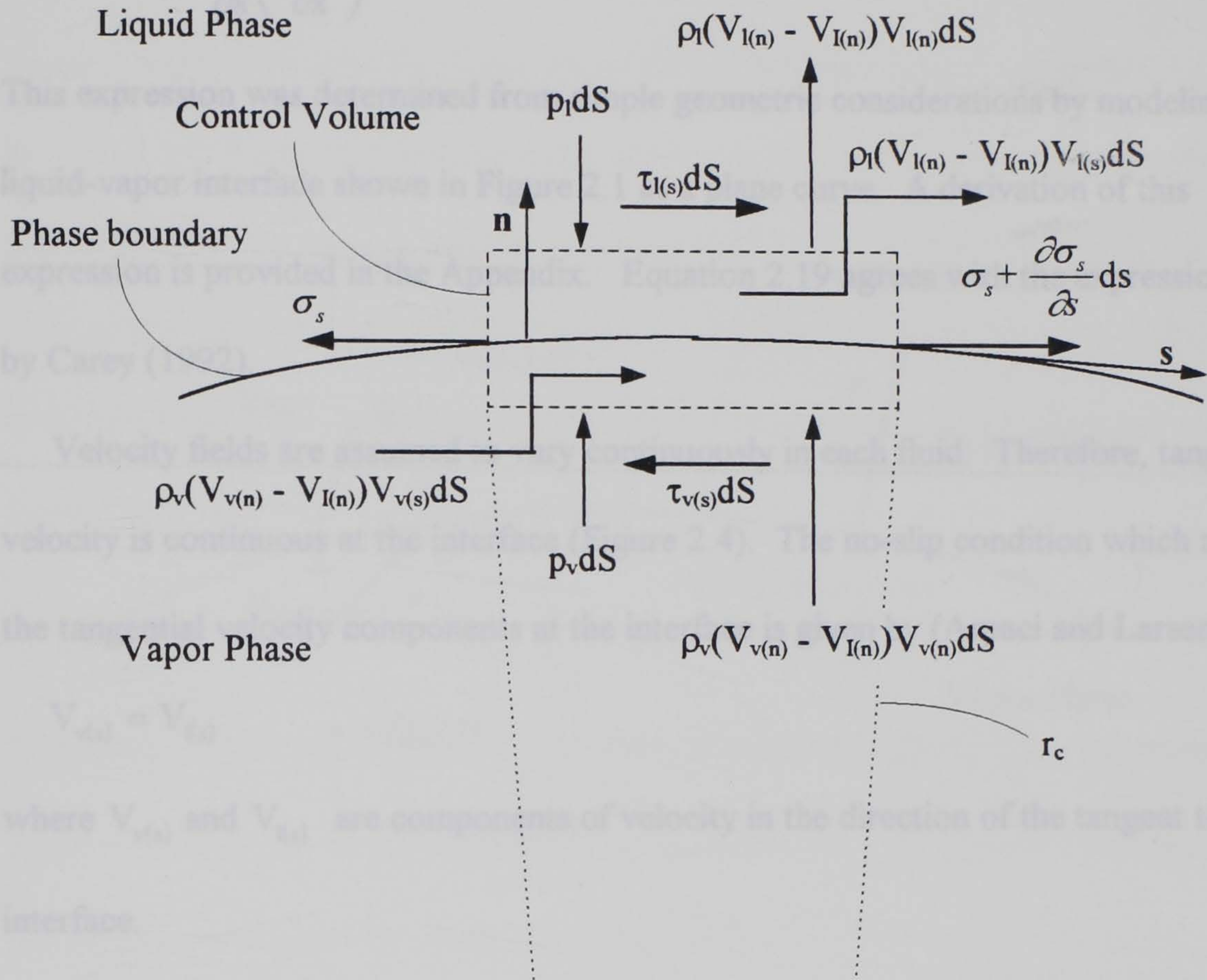


Figure 2.3. Differential control volume about a moving interface for the formulation of balance of momentum normal and tangent to the interface.

$$r_c = \frac{\left[1 + \left(\frac{\partial \delta_v}{\partial x} \right)^2 \right]^{\frac{3}{2}}}{-\frac{\partial}{\partial x} \left(\frac{\partial \delta_v}{\partial x} \right)} \quad (2.19)$$

This expression was determined from simple geometric considerations by modeling the liquid-vapor interface shown in Figure 2.1 as a plane curve. A derivation of this expression is provided in the Appendix. Equation 2.19 agrees with the expression given by Carey (1992).

Velocity fields are assumed to vary continuously in each fluid. Therefore, tangential velocity is continuous at the interface (Figure 2.4). The no-slip condition which applies to the tangential velocity components at the interface is given by (Arpaci and Larsen, 1984)

$$V_{v(s)} = V_{l(s)} \quad (2.20)$$

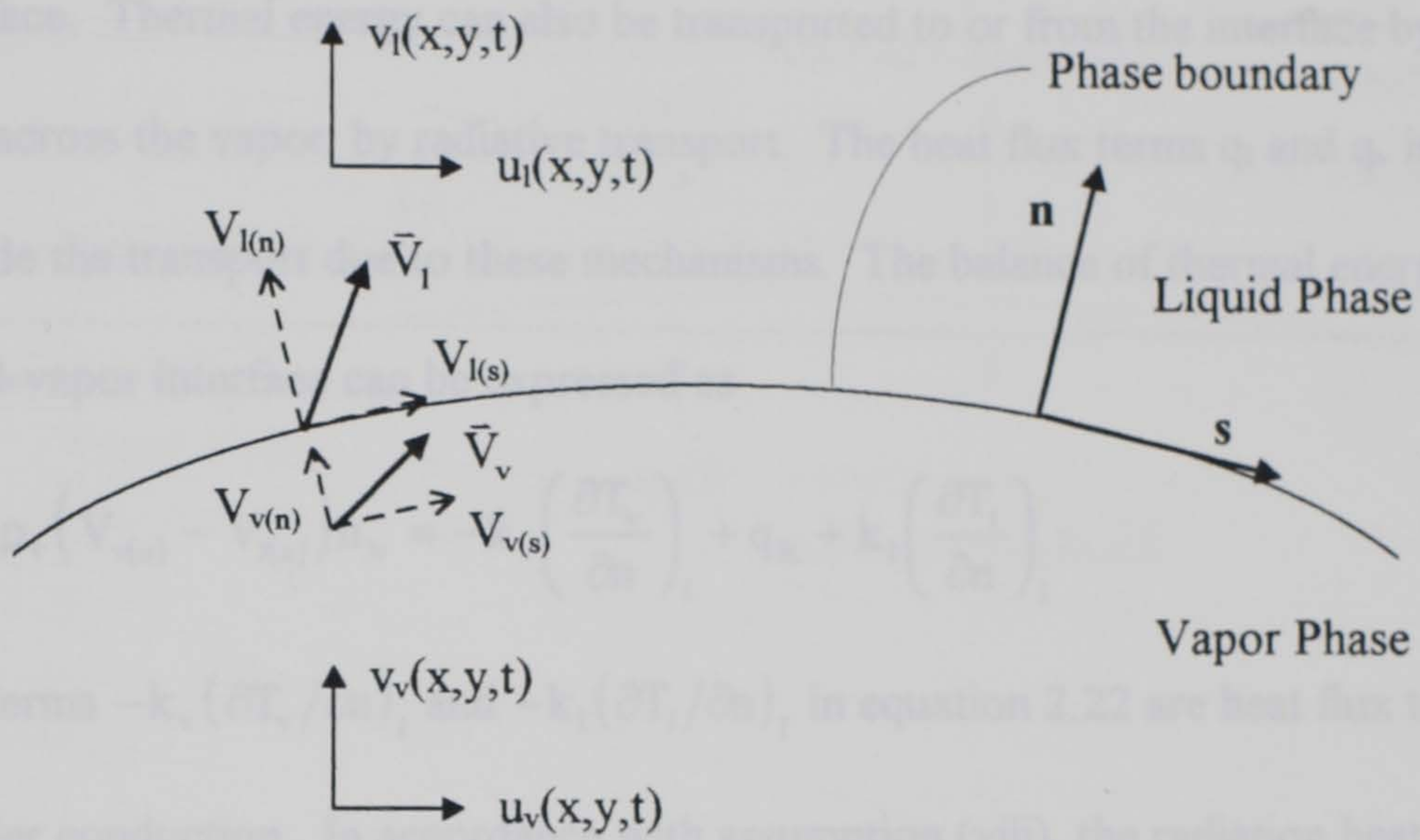
where $V_{v(s)}$ and $V_{l(s)}$ are components of velocity in the direction of the tangent to the interface.

For constant interfacial tension, the force and momentum balance in the direction of the unit tangent vector \hat{s} at the interface (Figure 2.3) reduces to an equality of the shear stress in the liquid and vapor on either side of the interface as the control volume thickness approaches zero.

$$\mu_v \left(\frac{\partial V_{v(s)}}{\partial n} \right)_I = \mu_l \left(\frac{\partial V_{l(s)}}{\partial n} \right)_I \quad (2.21)$$

In equation 2.21, n is the coordinate normal to the interface and the indice I denotes an interfacial location.

The balance of thermal energy at the liquid-vapor interface is depicted in Figure 2.5. As in the transport of mass and momentum, thermal energy is convected into the control volume moving with the interface at the velocity of the fluid relative to the interface. Phase change at the interface is accounted for by the latent heat of vaporization given by $h_v = (h_v - h_l)$. Local thermodynamic equilibrium is assumed to exist at the liquid-vapor interface.



The terms $-k_l (\partial T / \partial n)$ and $-k_v (\partial T / \partial n)$ in equation 2.22 are heat flux terms due to Fourier conduction. In accordance with assumption (viii), the radiation heat flux across the vapor layer is given by (Sparrow, 1964)

$$q_r = h_r (T_s - T) \tag{2.23}$$

where

$$h_r = \frac{1}{4} \sigma (T_s + T) \tag{2.24}$$

Figure 2.4. Normal and tangential velocity components at the liquid-vapor interface.

The conservation equations for energy and momentum in the vapor and liquid layers are coupled even when constant thermophysical properties are assumed. This coupling is due to the fact that the velocity of the liquid-vapor interface depends on the vaporization rate.

The balance of thermal energy at the liquid-vapor interface is depicted in Figure 2.5. As in the transport of mass and momentum, thermal energy is convected into the control volume moving with the interface at the velocity of the fluid relative to the interface. Phase change at the interface is accounted for by the latent heat of vaporization given by $h_{lv} = (h_v - h_l)$. Local thermodynamic equilibrium is assumed to exist at the liquid-vapor interface. Thermal energy can also be transported to or from the interface by conduction and, across the vapor, by radiative transport. The heat flux terms q_l and q_v in Figure 2.5 include the transport due to these mechanisms. The balance of thermal energy at the liquid-vapor interface can be expressed as

$$-\rho_v (V_{v(n)} - V_{l(n)}) h_{lv} = -k_v \left(\frac{\partial T_v}{\partial n} \right)_I + q_R + k_l \left(\frac{\partial T_l}{\partial n} \right)_I \quad (2.22)$$

The terms $-k_v (\partial T_v / \partial n)_I$ and $-k_l (\partial T_l / \partial n)_I$ in equation 2.22 are heat flux terms due to Fourier conduction. In accordance with assumption (viii), the radiation heat flux across the vapor layer is given by (Sparrow, 1964)

$$q_R = h_R (T_p - T_I) \quad (2.23)$$

where

$$h_R = \left[\frac{\epsilon_p \epsilon_I}{\epsilon_p + \epsilon_I - \epsilon_p \epsilon_I} \right] \left[\frac{\sigma (T_p^4 - T_I^4)}{T_p - T_I} \right] \quad (2.24)$$

The conservation equations for energy and momentum in the vapor and liquid layers are coupled even when constant thermophysical properties are assumed. This coupling is due to the fact that the velocity of the liquid-vapor interface depends on the vaporization rate.

Model Formulation

In order to apply the integral method to a transient problem, physically correct polynomial profiles are assumed for flow velocity and temperature in the vapor layer and in the liquid layer. Cess and Sparrow (1961) showed that the temperature and velocity profiles in the vapor are nearly linear for stationary plates when $Ja/P_1 \ll 10$ and $Ja \ll 12$, respectively. Since most vapors (and most liquids) have $P_1 \approx 1$ and $Ja < 1$ for most applications, both conditions are frequently satisfied. The validity of the boundary conditions given by equations 2.11 and 2.12 is also supported by the fact that the vapor layer thickness is small, assuming linear profiles in the vapor layer, the boundary conditions given by equations 2.11 and 2.12 are satisfied.

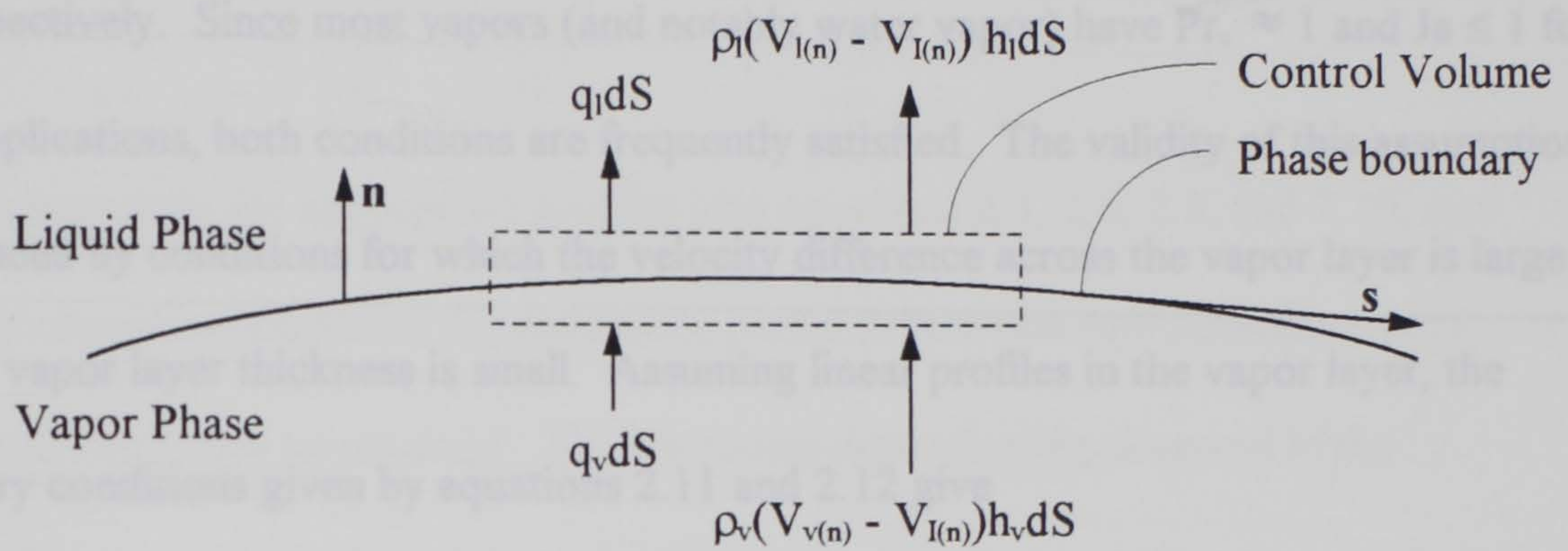


Figure 2.5. Differential control volume about a moving interface for the formulation of thermal energy conservation.

Second-degree polynomials are prescribed for the velocity and temperature profiles in the liquid subject to conditions given by equations 2.13, 2.14, and 2.15.

$$u_1 = u_w - 2 \frac{(u_w - u_\infty)}{\delta} y_1 + \frac{(u_w - u_\infty)}{\delta^2} y_1^2 \quad (2.27)$$

Model Formulation

In order to apply the integral method to a transient problem, physically correct polynomial profiles are assumed for flow velocity and temperature in the vapor layer and in the liquid layer. Cess and Sparrow (1961) showed that the temperature and velocity profiles in the vapor are nearly linear for stationary plates when $Ja/Pr_v \ll 30$ and $Ja \ll 12$, respectively. Since most vapors (and notably water vapor) have $Pr_v \approx 1$ and $Ja \leq 1$ for most applications, both conditions are frequently satisfied. The validity of this assumption is enhanced by conditions for which the velocity difference across the vapor layer is large and the vapor layer thickness is small. Assuming linear profiles in the vapor layer, the boundary conditions given by equations 2.11 and 2.12 give

$$u_v = v_p + \frac{(u_{vI} - v_p)}{\delta_v} y \quad (2.25)$$

and

$$T_v = T_p + \frac{(T_{vI} - T_p)}{\delta_v} y. \quad (2.26)$$

Transient effects are incorporated in the vapor layer velocity profile by equation 2.12a and by temporal changes in the thickness of the vapor layer. Similarly, transient effects are incorporated in the vapor layer temperature profile by equation 2.12b and by temporal changes in the thickness of the vapor layer.

Second-degree polynomials are prescribed for the velocity and temperature profiles in the liquid subject to conditions given by equations 2.13, 2.14, and 2.15.

$$u_l = u_{II} - 2 \frac{(u_{II} - u_{\infty})}{\delta} y_1 + \frac{(u_{II} - u_{\infty})}{\delta^2} y_1^2 \quad (2.27)$$

$$T_1 = T_{II} - 2 \frac{(T_{II} - T_{\infty})}{\Delta} y_1 + \frac{(T_{II} - T_{\infty})}{\Delta^2} y_1^2 \quad (2.28)$$

Transient effects are incorporated in the liquid layer velocity profile by equations 2.13a and 2.15a and by temporal changes in the thickness of the liquid velocity boundary layer. Similarly, transient effects are incorporated in the liquid layer temperature profile by equation 2.13b and by temporal changes in the thickness of the liquid thermal boundary layer.

By substituting the appropriate profiles into equations 2.4, 2.6, 2.8, and 2.10, and carefully observing functional dependencies, partial differential equations for $\delta_v(x,t)$, $\delta(x,t)$, and $\Delta(x,t)$ can be obtained. The functional dependencies observed in the formulation are given by $\delta_v = \delta_v(x,t)$, $\delta = \delta(x,t)$, $\Delta = \Delta(x,t)$, $u_v = u_v(x,y,t)$, $u_l = u_l(x,y,t)$, $u_{\infty} = u_{\infty}(x,t)$, $v_v = v_v(x,y,t)$, $v_l = v_l(x,y,t)$, $T_v = T_v(x,y,t)$, and $T_l = T_l(x,y,t)$. In addition, $p_v = p_v(x,t)$, $p_l = p_l(x,t)$, $u_{vl} = u_{vl}(x,t)$, $u_{ll} = u_{ll}(x,t)$, $u_l = u_l(x,t)$, $v_{vl} = v_{vl}(x,t)$, $v_{ll} = v_{ll}(x,t)$, $T_{vl} = T_{vl}(x,t)$, and $T_{ll} = T_{ll}(x,t)$. The terms v_p , T_p , and T_{∞} are constants. With the vapor layer velocity profile given by equation 2.25 and $\tau_{yx} = \mu_v \partial u_v / \partial y$ evaluated at $y = 0$ and $y = \delta_v$, equations 2.2 and 2.4 give the following expression for momentum conservation in the vapor layer.

$$\frac{\partial \bar{\delta}_v}{\partial t} \text{Sr}_w \left[\frac{1}{2} (\bar{u}_{vl} + \bar{v}_p) - \bar{u}_l \right] + \frac{\partial \bar{\delta}_v}{\partial x} \left[\frac{1}{3} (\bar{u}_{vl}^2 + \bar{v}_p \bar{u}_{vl} + \bar{v}_p^2) - \frac{1}{2} \bar{u}_l (\bar{u}_{vl} + \bar{v}_p) \right] + \left[\frac{1}{2} \text{Sr}_w \frac{\partial \bar{u}_{vl}}{\partial t} + \frac{\partial \bar{u}_{vl}}{\partial x} \left(\frac{1}{3} \bar{v}_p + \frac{2}{3} \bar{u}_{vl} - \frac{1}{2} \bar{u}_l \right) + \frac{1}{2} \frac{\partial \bar{p}_v}{\partial x} \right] \bar{\delta}_v = 0. \quad (2.29)$$

With the vapor layer velocity and temperature profiles given by equations 2.25 and 2.26, respectively, and $q_y = -k_v \partial T_v / \partial y$ evaluated at $y = 0$ and $y = \delta_v$, equation 2.6 gives the following equation for energy conservation in the vapor layer.

$$\begin{aligned} & \frac{\partial \bar{\delta}_v}{\partial t} \text{Sr}_w \left(-\frac{1}{2} \bar{T}_{vI} \right) + \frac{\partial \bar{\delta}_v}{\partial \bar{x}} \left[-\frac{1}{3} \bar{T}_{vI} \left(\frac{1}{2} \bar{u}_{vI} + \bar{v}_p \right) \right] + \\ & \left[\frac{1}{2} \text{Sr}_w \frac{\partial \bar{T}_{vI}}{\partial t} - \frac{1}{6} \bar{T}_{vI} \frac{\partial \bar{u}_{vI}}{\partial \bar{x}} + \frac{1}{3} \frac{\partial \bar{T}_{vI}}{\partial \bar{x}} \left(\frac{1}{2} \bar{v}_p + \bar{u}_{vI} \right) \right] \bar{\delta}_v = 0. \end{aligned} \quad (2.30)$$

Substituting the liquid layer velocity profile given by equation 2.27 into equation 2.8 with w_I given by equation 2.2 and $\tau_{yx} = \mu_l \partial u_l / \partial y$ evaluated at $y_1 = 0$ gives the following relationship for momentum conservation in the liquid layer.

$$\begin{aligned} & \frac{\partial \bar{\delta}}{\partial t} \text{Sr}_w \left[\frac{1}{3} (\bar{u}_{II} - \bar{u}_\infty) \right] + \frac{\partial \bar{\delta}}{\partial \bar{x}} \left[\frac{1}{5} \bar{u}_{II}^2 - \frac{1}{15} \bar{u}_{II} \bar{u}_\infty - \frac{2}{15} \bar{u}_\infty^2 \right] + \\ & \left[\frac{1}{3} \text{Sr}_w \frac{\partial \bar{u}_{II}}{\partial t} + \frac{2}{3} \text{Sr}_w \frac{\partial \bar{u}_\infty}{\partial t} + \frac{\partial \bar{u}_{II}}{\partial \bar{x}} \left(\frac{2}{5} \bar{u}_{II} - \frac{1}{15} \bar{u}_\infty \right) + \right. \\ & \left. \frac{\partial \bar{u}_\infty}{\partial \bar{x}} \left(\frac{4}{15} \bar{u}_{II} + \frac{2}{5} \bar{u}_\infty \right) + \frac{1}{2} \frac{\partial \bar{p}_1}{\partial \bar{x}} \right] \bar{\delta} + \left[-2 \frac{1}{\text{Re}_{wl}} (\bar{u}_{II} - \bar{u}_\infty) \right] \bar{\delta}^{-1} + \\ & \frac{\rho_v}{\rho_l} \left[\text{Sr}_w \frac{\partial \bar{\delta}_v}{\partial t} + \frac{1}{2} (\bar{u}_{vI} + \bar{v}_p) \frac{\partial \bar{\delta}_v}{\partial \bar{x}} + \frac{1}{2} \frac{\partial \bar{u}_{vI}}{\partial \bar{x}} \bar{\delta}_v \right] (\bar{u}_I - \bar{u}_\infty) = 0. \end{aligned} \quad (2.31)$$

With the liquid layer velocity and temperature profiles given by equations 2.27 and 2.28, respectively, equation 2.10 and equation 2.2 yield the following expression for energy conservation for the liquid layer.

$$\frac{\partial \bar{\Delta}}{\partial t} \text{Sr}_w \left[\frac{1}{3} \bar{T}_{II} \right] + \frac{\partial \bar{\Delta}}{\partial \bar{x}} \bar{T}_{II} \left[\frac{1}{3} \bar{u}_{II} + (\bar{u}_{II} - \bar{u}_{\infty}) \left(\frac{1}{10} \frac{\bar{\Delta}^2}{\bar{\delta}^2} - \frac{1}{3} \frac{\bar{\Delta}}{\bar{\delta}} \right) \right] +$$

$$\bar{\Delta}^3 \left[\frac{1}{30} \bar{T}_{II} \left(\frac{\partial \bar{u}_{II}}{\partial \bar{x}} - \frac{\partial \bar{u}_{\infty}}{\partial \bar{x}} \right) \bar{\delta}^{-2} + (\bar{u}_{II} - \bar{u}_{\infty}) \left(\frac{7}{10} \frac{\partial \bar{T}_{II}}{\partial \bar{x}} \bar{\delta}^{-2} - \frac{1}{15} \bar{T}_{II} \frac{\partial \bar{\delta}}{\partial \bar{x}} \bar{\delta}^{-3} \right) \right] +$$

$$\bar{\Delta}^2 \left[-\frac{1}{6} \bar{T}_{II} \left(\frac{\partial \bar{u}_{II}}{\partial \bar{x}} - \frac{\partial \bar{u}_{\infty}}{\partial \bar{x}} \right) \bar{\delta}^{-1} + (\bar{u}_{II} - \bar{u}_{\infty}) \left(-\frac{1}{6} \frac{\partial \bar{T}_{II}}{\partial \bar{x}} \bar{\delta}^{-1} + \frac{1}{6} \bar{T}_{II} \frac{\partial \bar{\delta}}{\partial \bar{x}} \bar{\delta}^{-2} \right) \right] +$$

$$\bar{\Delta} \left[\frac{1}{3} \text{Sr}_w \frac{\partial \bar{T}_{II}}{\partial t} + \frac{1}{3} \bar{T}_{II} \frac{\partial \bar{u}_{II}}{\partial \bar{x}} + \frac{1}{3} \bar{u}_{II} \frac{\partial \bar{T}_{II}}{\partial \bar{x}} \right] + \left[-2 \frac{1}{\text{Re}_w \text{Pr}_1} \bar{T}_{II} \right] \bar{\Delta}^{-1} +$$

$$\frac{\rho_v}{\rho_1} \bar{T}_{II} \left[\text{Sr}_w \frac{\partial \bar{\delta}_v}{\partial t} + \frac{1}{2} (\bar{u}_{vI} + \bar{v}_p) \frac{\partial \bar{\delta}_v}{\partial \bar{x}} + \frac{1}{2} \frac{\partial \bar{u}_{vI}}{\partial \bar{x}} \bar{\delta}_v \right] = 0.$$

(2.32)

In order to evaluate the additional relationships which must be satisfied at the liquid-vapor interface, the unit vectors in the normal and tangent directions to the interface, \hat{n} and \hat{s} in Figure 2.4, are related to the vapor layer thickness δ_v along the plate and are thereby defined as (Burelbach et al., 1988)

$$\hat{n} = \frac{-\frac{\partial \delta_v}{\partial x} \hat{i} + \hat{j}}{\left[1 + \left(\frac{\partial \delta_v}{\partial x} \right)^2 \right]^{\frac{1}{2}}} \quad (2.33)$$

and

$$\hat{s} = \frac{\hat{i} + \frac{\partial \delta_v}{\partial x} \hat{j}}{\left[1 + \left(\frac{\partial \delta_v}{\partial x} \right)^2 \right]^{\frac{1}{2}}} \quad (2.34)$$

Liquid velocity, vapor velocity, and interface velocity can be expressed in vector form as

$$\bar{V}_l = u_l \hat{i} + v_l \hat{j} \quad (2.35a)$$

$$\bar{V}_v = u_v \hat{i} + v_v \hat{j} \quad (2.35b)$$

$$\bar{V}_I = u_I \hat{i} + \frac{\partial \delta_v}{\partial t} \hat{j} \quad (2.35c)$$

respectively. In interfacial equations 2.17, 2.18, 2.20, 2.21, and 2.22, the velocity components directed normally and tangentially to the interface are obtained from the appropriate dot products involving the unit vectors defined in equations 2.33 and 2.34 and the velocity vectors defined in equation 2.35. In equations 2.21 and 2.22, the gradients in the direction normal to the interface are determined by evaluating the appropriate directional derivative (Thomas and Finney, 1988). The resulting interfacial relationships are expressed in dimensionless forms in equations 2.36 through 2.40. Upon using equations 2.33 and 2.35 to obtain velocity components directed normally to the interface, equation 2.17 yields the following expression for conservation of mass at the liquid-vapor interface.

$$\left(\bar{v}_{II} - \bar{u}_{II} \frac{\partial \bar{\delta}_v}{\partial \bar{x}} \right) - \frac{\rho_v}{\rho_l} \left(\bar{v}_{vI} - \bar{u}_{vI} \frac{\partial \bar{\delta}_v}{\partial \bar{x}} \right) = \left(1 - \frac{\rho_v}{\rho_l} \right) \left[Sr_w \frac{\partial \bar{\delta}_v}{\partial \bar{t}} - \bar{u}_I \frac{\partial \bar{\delta}_v}{\partial \bar{x}} \right]. \quad (2.36)$$

Similarly, equations 2.33 and 2.35 can be used with equation 2.18 to get the following expression for the momentum balance in the direction of the normal to the interface.

$$\begin{aligned}
& \left(S r_w \frac{\partial \bar{\delta}_v}{\partial \bar{t}} - \bar{u}_I \frac{\partial \bar{\delta}_v}{\partial \bar{x}} \right) \left[\frac{\rho_v}{\rho_1} \left(\bar{v}_{vI} - \bar{u}_{vI} \frac{\partial \bar{\delta}_v}{\partial \bar{x}} \right) - \left(\bar{v}_{II} - \bar{u}_{II} \frac{\partial \bar{\delta}_v}{\partial \bar{x}} \right) \right] + \\
& \left(\bar{v}_{II} - \bar{u}_{II} \frac{\partial \bar{\delta}_v}{\partial \bar{x}} \right)^2 - \frac{\rho_v}{\rho_1} \left(\bar{v}_{vI} - \bar{u}_{vI} \frac{\partial \bar{\delta}_v}{\partial \bar{x}} \right)^2 = \\
& \bar{\sigma}_s \frac{\partial^2 \bar{\delta}_v}{\partial \bar{x}^2} \left[1 + \left(\frac{\partial \bar{\delta}_v}{\partial \bar{x}} \right)^2 \right]^{-\frac{1}{2}} + \frac{1}{2} \left(\frac{\rho_v}{\rho_1} \bar{p}_v - \bar{p}_1 \right) \left[1 + \left(\frac{\partial \bar{\delta}_v}{\partial \bar{x}} \right)^2 \right].
\end{aligned}
\tag{2.37}$$

Upon using equations 2.34, 2.35a, and 2.35b to obtain velocity components directed tangentially to the interface, equation 2.20 yields the following relationship for the no slip condition at the interface.

$$(\bar{u}_{II} - \bar{u}_{vI}) + (\bar{v}_{II} - \bar{v}_{vI}) \frac{\partial \bar{\delta}_v}{\partial \bar{x}} = 0.
\tag{2.38}$$

In equation 2.21, the gradients directed normally to the interface can be determined using equations 2.33 and 2.34 with equations 2.35a and 2.35b. The resulting expression for the shear stress balance at the interface is given by

$$\begin{aligned}
& \frac{\partial \bar{\delta}_v}{\partial \bar{x}} \left[\frac{\partial \bar{v}_{vI}}{\partial \bar{y}} - \frac{\partial \bar{u}_{vI}}{\partial \bar{x}} - \frac{\mu_1}{\mu_v} \left(\frac{\partial \bar{v}_{II}}{\partial \bar{y}} - \frac{\partial \bar{u}_{II}}{\partial \bar{x}} \right) \right] + \\
& \left\{ -\frac{\partial \bar{\delta}_v}{\partial \bar{x}} \frac{\partial^2 \bar{\delta}_v}{\partial \bar{x}^2} + \left(\frac{\partial \bar{\delta}_v}{\partial \bar{x}} \right)^3 \left[1 + \left(\frac{\partial \bar{\delta}_v}{\partial \bar{x}} \right)^2 \right]^{-1} \frac{\partial^2 \bar{\delta}_v}{\partial \bar{x}^2} \right\} \left(\bar{v}_{vI} - \frac{\mu_1}{\mu_v} \bar{v}_{II} \right) + \\
& \left(\frac{\partial \bar{\delta}_v}{\partial \bar{x}} \right)^2 \left[1 + \left(\frac{\partial \bar{\delta}_v}{\partial \bar{x}} \right)^2 \right]^{-1} \frac{\partial^2 \bar{\delta}_v}{\partial \bar{x}^2} \left(\bar{u}_{vI} - \frac{\mu_1}{\mu_v} \bar{u}_{II} \right) + \\
& - \left(\frac{\partial \bar{\delta}_v}{\partial \bar{x}} \right)^2 \left(\frac{\partial \bar{v}_{vI}}{\partial \bar{x}} - \frac{\mu_1}{\mu_v} \frac{\partial \bar{v}_{II}}{\partial \bar{x}} \right) + (\bar{u}_{vI} - \bar{v}_p) \bar{\delta}_v^{-1} + \\
& 2 \frac{\mu_1}{\mu_v} (\bar{u}_{II} - \bar{u}_\infty) \bar{\delta}_v^{-1} = 0.
\end{aligned} \tag{2.39}$$

The gradients directed normally to the interface in equation 2.22 can be determined by using equation 2.33 with the temperature profiles given by equations 2.26 and 2.28. Upon using equations 2.33, 2.35b, and 2.35c to obtain velocity components directed normally to the interface, equation 2.22 yields the following expression for the balance of thermal energy at the liquid-vapor interface.

$$-\frac{1}{\text{Ja}} \text{Pr}_v \text{Re}_{ww} \left[\left(\bar{v}_{vi} - \bar{u}_{vi} \frac{\partial \bar{\delta}_v}{\partial \bar{x}} \right) - \left(\text{Sr}_w \frac{\partial \bar{\delta}_v}{\partial \bar{t}} - \bar{u}_I \frac{\partial \bar{\delta}_v}{\partial \bar{x}} \right) \right] =$$

$$\frac{\partial \bar{T}_{vi}}{\partial \bar{x}} \frac{\partial \bar{\delta}_v}{\partial \bar{x}} - \bar{T}_{vi} \bar{\delta}_v^{-1} \left[1 + \left(\frac{\partial \bar{\delta}_v}{\partial \bar{x}} \right)^2 \right] +$$

$$-\frac{wh_R}{k_v} \bar{T}_{vi} \left[1 + \left(\frac{\partial \bar{\delta}_v}{\partial \bar{x}} \right)^2 \right]^{\frac{1}{2}} - \beta \frac{\mu_l}{\mu_v} \left(\frac{\partial \bar{T}_{li}}{\partial \bar{x}} \frac{\partial \bar{\delta}_v}{\partial \bar{x}} + 2 \bar{T}_{li} \bar{\Delta}^{-1} \right).$$

(2.40)

The terms $\partial \bar{v}_{vi} / \partial \bar{y}$ and $\partial \bar{v}_{li} / \partial \bar{y}$ which appear in equation 2.39 are replaced by using the differential form of continuity applied at the interface. For the vapor layer, equation 2.1 applied at the interface gives

$$\partial \bar{v}_{vi} / \partial \bar{y} = -\partial \bar{u}_{vi} / \partial \bar{x}. \quad (2.41)$$

Similarly, for the liquid layer

$$\partial \bar{v}_{li} / \partial \bar{y} = -\partial \bar{u}_{li} / \partial \bar{x}. \quad (2.42)$$

Another useful equation is obtained by taking the derivative with respect to x of the no-slip condition given by equation 2.37. This relationship represents the interface curvature $\partial^2 \bar{\delta}_v / \partial \bar{x}^2$ in terms of the interfacial velocity components.

$$\frac{\partial \bar{u}_{li}}{\partial \bar{x}} - \frac{\partial \bar{u}_{vi}}{\partial \bar{x}} + (\bar{v}_{li} - \bar{v}_{vi}) \frac{\partial^2 \bar{\delta}_v}{\partial \bar{x}^2} + \frac{\partial \bar{\delta}_v}{\partial \bar{x}} \left(\frac{\partial \bar{v}_{li}}{\partial \bar{x}} - \frac{\partial \bar{v}_{vi}}{\partial \bar{x}} \right) = 0. \quad (2.43)$$

The local convective heat transfer coefficient h at the plate surface is obtained from Newton's law of cooling and equation 2.26 and is given by

$$h = \frac{-k_v \left. \frac{\partial T_v}{\partial y} \right|_{y=0}}{(T_p - T_s)} \quad (2.44a)$$

With h given by equation 2.44a, the local Nusselt number is defined as

$$Nu_v = \frac{hw}{k_v} \quad (2.44b)$$

If the simplifying assumption of constant interface temperature $T_{vi} = T_s$ is invoked, equation 2.44a gives

$$h = \frac{k_v}{\delta_v} \quad (2.44c)$$

Forcing Functions for Incident Flow

An important advantage of the present model is that boundary layer behavior can be predicted for any specified temporal variation in the free stream velocity $u_\infty(x, t)$ in equation 2.15a, as long as the variations are piecewise smooth. Since the precise characteristics of temporal flow variations are dependent on specific physical circumstances, the general features of a steady stagnation flow are assumed to apply so as to obtain forcing functions which converge on the steady flow case as forcing frequencies approach zero (Mladin and Zumbrunnen, 1994). The transient velocity flow field is assumed to resemble a steady state flow field at each instant in time where the velocity gradient at the stagnation line corresponds to the instantaneous incident velocity.

The steady state dimensionless pressure distribution in the liquid $\bar{p}_1(\bar{x})$ can be accurately expressed for $\bar{x} \leq x_*$ by (Zumbrunnen et al., 1992)

$$\bar{p}_{1,ss} = \left(\frac{\bar{x}}{x_*} \right)^2 \left(2 \frac{\bar{x}}{x_*} - 3 \right) + 1. \quad (2.45)$$

This general pressure distribution reflects the essential features of the dimensionless pressure distributions for a variety of jet velocity discharge profiles. Applicable values of x_* depend on the specific jet velocity profile of interest. Notably, for $\bar{x} = 0$, $\bar{p}_1 = 1$ and $d\bar{p}_1/d\bar{x} = 0$ and for $\bar{x} \geq x_*$, $\bar{p}_1 = 0$ and $d\bar{p}_1/d\bar{x} \cong 0$. This pressure distribution was used with Euler's equation, given by equation 2.16, to develop the steady state expressions for $d\bar{u}_\infty/d\bar{x}$ and \bar{u}_∞ . With $\bar{u}_\infty = 0$ at the stagnation line ($\bar{x} = 0$), the resulting expressions for \bar{u}_∞ and $d\bar{u}_\infty/d\bar{x}$ are

$$\bar{u}_{\infty,ss} \Big|_{0 \leq \bar{x} \leq x_*} = \left[3 \left(\frac{\bar{x}}{x_*} \right)^2 - 2 \left(\frac{\bar{x}}{x_*} \right)^3 \right]^{\frac{1}{2}} \quad (2.46a)$$

$$\bar{u}_{\infty,ss} \Big|_{\bar{x} > x_*} = 1 \quad (2.46b)$$

$$\frac{d\bar{u}_{\infty,ss}}{d\bar{x}} \Big|_{0 \leq \bar{x} \leq x_*} = \frac{3}{\bar{u}_{\infty,ss} x_*} \left[\frac{\bar{x}}{x_*} - \left(\frac{\bar{x}}{x_*} \right)^2 \right] \quad (2.47a)$$

$$\frac{d\bar{u}_{\infty,ss}}{d\bar{x}} \Big|_{\bar{x} > x_*} = 0. \quad (2.47b)$$

The steady state dimensionless free stream velocity gradient at the stagnation line was found from equations 2.46 and 2.47. In the limit as $\bar{x} \rightarrow 0$, it is given by

$$\bar{C} = \frac{d\bar{u}_{\infty,ss}}{d\bar{x}} \Big|_{\bar{x}=0} = \frac{\sqrt{3}}{x_*} \quad (2.48)$$

where $\bar{C} = 0.7854$ and $x_* = 2.2053$ for a planar jet with a uniform discharge velocity.

Sinusoidal forcing functions are specified about the initial, steady state values given by equations 2.46 and 2.47 and are given for $0 < \epsilon < 1$ by

$$\bar{u}_\infty|_{0 \leq \bar{x} \leq x_*} = \left[3 \left(\frac{\bar{x}}{x_*} \right)^2 - 2 \left(\frac{\bar{x}}{x_*} \right)^3 \right]^{\frac{1}{2}} \left[1 + \epsilon \cos(2\pi \bar{f} \bar{t}) \right] \quad (2.49)$$

$$\left. \frac{\partial \bar{u}_\infty}{\partial \bar{x}} \right|_{0 \leq \bar{x} \leq x_*} = \frac{3}{\bar{u}_{\infty,ss} x_*} \left[\frac{\bar{x}}{x_*} - \left(\frac{\bar{x}}{x_*} \right)^2 \right] \left[1 + \epsilon \cos(2\pi \bar{f} \bar{t}) \right] \quad (2.50a)$$

$$\left. \frac{\partial \bar{u}_\infty}{\partial \bar{x}} \right|_{\bar{x}=0} = \frac{\sqrt{3}}{x_*} \left[1 + \epsilon \cos(2\pi \bar{f} \bar{t}) \right]. \quad (2.50b)$$

Taking the derivative of equation 2.49 with respect to \bar{t} gives

$$\left. \frac{\partial \bar{u}_\infty}{\partial \bar{t}} \right|_{0 \leq \bar{x} \leq x_*} = -2\pi \bar{f} \epsilon \left[3 \left(\frac{\bar{x}}{x_*} \right)^2 - 2 \left(\frac{\bar{x}}{x_*} \right)^3 \right]^{\frac{1}{2}} \sin(2\pi \bar{f} \bar{t}). \quad (2.51)$$

The time varying dimensionless pressure distribution in the liquid $\bar{p}_1(\bar{x}, \bar{t})$ is determined

by using equations 2.49, 2.50, and 2.51 in the time-dependent Euler equation given by

equation 2.16 which may be expressed in dimensionless form as

$$Sr_w \frac{\partial \bar{u}_\infty}{\partial \bar{t}} + \bar{u}_\infty \frac{\partial \bar{u}_\infty}{\partial \bar{x}} = -\frac{1}{2} \frac{\partial \bar{p}_1}{\partial \bar{x}}. \quad (2.52)$$

The resulting dimensionless pressure gradient is given by

$$\left. \frac{\partial \bar{p}_1}{\partial \bar{x}} \right|_{0 \leq \bar{x} \leq x_*} = 4\pi \bar{f} \epsilon Sr_w \sin(2\pi \bar{f} \bar{t}) \bar{u}_{\infty,ss} - \frac{6}{x_*} \left[1 + \epsilon \cos(2\pi \bar{f} \bar{t}) \right]^2 \left[\frac{\bar{x}}{x_*} - \left(\frac{\bar{x}}{x_*} \right)^2 \right]. \quad (2.53)$$

The time-dependent dimensionless pressure distribution is obtained by integrating equation 2.53 with respect to \bar{x} . The term $f(\bar{t})$ is an unknown integration function of \bar{t} .

$$\begin{aligned} \bar{p}_1|_{0 \leq \bar{x} \leq x_*} = & 4\pi \bar{f} \varepsilon Sr_w \sin(2\pi \bar{f} \bar{t}) \frac{x_*^6}{4} \left(-\frac{2}{x_*^3} \bar{x} + \frac{3}{x_*^2} \right)^{\frac{3}{2}} \left[\frac{2}{5} \left(-\frac{2}{x_*^3} \bar{x} + \frac{3}{x_*^2} \right) - \frac{2}{x_*^2} \right] + \\ & -\frac{6}{x_*} \left[1 + \varepsilon \cos(2\pi \bar{f} \bar{t}) \right]^2 \left(\frac{1}{2} \frac{\bar{x}^2}{x_*} - \frac{1}{3} \frac{\bar{x}^3}{x_*^2} \right) + f(\bar{t}). \end{aligned} \quad (2.54)$$

The function $f(\bar{t})$ is determined by considering the pressure distribution along the stagnation streamline. The steady state local velocity component perpendicular to the surface in the free stream is given by (Schlichting, 1979)

$$\bar{v}_{\infty,ss}|_{\bar{x}=0} = -\bar{C}\bar{y}. \quad (2.55)$$

A sinusoidal forcing function consistent with equations 2.49 and 2.50 is specified about the initial steady state value defined in equation 2.55 and is given for $0 < \varepsilon < 1$ by

$$\bar{v}_{\infty}|_{\bar{x}=0} = -\bar{C}\bar{y} \left[1 + \varepsilon \cos(2\pi \bar{f} \bar{t}) \right]. \quad (2.56)$$

Taking the derivative of equation 2.56 with respect to \bar{t} gives

$$\left. \frac{\partial \bar{v}_{\infty}}{\partial \bar{t}} \right|_{\bar{x}=0} = 2\pi \bar{f} \varepsilon \bar{C}\bar{y} \sin(2\pi \bar{f} \bar{t}). \quad (2.57)$$

Similarly, taking the derivative of equation 2.56 with respect to \bar{y} gives

$$\left. \frac{\partial \bar{v}_{\infty}}{\partial \bar{y}} \right|_{\bar{x}=0} = -\bar{C} \left[1 + \varepsilon \cos(2\pi \bar{f} \bar{t}) \right]. \quad (2.58)$$

The time varying dimensionless pressure distribution in the liquid $\bar{p}_1(\bar{y}, \bar{t})$ is determined by using equations 2.56, 2.57, and 2.58 in the dimensionless form of the time-dependent

Euler equation given by

$$-\bar{g} - \frac{1}{2} \frac{\partial \bar{p}_1}{\partial \bar{y}} = \text{Sr}_w \frac{\partial \bar{v}_\infty}{\partial \bar{t}} + \bar{v}_\infty \frac{\partial \bar{v}_\infty}{\partial \bar{y}}. \quad (2.59)$$

The resulting dimensionless pressure gradient is given by

$$\left. \frac{\partial \bar{p}_1}{\partial \bar{y}} \right|_{\bar{x}=0} = \left\{ -4 \text{Sr}_w \pi \bar{f} \bar{\epsilon} \bar{C} \sin (2\pi \bar{f} \bar{t}) - 2 \bar{C}^2 [1 + \bar{\epsilon} \cos (2\pi \bar{f} \bar{t})]^2 \right\} \bar{y} - 2\bar{g}. \quad (2.60)$$

The time-dependent dimensionless pressure distribution along the stagnation line is obtained by integrating equation 2.60 using the condition $\bar{p}_1 = 0$ at $\bar{y} = \bar{H}$ to determine the resulting integration function of \bar{t} .

$$\begin{aligned} \bar{p}_1|_{\bar{x}=0} = & \left\{ -2 \text{Sr}_w \pi \bar{f} \bar{\epsilon} \bar{C} \sin (2\pi \bar{f} \bar{t}) - \bar{C}^2 [1 + \bar{\epsilon} \cos (2\pi \bar{f} \bar{t})]^2 \right\} (\bar{y}^2 - \bar{H}^2) + \\ & -2\bar{g}(\bar{y} - \bar{H}). \end{aligned} \quad (2.61)$$

By evaluating equation 2.61 at $\bar{y} = 0$, the condition for determining the unknown function $f(\bar{t})$ in equation 2.54 can be obtained. At $\bar{x} = 0$,

$$\bar{p}_1 = 2 \text{Sr}_w \pi \bar{f} \bar{\epsilon} \bar{C} \sin (2\pi \bar{f} \bar{t}) \bar{H}^2 + \bar{C}^2 [1 + \bar{\epsilon} \cos (2\pi \bar{f} \bar{t})]^2 \bar{H}^2 + 2\bar{g}\bar{H}. \quad (2.62)$$

The time-dependent dimensionless pressure distribution of equation 2.54 becomes

$$\begin{aligned} \bar{p}_1|_{0 \leq \bar{x} \leq x_*} = & 4\pi \bar{f} \bar{\epsilon} \text{Sr}_w \sin (2\pi \bar{f} \bar{t}) \frac{x_*^6}{4} \left(-\frac{2}{x_*^3} \bar{x} + \frac{3}{x_*^2} \right)^{\frac{3}{2}} \left[\frac{2}{5} \left(-\frac{2}{x_*^3} \bar{x} + \frac{3}{x_*^2} \right) - \frac{2}{x_*^2} \right] + \\ & -\frac{6}{x_*} [1 + \bar{\epsilon} \cos (2\pi \bar{f} \bar{t})]^2 \left(\frac{1}{2} \frac{\bar{x}^2}{x_*} - \frac{1}{3} \frac{\bar{x}^3}{x_*^2} \right) + 2 \text{Sr}_w \pi \bar{f} \bar{\epsilon} \bar{C} \sin (2\pi \bar{f} \bar{t}) \bar{H}^2 + \\ & \bar{C}^2 [1 + \bar{\epsilon} \cos (2\pi \bar{f} \bar{t})]^2 \bar{H}^2 + 2\bar{g}\bar{H} + \frac{4}{5} \text{Sr}_w \pi \bar{f} \bar{\epsilon} \sin (2\pi \bar{f} \bar{t}) x_* (3)^{\frac{3}{2}}. \end{aligned} \quad (2.63)$$

CHAPTER III

SOLUTION METHODOLOGY AND MODEL VERIFICATION

The set of nonlinear partial differential equations 2.29-2.32, 2.36-2.40, and 2.43 govern the transient and spatial boundary layer responses of $\bar{\delta}_v$, $\bar{\delta}$, and $\bar{\Delta}$. This set of equations consists of momentum and energy conservation in the vapor and liquid layers coupled with the following conditions at the liquid-vapor interface: conservation of mass, balance of force and momentum, balance of shear stress, balance of thermal energy, and the no-slip relationship. The governing parameters for this set of equations include Strouhal number Sr_w , which defines the forcing frequency for the incident flow, Jakob number Ja , which is a measure of vapor superheat, and subcooling parameter β , which is a measure of the relative temperature differences across the vapor and liquid. Other parameters include the ratios of liquid density to vapor density and liquid viscosity to vapor viscosity. Reynolds numbers Re_{wl} and Re_{wv} , and Prandtl numbers Pr_l and Pr_v , for the liquid and the vapor are also governing parameters. The effects of interfacial tension and radiation heat transfer are taken into account by the dimensionless interfacial tension parameter $\bar{\sigma}$, and the dimensionless parameter wh_R/k_v . The free stream velocity distribution and the pressure distribution in the liquid and the vapor must also be specified for the governing equations.

The governing equations have the potential to extend previous steady state studies of forced convection boundary layer flow in the film boiling regime on a flat isothermal plate. The current model retains transient terms that were omitted from the steady state studies

in which spatial boundary layer variation was investigated. Therefore, the current model is capable of investigating boundary layer behavior in the vicinity of a stagnation flow as the boundary layers vary spatially and temporally. However, only the equations pertaining to the stagnation line temporal response will be solved within the scope of this study.

Solution Methodology for Stagnation Line Temporal Response

The equations governing the boundary layer responses can be simplified at the stagnation line by recognizing the symmetry in the dividing flow about the stagnation streamline as shown in Figure 2.1. Based on this symmetry, $\partial \bar{\delta}_v / \partial \bar{x} = 0$, $\partial \bar{\delta} / \partial \bar{x} = 0$, and $\partial \bar{\Delta} / \partial \bar{x} = 0$ at $\bar{x} = 0$. The validity of this assumption of boundary layer symmetry is obvious for a stationary plate but must be carefully considered for $\bar{v}_p \neq 0$. Boundary layer symmetry about the stagnation streamline on a moving plate was applied by Zumbrennen et al. (1992) in an integral formulation for single-phase flow with resulting model predictions agreeing with an exact analysis (Zumbrennen, 1991) where symmetry was not assumed to within 2%. Thus, the conditions $\partial \bar{\delta} / \partial \bar{x} = 0$ and $\partial \bar{\Delta} / \partial \bar{x} = 0$ at the stagnation line ($\bar{x} = 0$) were concluded to provide results within the accuracy of the integral formulation. Therefore, these conditions were applied in the present model and were extended to include $\partial \bar{\delta}_v / \partial \bar{x} = 0$ at $\bar{x} = 0$.

Similarly, symmetry in the pressure distribution about the stagnation streamline gives $\partial \bar{p}_1 / \partial \bar{x} = 0$ and $\partial \bar{p}_v / \partial \bar{x} = 0$ at $\bar{x} = 0$. The assumption of local thermodynamic equilibrium at the interface between vapor and liquid phases of a pure substance implies a unique relationship between the temperature and the vapor pressure at the interface.

Therefore, the temperature gradients at the stagnation line are $\partial \bar{T}_w / \partial \bar{x} = 0$ and $\partial \bar{T}_{vi} / \partial \bar{x} = 0$ as a result of the symmetry in the pressure distribution at the stagnation line. Because \bar{u}_∞ has a constant zero value ($\bar{u}_\infty = 0$) at $\bar{x} = 0$ even in a time-varying flow, it follows that the time derivative $\partial \bar{u}_\infty / \partial \bar{t}$ is zero along the stagnation streamline. The temperature of the interface may vary with time and position along the interface as long as local thermodynamic equilibrium is maintained between saturation temperature and saturation pressure. Therefore, equations 2.30, 2.32, and 2.40 were developed assuming the temperature of the interface is not a constant. However, for the sample cases presented in this study, it is assumed that the interface temperature is constant and the solution methodology is presented based on this simplifying assumption. Although pulsing the flow induces pressure oscillations which are accompanied by oscillations in saturation temperature, the assumption of constant interface temperature is appropriate for small oscillations in saturation temperature. If the dependence of interface temperature on time and position were retained, the same solution methodology would apply. Invoking the simplifying conditions which arise at the stagnation line along with the assumption that interface temperature is a constant in equations 2.29-2.32, 2.36-2.40, and 2.43 results in a set of nonlinear ordinary differential equations with respect to time which governs the transient responses in the vicinity of the stagnation line. Momentum conservation for the vapor layer given by equation 2.29 simplifies at the stagnation line to give

$$\frac{\partial \bar{\delta}_v}{\partial \bar{t}} \text{Sr}_w \left[\frac{1}{2} (\bar{u}_{vi} + \bar{v}_p) - \bar{u}_I \right] + \left[\frac{1}{2} \text{Sr}_w \frac{\partial \bar{u}_{vi}}{\partial \bar{t}} + \frac{\partial \bar{u}_{vi}}{\partial \bar{x}} \left(\frac{1}{3} \bar{v}_p + \frac{2}{3} \bar{u}_{vi} - \frac{1}{2} \bar{u}_I \right) \right] \bar{\delta}_v = 0.$$

(3.1)

Energy conservation for the vapor layer, equation 2.30, becomes

$$\frac{\partial \bar{\delta}_v}{\partial t} \left(-\frac{1}{2} \text{Sr}_w \right) - \frac{1}{6} \frac{\partial \bar{u}_{vi}}{\partial \bar{x}} \bar{\delta}_v = 0. \quad (3.2)$$

Similarly, equations 2.31 and 2.32 for momentum and energy conservation in the liquid layer can be simplified at the stagnation line to give equations 3.3 and 3.4, respectively.

$$\begin{aligned} & \frac{\partial \bar{\delta}}{\partial t} \text{Sr}_w \left(\frac{1}{3} \bar{u}_{II} \right) + \left(\frac{1}{3} \text{Sr}_w \frac{\partial \bar{u}_{II}}{\partial t} + \frac{2}{5} \bar{u}_{II} \frac{\partial \bar{u}_{II}}{\partial \bar{x}} + \frac{4}{15} \bar{u}_{II} \frac{\partial \bar{u}_{\infty}}{\partial \bar{x}} \right) \bar{\delta} + \\ & \frac{\rho_v}{\rho_l} \left(\text{Sr}_w \frac{\partial \bar{\delta}_v}{\partial t} + \frac{1}{2} \frac{\partial \bar{u}_{vi}}{\partial \bar{x}} \bar{\delta}_v \right) \bar{u}_I - \frac{2}{\text{Re}_{wl}} \bar{u}_{II} \bar{\delta}^{-1} = 0. \end{aligned} \quad (3.3)$$

$$\begin{aligned} & \frac{\partial \bar{\Delta}}{\partial t} \left(\frac{1}{3} \text{Sr}_w \right) + \bar{\Delta}^3 \left[\frac{1}{30} \left(\frac{\partial \bar{u}_{II}}{\partial \bar{x}} - \frac{\partial \bar{u}_{\infty}}{\partial \bar{x}} \right) \bar{\delta}^{-2} \right] + \bar{\Delta}^2 \left[-\frac{1}{6} \left(\frac{\partial \bar{u}_{II}}{\partial \bar{x}} - \frac{\partial \bar{u}_{\infty}}{\partial \bar{x}} \right) \bar{\delta}^{-1} \right] + \\ & \bar{\Delta} \left(\frac{1}{3} \frac{\partial \bar{u}_{II}}{\partial \bar{x}} \right) + \left[-2 \frac{1}{\text{Re}_{wl} \text{Pr}_l} \right] \bar{\Delta}^{-1} + \frac{\rho_v}{\rho_l} \left(\text{Sr}_w \frac{\partial \bar{\delta}_v}{\partial t} + \frac{1}{2} \frac{\partial \bar{u}_{vi}}{\partial \bar{x}} \bar{\delta}_v \right) = 0. \end{aligned} \quad (3.4)$$

At the stagnation line, equation 2.36 for conservation of mass at the liquid-vapor interface becomes

$$\bar{v}_{II} = \left(1 - \frac{\rho_v}{\rho_l} \right) \text{Sr}_w \frac{\partial \bar{\delta}_v}{\partial t} + \frac{\rho_v}{\rho_l} \bar{v}_{vi} \quad (3.5)$$

while the force and momentum balance in the direction of the normal to the interface, equation 2.37, simplifies to

$$\text{Sr}_w \frac{\partial \bar{\delta}_v}{\partial t} \left(\frac{\rho_v}{\rho_l} \bar{v}_{vi} - \bar{v}_{II} \right) + \bar{v}_{II}^2 - \frac{\rho_v}{\rho_l} \bar{v}_{vi}^2 = \bar{\sigma}_s \frac{\partial^2 \bar{\delta}_v}{\partial \bar{x}^2} + \frac{1}{2} \left(\frac{\rho_v}{\rho_l} \bar{p}_v - \bar{p}_l \right). \quad (3.6)$$

Upon invoking the symmetry conditions at the stagnation line, the no-slip relationship at the liquid-vapor interface given by equation 2.38 reduces to

$$\bar{u}_{II} = \bar{u}_{vI} \quad (3.7)$$

and the interfacial shear stress balance given by equation 2.39 becomes

$$\left(\bar{u}_{vI} - \bar{v}_p\right)\bar{\delta}_v^{-1} + 2\frac{\mu_l}{\mu_v}\bar{u}_{II}\bar{\delta}^{-1} = 0. \quad (3.8)$$

Equation 2.40 for the balance of thermal energy at the liquid-vapor interface simplifies to

$$-\frac{1}{Ja}Pr_v Re_{ww} \left(\bar{v}_{vI} - Sr_w \frac{\partial \bar{\delta}_v}{\partial \bar{t}} \right) = -\bar{T}_{vI}\bar{\delta}_v^{-1} - \frac{wh_R}{k_v}\bar{T}_{vI} - 2\beta\frac{\mu_l}{\mu_v}\bar{T}_{II}\bar{\Delta}^{-1}. \quad (3.9)$$

At the stagnation line, equation 2.43 gives

$$\frac{\partial^2 \bar{\delta}_v}{\partial \bar{x}^2} = -\left(\frac{\partial \bar{u}_{II}}{\partial \bar{x}} - \frac{\partial \bar{u}_{vI}}{\partial \bar{x}} \right) \frac{1}{(\bar{v}_{II} - \bar{v}_{vI})}. \quad (3.10)$$

Equations 3.1-3.10 can be combined to produce a set of three nonlinear ordinary differential equations which govern the transient response of the boundary layers $\bar{\delta}_v$, $\bar{\delta}$, and $\bar{\Delta}$ in the vicinity of the stagnation line. The differential control volumes used to develop the relationships for conservation of mass, momentum and energy at the liquid-vapor interface (Figures 2.2, 2.3, and 2.5) indicate that the velocity of the liquid at the interface, the velocity of the vapor at the interface, and the velocity of the liquid-vapor interface itself are separate quantities. Because the x-components of liquid and vapor velocity at the interface are equal at the stagnation line according to equation 3.7, and the liquid-vapor interface lies between the liquid and vapor layers, equation 3.7 may be generalized to also include the x-component of interface velocity \bar{u}_I .

$$\bar{u}_{II} = \bar{u}_I = \bar{u}_{vI}. \quad (3.11)$$

Because \bar{u}_{II} , \bar{u}_I , and \bar{u}_{vI} are always equal at the stagnation line, their time derivatives are also equal at the stagnation line.

$$\frac{\partial \bar{u}_{II}}{\partial \bar{t}} = \frac{\partial \bar{u}_I}{\partial \bar{t}} = \frac{\partial \bar{u}_{vI}}{\partial \bar{t}}. \quad (3.12)$$

However, \bar{u}_{II} and \bar{u}_{vI} are constrained to be equal only at the stagnation line where there is symmetry in the flow. Away from the stagnation line, \bar{u}_{II} and \bar{u}_{vI} may vary independently. Therefore, the gradients $\partial \bar{u}_{II} / \partial \bar{x}$ and $\partial \bar{u}_{vI} / \partial \bar{x}$ at the stagnation line are not assumed to be equal. Upon invoking equations 3.11 and 3.12, there is no need to distinguish between the terms \bar{u}_{II} , \bar{u}_I , and \bar{u}_{vI} . Therefore, the x-components of velocity in the vapor and the liquid layers at the liquid-vapor interface as well as the x-component of the velocity of the liquid-vapor interface itself can be denoted as \bar{u}_I . Similarly, the time derivatives of \bar{u}_{II} , \bar{u}_I , and \bar{u}_{vI} are all equal and can be denoted as $\partial \bar{u}_I / \partial \bar{t}$.

In order to develop a resulting set of three nonlinear ordinary differential equations which depend only on the dependent variables $\bar{\delta}_v$, $\bar{\delta}$, and $\bar{\Delta}$, all other dependent variables which appear in equations 3.1-3.10 must be expressed in terms of these four variables. For example, the nonlinear ordinary differential equation for $\partial \bar{\delta}_v / \partial \bar{t}$ will be developed from equation 3.1 and the variables \bar{u}_I , $\partial \bar{u}_I / \partial \bar{t}$, and $\partial \bar{u}_{vI} / \partial \bar{x}$ which appear in equation 3.1 will be expressed in terms of the variables $\bar{\delta}_v$, $\bar{\delta}$, $\bar{\Delta}$, and \bar{t} . Observing the equalities established by equations 3.11 and 3.12, equations 3.1 and 3.2 can be combined and rearranged to develop expressions for $\partial \bar{\delta}_v / \partial \bar{t}$ and $\partial \bar{u}_{vI} / \partial \bar{x}$.

$$\frac{\partial \bar{\delta}_v}{\partial \bar{t}} = \frac{1}{(\bar{v}_p + 2\bar{u}_I)} \frac{\partial \bar{u}_I}{\partial \bar{t}} \bar{\delta}_v. \quad (3.13)$$

$$\frac{\partial \bar{u}_{vI}}{\partial \bar{x}} = -3\text{Sr}_w \frac{1}{(\bar{v}_p + 2\bar{u}_I)} \frac{\partial \bar{u}_I}{\partial \bar{t}}. \quad (3.14)$$

The nonlinear ordinary differential equations for $\partial \bar{\delta}/\partial \bar{t}$ and $\partial \bar{\Delta}/\partial \bar{t}$ will be developed from equations 3.3 and 3.4, respectively. Equations 3.5, 3.9, and 3.10 can be used to eliminate the variables \bar{v}_{II} , \bar{v}_{vI} , and $\partial^2 \bar{\delta}_v / \partial \bar{x}^2$, respectively, as necessary. Using equations 3.5, 3.9, and 3.10 in equation 3.6 results in an expression for the gradient $\partial \bar{u}_{II} / \partial \bar{x}$.

$$\begin{aligned} \frac{\partial \bar{u}_{II}}{\partial \bar{x}} = & \frac{\partial \bar{u}_{vI}}{\partial \bar{x}} + \frac{1}{\bar{\sigma}_s} \left(\frac{\rho_v}{\rho_1} - 1 \right) \frac{\text{Ja}}{\text{Pr}_v \text{Re}_{ww}} \left(\frac{\bar{T}_{vI}}{\bar{\delta}_v} + \frac{wh_R}{k_v} \bar{T}_{vI} + 2\beta \frac{\mu_1}{\mu_v} \bar{T}_{II} \bar{\Delta}^{-1} \right) \left[\frac{1}{2} \left(\frac{\rho_v}{\rho_1} \bar{p}_v - \bar{p}_1 \right) - \right. \\ & \left. \left(1 - \frac{\rho_1}{\rho_v} \right) \left(\frac{\text{Ja}}{\text{Pr}_v \text{Re}_{ww}} \frac{\rho_v}{\rho_1} \right)^2 \left(\frac{\bar{T}_{vI}}{\bar{\delta}_v} + \frac{wh_R}{k_v} \bar{T}_{vI} + 2\beta \frac{\mu_1}{\mu_v} \bar{T}_{II} \bar{\Delta}^{-1} \right)^2 \right]. \end{aligned} \quad (3.15)$$

The expression for \bar{u}_I is obtained by using equation 3.11 in equation 3.8 which gives

$$\bar{u}_I = \frac{\bar{v}_p}{\left(1 + 2 \frac{\mu_1}{\mu_v} \frac{\bar{\delta}_v}{\bar{\delta}} \right)}. \quad (3.16)$$

It is evident from equations 3.13 and 3.14 that an expression for $\partial \bar{u}_I / \partial \bar{t}$ is needed. This expression can be obtained by differentiating with respect to time the shear stress balance at the interface given by equation 2.39. Invoking the symmetry conditions which apply at the stagnation line, the derivative with respect to time of equation 2.39 gives

$$\frac{\partial \bar{u}_I}{\partial \bar{t}} = \left[(\bar{u}_I - \bar{v}_p) \frac{1}{\bar{\delta}_v^2} \frac{\partial \bar{\delta}_v}{\partial \bar{t}} + 2 \frac{\mu_1}{\mu_v} \bar{u}_I \frac{1}{\bar{\delta}^2} \frac{\partial \bar{\delta}}{\partial \bar{t}} \right] \left(\frac{1}{\bar{\delta}_v} + 2 \frac{\mu_1}{\mu_v} \frac{1}{\bar{\delta}} \right)^{-1} \quad (3.17)$$

The set of three nonlinear ordinary differential equations which depend only on the dependent variables $\bar{\delta}_v$, $\bar{\delta}$, and $\bar{\Delta}$ are given by equations 3.13, 3.3, and 3.4 upon substituting for the terms $\partial \bar{u}_{vI} / \partial \bar{x}$, $\partial \bar{u}_{II} / \partial \bar{x}$, \bar{u}_I , and $\partial \bar{u}_I / \partial \bar{t}$ with the expressions above. Observing the equalities established by equations 3.11 and 3.12, equations 3.3 and 3.4 can be expressed as

$$\frac{\partial \bar{\delta}}{\partial \bar{t}} = \left[-\frac{1}{\bar{u}_I} \frac{\partial \bar{u}_I}{\partial \bar{t}} - \frac{4}{5} \frac{1}{\text{Sr}_w} \frac{\partial \bar{u}_\infty}{\partial \bar{x}} - \frac{6}{5} \frac{1}{\text{Sr}_w} \frac{\partial \bar{u}_{II}}{\partial \bar{x}} \right] \bar{\delta} + \frac{3}{2} \frac{\rho_v}{\rho_l} \frac{\partial \bar{\delta}_v}{\partial \bar{t}} + 6 \frac{1}{\text{Sr}_w \text{Re}_{wl}} \bar{\delta}^{-1} \quad (3.18)$$

and

$$\begin{aligned} \frac{\partial \bar{\Delta}}{\partial \bar{t}} = & \frac{1}{\text{Sr}_w} \frac{\partial \bar{u}_{II}}{\partial \bar{x}} \left(-\frac{1}{10} \frac{\bar{\Delta}^3}{\bar{\delta}^2} + \frac{1}{2} \frac{\bar{\Delta}^2}{\bar{\delta}} - \bar{\Delta} \right) + \frac{1}{\text{Sr}_w} \frac{\partial \bar{u}_\infty}{\partial \bar{x}} \left(\frac{1}{10} \frac{\bar{\Delta}^3}{\bar{\delta}^2} - \frac{1}{2} \frac{\bar{\Delta}^2}{\bar{\delta}} \right) + \\ & 6 \frac{1}{\text{Sr}_w \text{Re}_{wl} \text{Pr}_l} \bar{\Delta}^{-1} + \frac{3}{2} \frac{\rho_v}{\rho_l} \frac{\partial \bar{\delta}_v}{\partial \bar{t}} \end{aligned} \quad (3.19)$$

respectively. Upon substituting for $\partial \bar{u}_{vI} / \partial \bar{x}$, $\partial \bar{u}_{II} / \partial \bar{x}$, \bar{u}_I , and $\partial \bar{u}_I / \partial \bar{t}$ from equations 3.14, 3.15, 3.16, and 3.17, respectively, equations 3.13, 3.18, and 3.19 form the set of three nonlinear ordinary differential equations which govern the transient response of the vapor layer and the velocity and thermal boundary layers in the liquid in the vicinity of the stagnation line in terms of the dimensionless variables $\bar{\delta}_v$, $\bar{\delta}$, and $\bar{\Delta}$. Because the governing equations were developed to include the influence of surface motion, the model depends on the surface motion parameter \bar{v}_p . As a consequence, the condition $\bar{v}_p \neq 0$ must be observed or a singularity will result upon using equation 3.16. If subsequent

studies investigate boundary layer behavior away from the stagnation line using the governing equations which include spatial dependency, another singularity point may arise. This singularity may be encountered as the interface velocity approaches the velocity of the plate at locations away from the stagnation line.

An automatic step size Runge-Kutta-Fehlberg integration method was implemented within the commercial software package MATLAB (Natick, Massachusetts) to obtain numerical solutions to the three ordinary, nonlinear differential equations 3.13, 3.18, and 3.19 for $\bar{\delta}_v$, $\bar{\delta}$, and $\bar{\Delta}$. An automatic step size was used where larger steps are taken when the solution is changing more slowly. A fourth- and fifth-order pair of formulas was used for higher accuracy. In obtaining numerical results for model verification, a tolerance of 10^{-6} was specified for the differential equation solver. This tolerance means that time steps are successively halved until the absolute error between successive computations is within 10^{-6} . At this tolerance and lower, the boundary layers converged to the same steady state response for the case of no external forcing. The boundary layer thicknesses approached steady state values in an asymptotic fashion with steady state being established when $\bar{\delta}_v$, $\bar{\delta}$, and $\bar{\Delta}$ were no longer changing within an absolute error of 10^{-6} . In obtaining numerical solutions for forced response cases, a tolerance of 10^{-9} was specified for the differential equation solver. This tolerance means that time steps are successively halved until the absolute error between successive computations is within 10^{-9} . At this tolerance and lower, the boundary layers converged to the same forced response as determined by visual comparison of the output plots. Initial values for the forced response cases were given by the steady state values of $\bar{\delta}_v$, $\bar{\delta}$, and $\bar{\Delta}$ for the condition of no flow pulsation.

These initial values were determined by allowing the transient model to run to steady state with steady state being established when $\bar{\delta}_v$, $\bar{\delta}$, and $\bar{\Delta}$ were no longer changing within an absolute error of 10^{-9} .

Liquid-Vapor Interface Shape in the Vicinity of the Stagnation Line

Upon solving the governing equations for the dimensionless boundary layer thicknesses $\bar{\delta}_v$, $\bar{\delta}$, and $\bar{\Delta}$ at the stagnation line ($\bar{x} = 0$), it is possible to construct the shape of the liquid-vapor interface in the vicinity of the stagnation line. A second order polynomial $y(x)$ is assumed to model the liquid-vapor interface at an instant in time. The interface profile is governed by the symmetry in the dividing flow about the stagnation streamline. At the stagnation line ($x = 0$),

$$y = \delta_v \quad (3.20a)$$

and

$$dy/dx = d\delta_v/dx = 0. \quad (3.20b)$$

In addition, the curvature of the interface $d^2y/dx^2 = d^2\delta_v/dx^2$ is known at $x = 0$ from equation 3.10. Based on these three conditions, the resulting dimensionless liquid-vapor interface in the vicinity of the stagnation line at an instant in time is given by

$$\bar{\delta}_v(\bar{x}) = \frac{1}{2} \left(\left. \frac{d^2\bar{\delta}_v}{d\bar{x}^2} \right|_{\bar{x}=0} \right) \bar{x}^2 + \left(\bar{\delta}_v \Big|_{\bar{x}=0} \right). \quad (3.21)$$

Liquid Layer Model Verification

The liquid boundary layer response without flow pulsation was verified by comparison under steady state conditions to a known similarity solution for a two-dimensional

stagnation flow. The ratio $Nu/Re^{1/2}$ for a single-phase stagnation flow with constant free stream and wall temperature is tabulated by Evans (1962). This data was used as the basis to verify the current model. In order to solve equations 3.13, 3.18, and 3.19 to approximate a single-phase flow, several assumptions had to be made in specifying the input parameters. First, each vapor property was assigned the same value as the corresponding liquid property. Dimensionless interfacial tension was made very small such that the interface was passive. Radiation across the vapor layer was set to zero by specifying $wh_R/k_v = 0$. The influence of the vapor layer can be diminished by modeling it as having a low thermal resistance. Therefore, the difference between plate and interface temperatures was decreased to 0.1 °C. The comparison was run for a liquid free stream temperature of 20 °C, an interface temperature of 100 °C, and a plate temperature of 100.1 °C.

Equations 3.13, 3.18, and 3.19 model the transient boundary layer response of $\bar{\delta}_v$, $\bar{\delta}$, and $\bar{\Delta}$. These transient equations are used to determine a steady state response by specifying approximate initial conditions and then allowing the model to run to steady state. To approximate the single-phase case, the initial vapor layer thickness was made sufficiently small such that it had negligible influence on the response of the liquid boundary layers. The initial values for the liquid thermal and velocity boundary layer thicknesses were determined from the steady stagnation flow solution for Hiemenz flow given by (Schlichting, 1979)

$$\delta = 2.4 \sqrt{\frac{\mu/\rho}{C}} \quad (3.22)$$

Given δ from equation 3.22, Δ can be determined from equation 3.23.

$$\frac{\delta}{\Delta} = \text{Pr}^{1/3}. \quad (3.23)$$

The heat transfer coefficient for the single-phase case can be calculated by

$$h = \frac{-k_1 \left. \frac{\partial T_1}{\partial y_1} \right|_{y_1=0}}{(T_p - T_\infty)} = \frac{2k_1}{\Delta}. \quad (3.24)$$

The calculated values of $\text{Nu}/\text{Re}^{1/2}$, where $\text{Nu} = hx/k$ and $\text{Re} = (Cx^2\rho/\mu)^{1/2}$, were determined to be within 0.9-3.8% of those obtained from the similarity solutions tabulated by Evans (1962) for a two-dimensional stagnation flow for $1.0 < \text{Pr} < 10.0$. These values are listed in Table 3.1.

Table 3.1. Comparison of model predictions of $\text{Nu}/\text{Re}^{1/2}$ to those of a similarity solution for two-dimensional stagnation flow.

	Pr		
	1.0	5.0	10.0
Evans (1962)	0.570	1.043	1.344
Current Model	0.565	1.014	1.293

Vapor Layer Model Verification

The vapor layer response without flow pulsation was verified by comparison under steady state conditions to a known theoretical correlation for experimental data for forced convection film boiling heat transfer from a horizontal cylinder in a subcooled cross-flow.

Liu et al. (1992) compare their experimental data with the correlation of Epstein and Hauser (1980) for subcooled forced convection film boiling heat transfer from a cylinder. Epstein and Hauser's semi-theoretical correlation for flow rates $U > (gD)^{1/2}$ is given by

$$\beta_* \text{Nu}_v / (\text{Re}_l)^{1/2} = 2.5Z^4 \quad (3.25)$$

where $\text{Nu}_v = h_{co}D/k_v$, Re_l is the liquid flow Reynolds number given by $\text{Re}_l = UD\rho_l/\mu_l$, and Z is the nondimensional parameter given by

$$Z = 1/(27A_1) + (4/(3\pi))^2(B_1/A_1)^4. \quad (3.26)$$

The nondimensional parameters β_* , A_1 , and B_1 in the expression for Z are defined as:

$$\beta_* = \left[\left(\frac{\rho_v}{\rho_l} \right)^{1/2} \left(\frac{\mu_v/\rho_v}{\mu_l/\rho_l} \right) \right]^2. \quad (3.27)$$

$$A_1 = c_{pv}\Delta T_{sat}/(Pr_v L). \quad (3.28)$$

$$B_1 = \beta_*(k_l/k_v)[c_{pv}\Delta T_{sub}/(Pr_v L)]Pr_l^{1/2}. \quad (3.29)$$

The heat transfer coefficient h_{co} is the area-averaged film boiling heat transfer coefficient if there were no radiation heat transfer, D is the diameter of the cylinder heater, g is the acceleration due to gravity, and U is the liquid flow rate. The heater surface superheat is given by $\Delta T_{sat} = T_w - T_{sat}$, where T_w is the cylinder wall temperature and T_{sat} is saturation temperature. The liquid subcooling below saturation temperature is given by $\Delta T_{sub} = T_{sat} - T_l$, and L is the latent heat of vaporization.

Although the current model solution returns the local heat transfer coefficient in the vicinity of the stagnation line, available experimental data and equation 3.25 pertain to a heat transfer coefficient averaged over the entire cylinder surface. Therefore, the local

the vicinity of the stagnation line correlates well with the average heat transfer coefficient based on the entire surface of the cylinder as given by equation 3.25. The accuracy of the correlation given by equation 3.25 was investigated by Liu et al. (1992). The experimental data of Liu et al. (1992) has nearly the same slope as the correlation of equation 3.25, but the correlation predicts values that are higher than the experimental data. The maximum difference is 32% for a 3mm diameter cylinder in water. Thus, the model of this study returns Nusselt numbers that are in good agreement with experimental data.

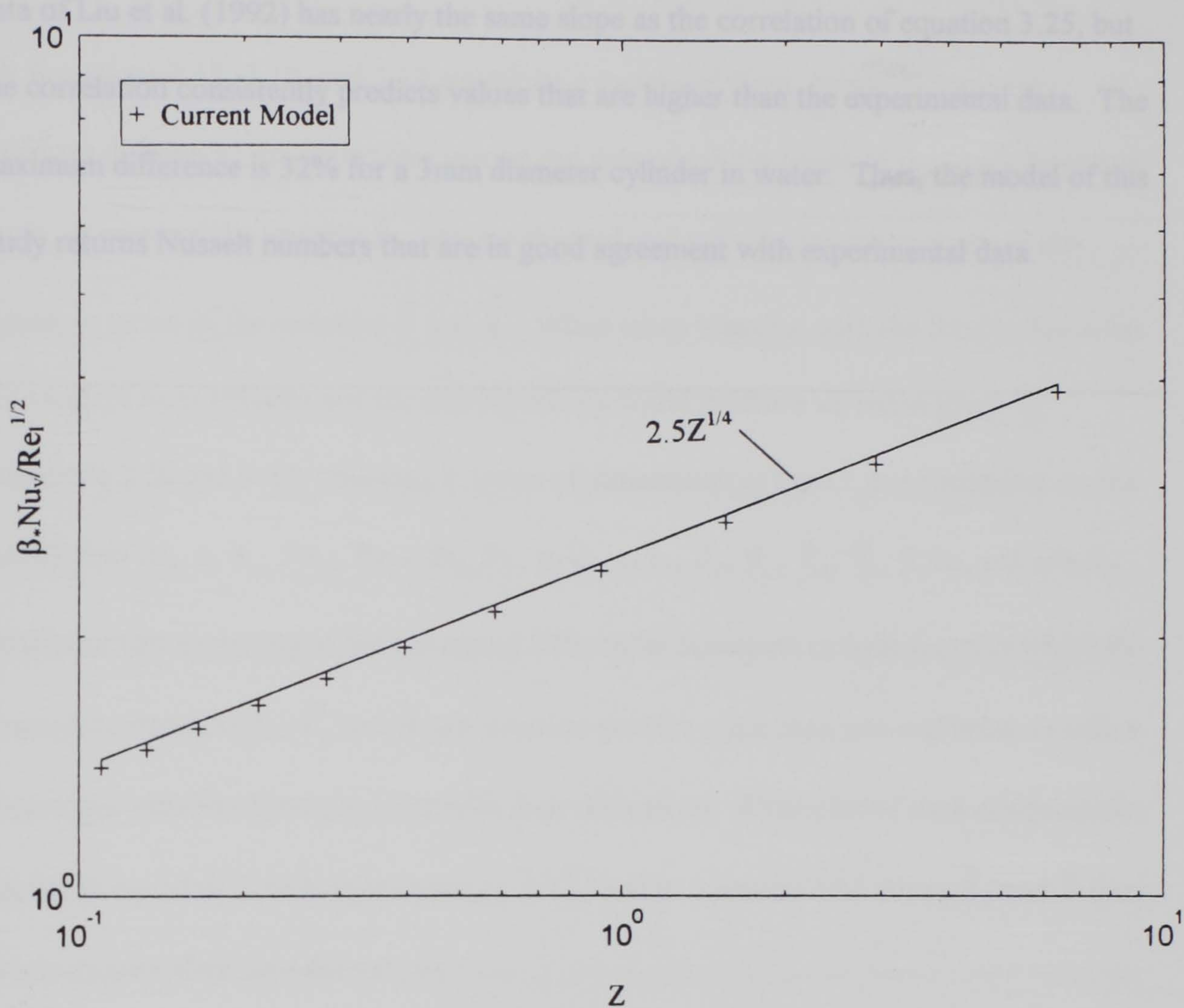


Figure 3.1. Comparison of predicted Nusselt numbers for film boiling with water with those given by Epstein and Hauser's correlation (equation 3.25) with $Re_{wl} = 1742$, $Re_{ww} = 8.4$, $Pr_l = 1.9$, $Pr_v = 1.0$, $\mu_l/\mu_v = 13.5$, $\rho_l/\rho_v = 2789$, $\bar{\sigma}_s = 0.6$, $\beta = 0.03$, $Ja = 0.5$, and $wh_R/k_v = 0$.

the vicinity of the stagnation line correlates well with the average heat transfer coefficient based on the entire surface of the cylinder as given by equation 3.25. The accuracy of the correlation given by equation 3.25 was investigated by Liu et al. (1992). The experimental data of Liu et al. (1992) has nearly the same slope as the correlation of equation 3.25, but the correlation consistently predicts values that are higher than the experimental data. The maximum difference is 32% for a 3mm diameter cylinder in water. Thus, the model of this study returns Nusselt numbers that are in good agreement with experimental data.

CHAPTER IV

RESULTS AND DISCUSSION

Equations 3.13, 3.18, and 3.19 constitute a system of three, coupled, nonlinear, ordinary differential equations that govern the dynamical responses of the vapor boundary layer, in terms of the variable $\bar{\delta}_v$, and the thermal and velocity boundary layers in the liquid, in terms of the variables $\bar{\delta}$ and $\bar{\Delta}$. When taken together with the forcing functions for incident flow velocity and the corresponding liquid pressure variation given by equations 2.50 and 2.63, solutions in terms of dimensionless time \bar{t} are dependent on the parameters Sr_w , ϵ , \bar{v}_p , Re_{wl} , Re_{ww} , Pr_l , Pr_v , μ_l/μ_v , ρ_l/ρ_v , $\bar{\sigma}_s$, \bar{p}_v , \bar{T}_{vl} , \bar{T}_{ll} , β , Ja , and wh_R/k_v . Nonlinearities appearing in the governing differential equations include terms in which the dependent variables $\bar{\delta}_v$, $\bar{\delta}$, and $\bar{\Delta}$ are raised to powers other than one and terms in which dependent variables form products with their derivatives. Examples of such nonlinearities appear in equation 3.19 in terms such as $\bar{\Delta}^3/\bar{\delta}^2$ and in equation 3.17 where $\bar{\delta}_v$ and $\bar{\delta}$ form products with their time derivatives.

Because this model retains nonlinear terms, it is capable of investigating distinctive phenomena associated with the complex responses of nonlinear systems (Moon, 1992). For example, nonlinear behavior implies the potential for multiple equilibrium states and the possibility of periodic solutions with subharmonic and superharmonic frequency components. Other nonlinear phenomena which may be discovered in the present model include quasiperiodic oscillations in response to periodic inputs. The possibility of self-excited oscillations can also be investigated. Frequency locking in response to a periodic

driving force, another well known phenomena in nonlinear oscillations, could also be investigated. Retaining nonlinear terms in the current model allows many aspects of boundary layer response to be investigated which would not be possible in a study based on linearizations.

The purpose of the results presented in this study is to demonstrate the model's performance and to suggest how it may be used in subsequent studies. A parametric study is not performed. The effect of flow pulsations, interfacial tension, and radiation on the stability of the vapor layer will be briefly investigated for one specific condition that roughly pertains to metals cooling.

The responses of equations 3.13, 3.18, and 3.19 with no external forcing can be used to establish a set of steady state boundary layer thicknesses, $\bar{\delta}_v$, $\bar{\delta}$, and $\bar{\Delta}$, for a given set of parameters. These steady state values are determined by allowing the model to pass through an initial transient beginning with prescribed estimates and then achieve steady state. However, the model does not predict a unique set of steady state boundary layer thicknesses, $\bar{\delta}_v$, $\bar{\delta}$, and $\bar{\Delta}$, based on a given set of parameters alone. Rather, the steady state response also depends on the initial values specified for $\bar{\delta}_v$, $\bar{\delta}$, and $\bar{\Delta}$. For example, given the same set of parameters, two different sets of initial values for $\bar{\delta}_v$, $\bar{\delta}$, and $\bar{\Delta}$ would result in two different steady states being achieved.

The occurrence of multiple steady states can be explained physically by considering the balance of thermal energy at the liquid-vapor interface (equation 2.22). In stable film boiling for a given parametric range, several different vapor layer thicknesses which satisfy the balance of thermal energy at the interface may be possible. Vapor layer thickness is

influenced by vaporization rate. A high rate of vaporization resulting in a relatively large vapor layer thickness is supported by a high rate of energy transfer to the interface by conduction and radiation. Likewise, a low vaporization rate resulting in a relatively thinner vapor layer is produced by the transfer of less energy to the interface. The interaction of all three boundary layers results in multiple combinations of boundary layer thicknesses which maintain the balance of thermal energy at the liquid-vapor interface.

However, there seems to be a certain range of initial conditions within which the model achieves a steady state response and outside that range, the model becomes unstable. Therefore, the model results are very dependent on the initial values specified for $\bar{\delta}_v$, $\bar{\delta}$, and $\bar{\Delta}$. Physically plausible initial values for $\bar{\delta}$ and $\bar{\Delta}$ which are consistent with a given parametric range can be determined from the Hiemenz flow solution given by equations 3.22 and 3.23. Similarly, an initial value for $\bar{\delta}_v$ which is consistent with a given parametric range can be determined from Epstein and Hauser's correlation given by equation 3.25. Because the data available for determining initial values of $\bar{\delta}_v$ is based on the stagnation flow of a cylinder in cross-flow, it was decided to present results of this study for this geometry.

The governing equations and boundary conditions of the current model were developed with the potential to investigate film boiling boundary layer behavior both spatially and temporally on a moving plate. Surface motion can significantly influence heat transfer in film boiling at regions away from the stagnation line, especially when surface speed greatly exceeds the liquid velocity. Thus, the model was developed to include the influence of the surface motion at regions away from the stagnation line. As a

consequence, the model depends on the surface motion parameter \bar{v}_p . In equation 3.16 $\bar{v}_p \neq 0$ or a singularity will result. However, a cylinder in cross-flow may not pertain to surface motion. Although surface motion can significantly influence heat transfer in film boiling at regions away from the stagnation line, surface motion has little influence on heat transfer near the stagnation line when surface temperature is constant (Zumbrunnen et al., 1989; Zumbrunnen et al., 1992). The current stagnation line model assumes a constant surface temperature. Therefore, heat transfer in this model is not expected to be significantly influenced by surface motion. This was investigated in the current model by varying \bar{v}_p from a value of 1 to $\bar{v}_p = 5$ for one specific condition. The same steady state response was predicted. On this basis, the initial value of $\bar{\delta}_v$ determined from Epstein and Hauser's correlation for a stationary surface is assumed to be a good approximation.

The present model assumes constant thermophysical properties. Film temperature T_f ($= (T_1 + T_2)/2$, where T_1 and T_2 are the temperatures across the boundary layer in the liquid or vapor) was used to estimate the values of thermophysical properties for the evaluation of parameters and the selection of parametric ranges. Boundary layer response was investigated for water with properties based on a free stream temperature of $T_\infty = 87$ °C, an interface saturation temperature of $T_s = 102$ °C, and a plate temperature of $T_p = 352$ °C. Results were determined for a cylinder diameter of 3mm and a flow velocity of 0.18 m/s. In order to move into a possibly more interesting parametric range, the Prandtl number of the liquid was taken to be $Pr_l = 4.0$ in order to emphasize the difference between the thermal and velocity boundary layers in the liquid. The actual liquid Prandtl number for the film temperature specified is about 2.0, which gives velocity and thermal

boundary layers in the liquid close to the same value. The value of \bar{v}_p is taken to be 1, whereby surface speed is equal to flow velocity. For a constant value of the interface temperature T_s , $\bar{T}_{vI} = -1$ and $\bar{T}_{II} = 1$. Other input parameters are given by $Re_{wl} = 1700$, $Re_{ww} = 15$, $Pr_v = 1.0$, $\mu_l/\mu_v = 20$, $\rho_l/\rho_v = 2200$, $\bar{\sigma}_s = 0.6$, $\beta = 0.03$, and $Ja = 0.2$. Although property values were based on film temperature in this study, it may be more appropriate to evaluate interfacial properties such as interfacial tension at the temperature of the interface.

The pressure imposed on the vapor boundary layer is an input parameter which must be determined. It is directly related to the pressure in the liquid boundary layer given by equation 2.63. A simplified version of equation 2.18 is used to approximate the pressure in the vapor boundary layer. For some phase change processes, the motion of the interface is limited by the heat transfer to or from it and the interface motion is usually relatively slow (Carey, 1992). For these conditions, the liquid and vapor momentum terms in equation 2.18 are very small. Therefore, pressure differences across the liquid-vapor interface arise principally from the curvature of the interface. This is used as a basis to approximate the value of pressure in the vapor boundary layer.

The pressure in the vapor layer is estimated by $p_v = p_l + \sigma_s/r_c$. In using this expression, radius of curvature is estimated equal to cylinder diameter and liquid pressure is specified at the time-averaged value. This expression is used in the current study only as a means to approximate a constant value for vapor pressure. In a physical system, p_v could change as r_c and p_l change according to equations 2.63 and 2.19, respectively. However, the limiting assumption of a constant value of p_v is necessary in the current study in order to obtain

closure in the system of equations under consideration. Physically, this restricts the model to smaller pulse amplitudes. The influence of interfacial tension on vapor pressure is included in the current model unlike the studies of Walsh and Wilson (1979) and Chappidi et al. (1991) which assumed $p_v = p_l$. Note that equation 2.18 without any simplification was used in developing the set of nonlinear partial differential equations which governs transient and spatial boundary layer response.

For the specified parametric condition, initial estimates of liquid layer velocity and thermal boundary layer thicknesses, $\bar{\delta}$ and $\bar{\Delta}$, were determined from the Hiemenz flow solution given by equations 3.22 and 3.23. Similarly, the initial estimate of vapor boundary layer thickness $\bar{\delta}_v$ was determined from Epstein & Hauser's correlation given by equation 3.25 for the specified parametric condition. These estimates were used in the present model as initial conditions to determine steady state values for the condition of no external forcing. These steady state values for the condition of no external forcing were used as initial conditions for the forced response cases which investigate the effects of flow pulsation. Two sets of initial values based on no external forcing were determined for the given parametric conditions for radiation parameter values of $wh_R/k_v = 0$ and $wh_R/k_v = 10$. The initial values of $\bar{\delta}_{v0} = 0.006500068$, $\bar{\delta}_0 = 0.057726632$, and $\bar{\Delta}_0 = 0.051433868$ correspond to the given parametric conditions for $wh_R/k_v = 0$. Likewise, for $wh_R/k_v = 10$, initial values are given by $\bar{\delta}_{v0} = 0.006561428$, $\bar{\delta}_0 = 0.063421017$, and $\bar{\Delta}_0 = 0.057488483$. With no external forcing, the steady state vapor layer thickness $\bar{\delta}_v$ with radiation is greater than the steady state vapor layer thickness with zero radiation as expected. The increased heat transfer due to radiation increases the thickness of the vapor

boundary layer because more liquid is vaporized. A thicker vapor layer and corresponding thermal resistance are required to establish thermal equilibrium.

Forced responses are presented for cases both with and without radiation for a forcing frequency of 10 Hz ($Sr_w = 0.1667$) with pulse amplitudes of 0.1, 0.2, and 0.3. The results are presented in terms of the instantaneous boundary layer thicknesses $\bar{\delta}_v$, $\bar{\delta}$, and $\bar{\Delta}$ normalized by their initial values $\bar{\delta}_{v0}$, $\bar{\delta}_0$, and $\bar{\Delta}_0$. Normalized Nu_* , defined as $Nu_* = Nu_v / Nu_{v0}$, is also presented to show the influence of the boundary layer dynamics on heat transfer.

First, the forced response without radiation will be considered. The boundary layer response for a pulse amplitude $\varepsilon = 0.1$ is shown in Figure 4.1a. Although flow pulsations are induced by sinusoidal forcing functions given by equations 2.50 and 2.63, the three boundary layers undergo non-sinusoidal oscillations due to the nonlinear content of equations 3.13, 3.18, and 3.19 as expected. The sinusoidal forcing functions specified by equations 2.50 and 2.63 begin pulsation with a zero slope. This zero slope facilitates a smooth transition from the initial condition as flow pulsation is imposed. As a result, a steady periodic boundary layer response is obtained after a small starting transient. When subject to flow pulsation for $\varepsilon = 0.1$, the oscillation of the liquid boundary layers $\bar{\delta}$ and $\bar{\Delta}$ reaches peaks of approximately 3 times their initial values. The response of the thermal boundary layer $\bar{\Delta}$ tends to lag behind the response of the velocity boundary layer $\bar{\delta}$. Physically, this behavior is expected because the velocity boundary layer responds directly to flow pulsation. Changes in the velocity boundary layer influence energy advection and these effects are reflected in the thermal boundary layer. In contrast, the minimum values

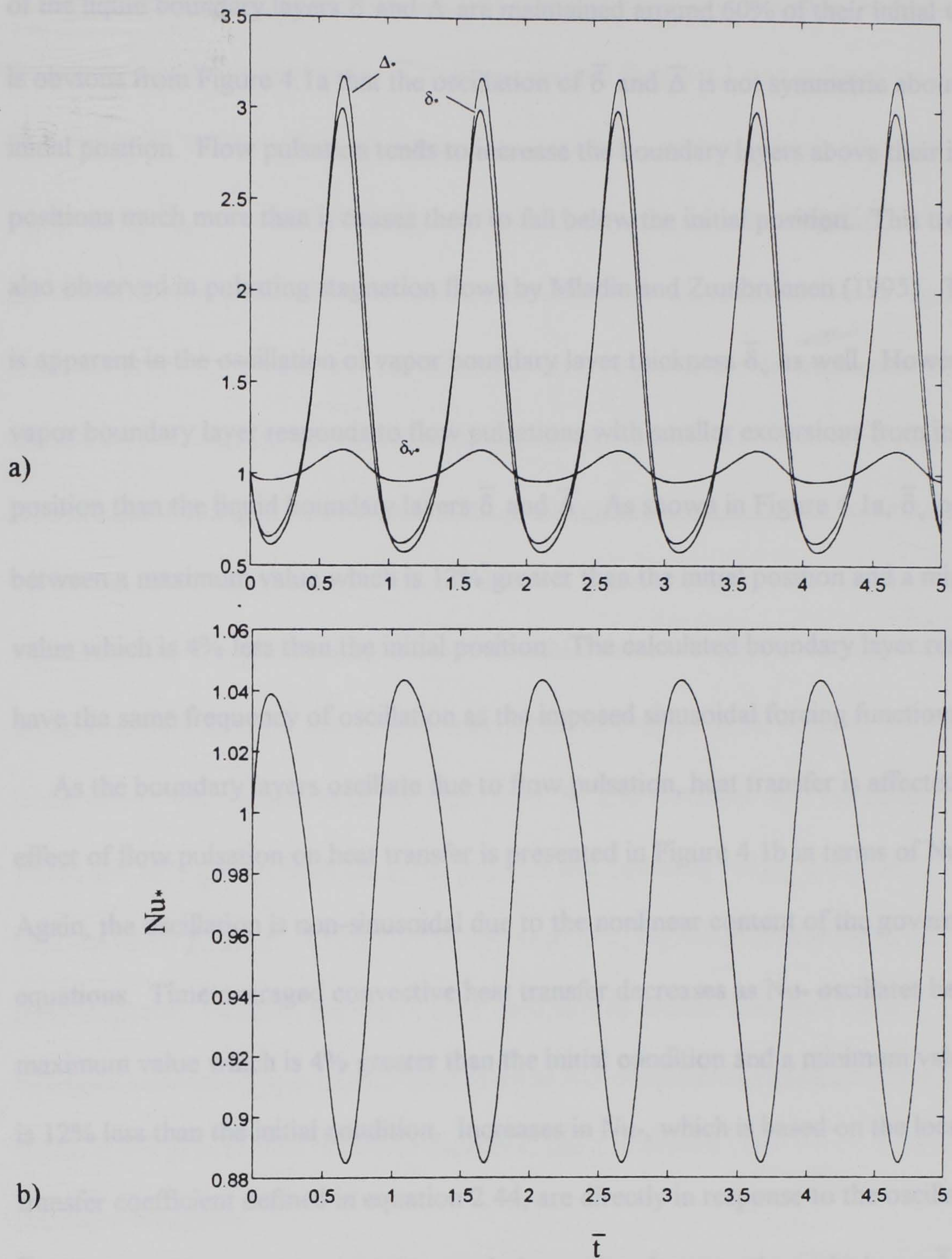


Figure 4.1. Response for sinusoidal flow pulsations: (a) normalized boundary layer thicknesses, (b) normalized Nusselt number with $Sr_w = 0.1667$, $\varepsilon = 0.1$, $\bar{v}_p = 1$, $Re_{wl} = 1700$, $Re_{ww} = 15$, $Pr_l = 4.0$, $Pr_v = 1.0$, $\mu_l/\mu_v = 20$, $\rho_l/\rho_v = 2200$, $\bar{\sigma}_s = 0.6$, $\beta = 0.03$, $Ja = 0.2$, $wh_R/k_v = 0$, $\bar{\delta}_{v0} = 0.006500068$, $\bar{\delta}_0 = 0.057726632$, and $\bar{\Delta}_0 = 0.051433868$.

of the liquid boundary layers $\bar{\delta}$ and $\bar{\Delta}$ are maintained around 60% of their initial values. It is obvious from Figure 4.1a that the oscillation of $\bar{\delta}$ and $\bar{\Delta}$ is not symmetric about the initial position. Flow pulsation tends to increase the boundary layers above their initial positions much more than it causes them to fall below the initial position. This trend was also observed in pulsating stagnation flows by Mladin and Zumbrunnen (1995). The trend is apparent in the oscillation of vapor boundary layer thickness $\bar{\delta}_v$ as well. However, the vapor boundary layer responds to flow pulsations with smaller excursions from its initial position than the liquid boundary layers $\bar{\delta}$ and $\bar{\Delta}$. As shown in Figure 4.1a, $\bar{\delta}_v$ oscillates between a maximum value which is 12% greater than the initial position and a minimum value which is 4% less than the initial position. The calculated boundary layer responses have the same frequency of oscillation as the imposed sinusoidal forcing functions.

As the boundary layers oscillate due to flow pulsation, heat transfer is affected. The effect of flow pulsation on heat transfer is presented in Figure 4.1b in terms of Nu_* . Again, the oscillation is non-sinusoidal due to the nonlinear content of the governing equations. Time-averaged convective heat transfer decreases as Nu_* oscillates between a maximum value which is 4% greater than the initial condition and a minimum value which is 12% less than the initial condition. Increases in Nu_* , which is based on the local heat transfer coefficient defined in equation 2.44, are directly in response to the oscillation of $\bar{\delta}_v$ below its initial position. As expected, decreasing the vapor layer thickness $\bar{\delta}_v$ improves heat transfer. Likewise, Nu_* falls below the initial value when $\bar{\delta}_v$ increases due to flow pulsation. An increase in vapor layer thickness hampers heat transfer as expected.

$\bar{\delta}$ and $\bar{\Delta}$ are maintained around 50% of their corresponding initial values. Although the

In order to investigate the influence of interfacial tension on boundary layer response, the interfacial tension parameter $\bar{\sigma}_s$ used to produce Figure 4.1 was reduced by 20% from $\bar{\sigma}_s = 0.6$ to $\bar{\sigma}_s = 0.48$. With all other parameters held constant, initial values for this case are given by $\bar{\delta}_{v_0} = 0.006776778$, $\bar{\delta}_0 = 0.086052238$, and $\bar{\Delta}_0 = 0.081337101$. Note that the decrease in interfacial tension for the case of no flow pulsation results in larger steady state values for $\bar{\delta}_v$, $\bar{\delta}$, and $\bar{\Delta}$. The boundary layer response for the decreased interfacial tension case is characterized by the same asymmetric oscillation observed in Figure 4.1a but with greater magnitudes of oscillation as shown in Figure 4.2. The maximum oscillation of the liquid boundary layers $\bar{\delta}$ and $\bar{\Delta}$ increased from values 3 times the initial value to peaks of approximately 6 times the initial value. Similarly, minimum values of the liquid boundary layers $\bar{\delta}$ and $\bar{\Delta}$ decreased from 60% of the initial value to 50% of the initial value. The oscillation of the vapor layer $\bar{\delta}_v$ also increases with maximum values which are 18% greater than the initial position and minimum values which are 8% less than the initial position. Thus, a 20 % decrease in $\bar{\sigma}_s$ significantly influences the boundary layer response. Notably, the vapor layer oscillates to smaller minimum values. Time-averaged convective heat transfer decreases as Nu^* oscillates between a maximum value which is 8% greater than the initial condition and a minimum value which is 18% less than the initial condition.

Similar trends are observed at the higher pulse amplitudes of $\varepsilon = 0.2$ and $\varepsilon = 0.3$ in Figures 4.3 and 4.4, respectively. A pulse amplitude of $\varepsilon = 0.2$ results in liquid thermal and velocity boundary layer peaks about 16 times the initial value. The minimum values of $\bar{\delta}$ and $\bar{\Delta}$ are maintained around 50% of their corresponding initial values. Although the

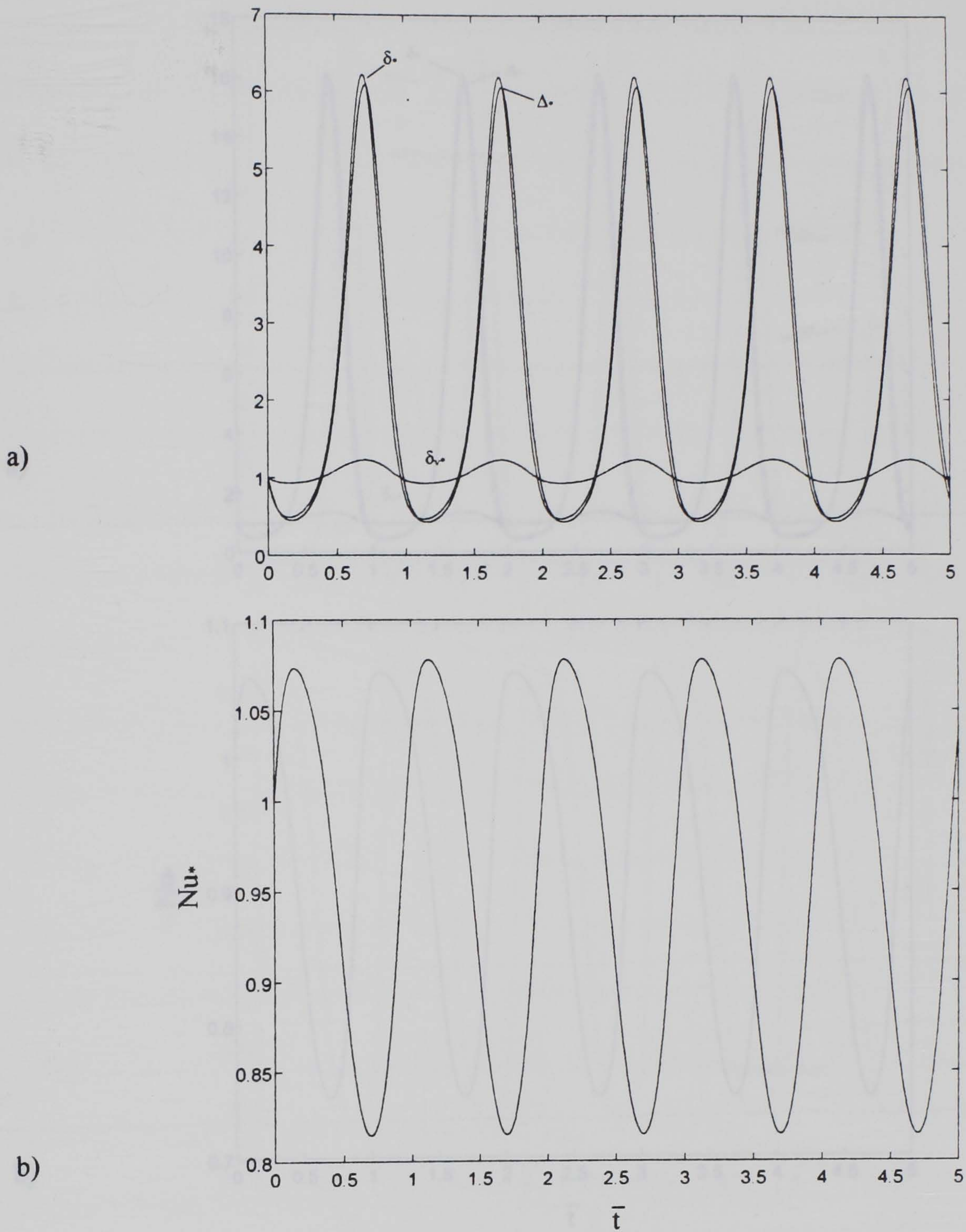


Figure 4.2. Response for sinusoidal flow pulsations: (a) normalized boundary layer thicknesses, (b) normalized Nusselt number with $Sr_w = 0.1667$, $\varepsilon = 0.1$, $\bar{v}_p = 1$, $Re_{wl} = 1700$, $Re_{ww} = 15$, $Pr_l = 4.0$, $Pr_v = 1.0$, $\mu_l/\mu_v = 20$, $\rho_l/\rho_v = 2200$, $\bar{\sigma}_s = 0.48$, $\beta = 0.03$, $Ja = 0.2$, $wh_R/k_v = 0$, $\bar{\delta}_{v0} = 0.006776778$, $\bar{\delta}_0 = 0.086052238$, and $\bar{\Delta}_0 = 0.081337101$.

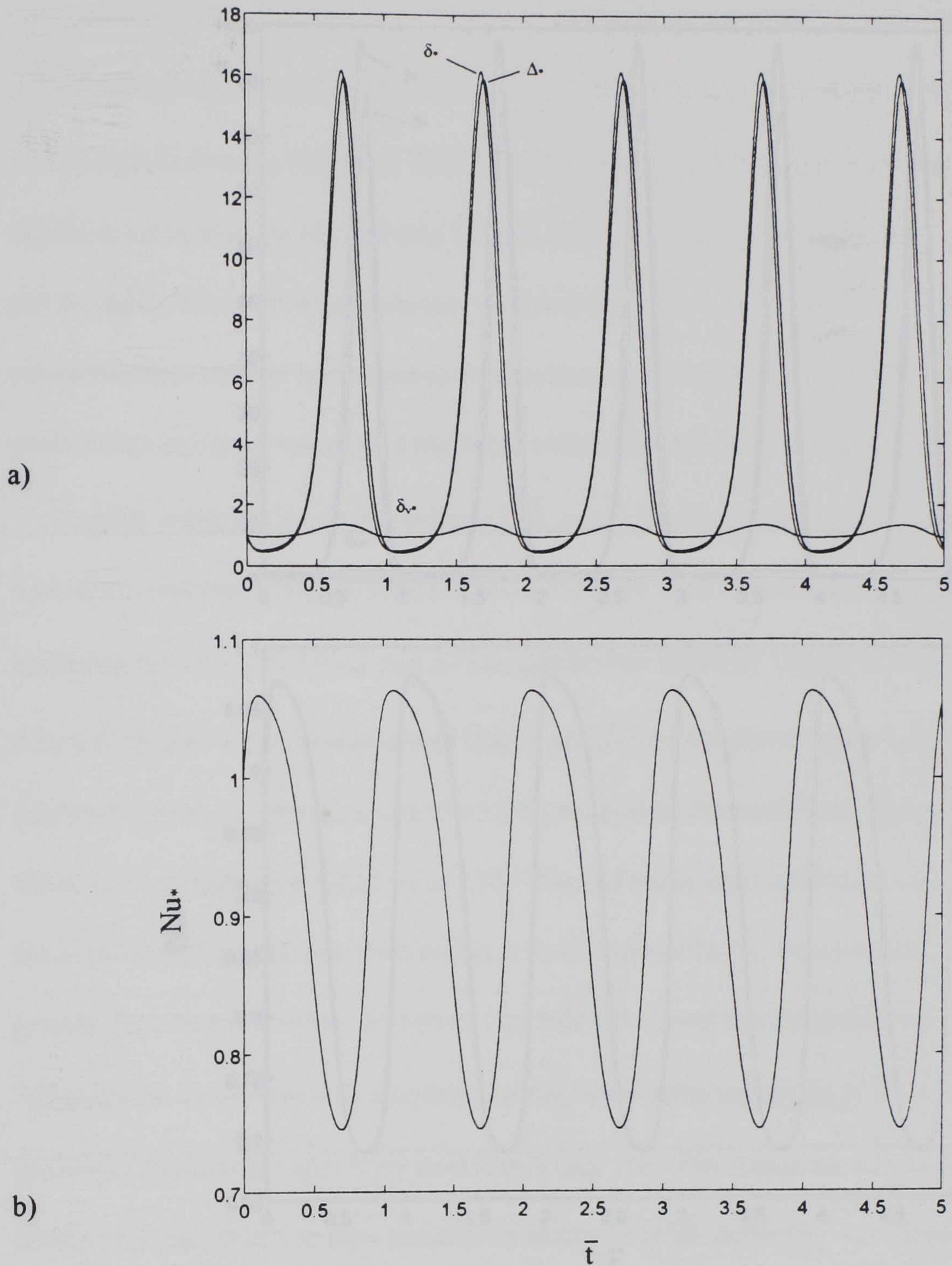


Figure 4.3. Response for sinusoidal flow pulsations: (a) normalized boundary layer thicknesses, (b) normalized Nusselt number with $Sr_w = 0.1667$, $\varepsilon = 0.2$, $\bar{v}_p = 1$, $Re_{wl} = 1700$, $Re_{ww} = 15$, $Pr_l = 4.0$, $Pr_v = 1.0$, $\mu_l/\mu_v = 20$, $\rho_l/\rho_v = 2200$, $\bar{\sigma}_s = 0.6$, $\beta = 0.03$, $Ja = 0.2$, $wh_R/k_v = 0$, $\bar{\delta}_{v0} = 0.006500068$, $\bar{\delta}_0 = 0.057726632$, and $\bar{\Delta}_0 = 0.051433868$.

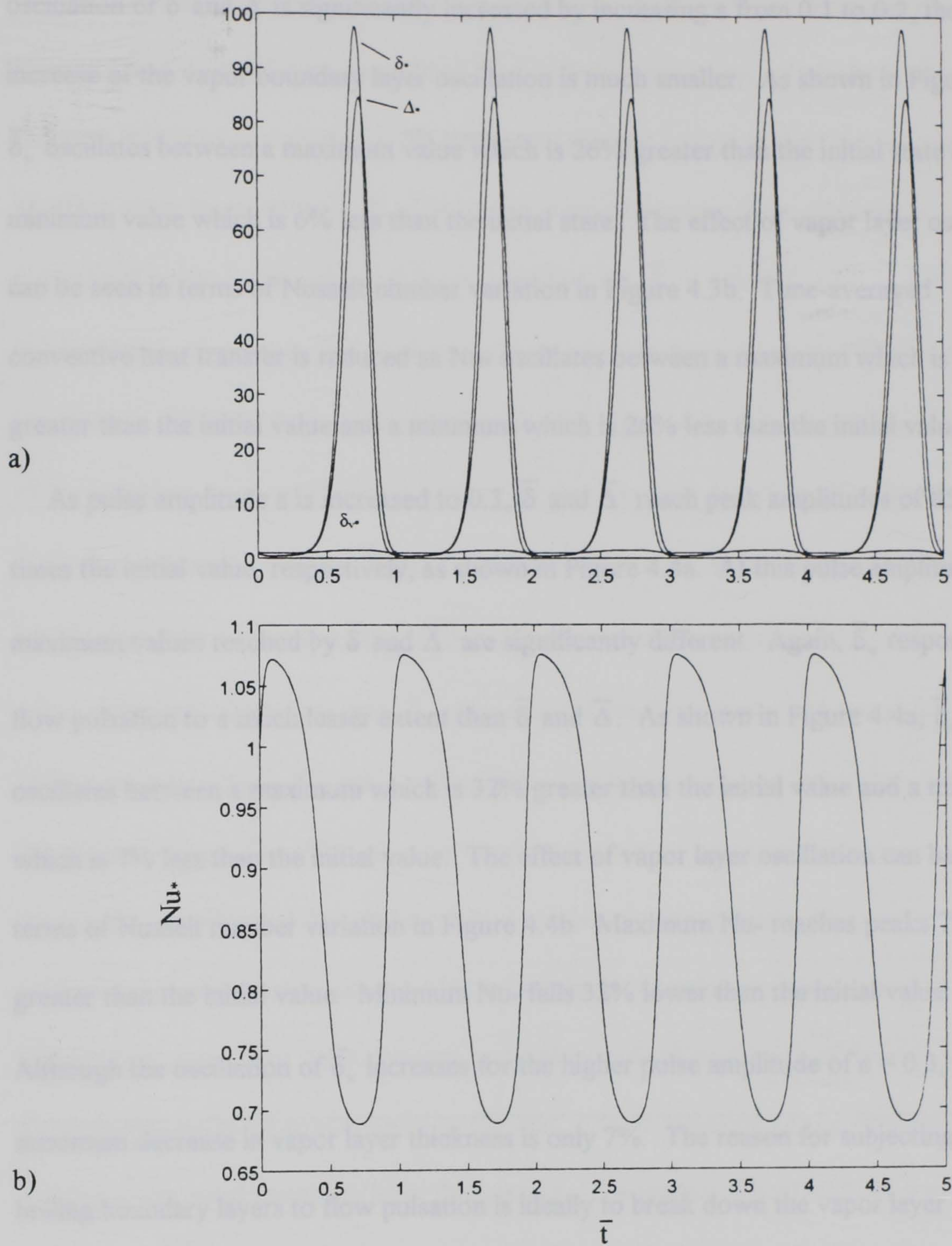


Figure 4.4. Response for sinusoidal flow pulsations: (a) normalized boundary layer thicknesses, (b) normalized Nusselt number with $Sr_w = 0.1667$, $\varepsilon = 0.3$, $\bar{v}_p = 1$, $Re_{wl} = 1700$, $Re_{ww} = 15$, $Pr_l = 4.0$, $Pr_v = 1.0$, $\mu_l/\mu_v = 20$, $\rho_l/\rho_v = 2200$, $\bar{\sigma}_s = 0.6$, $\beta = 0.03$, $Ja = 0.2$, $wh_R/k_v = 0$, $\bar{\delta}_{v0} = 0.006500068$, $\bar{\delta}_0 = 0.057726632$, and $\bar{\Delta}_0 = 0.051433868$.

oscillation of $\bar{\delta}$ and $\bar{\Delta}$ is significantly increased by increasing ε from 0.1 to 0.2, the increase of the vapor boundary layer oscillation is much smaller. As shown in Figure 4.3a, $\bar{\delta}_v$ oscillates between a maximum value which is 26% greater than the initial state and a minimum value which is 6% less than the initial state. The effect of vapor layer oscillation can be seen in terms of Nusselt number variation in Figure 4.3b. Time-averaged convective heat transfer is reduced as Nu_* oscillates between a maximum which is 6% greater than the initial value and a minimum which is 26% less than the initial value.

As pulse amplitude ε is increased to 0.3, $\bar{\delta}$ and $\bar{\Delta}$ reach peak amplitudes of 85 and 98 times the initial value, respectively, as shown in Figure 4.4a. At this pulse amplitude, the maximum values reached by $\bar{\delta}$ and $\bar{\Delta}$ are significantly different. Again, $\bar{\delta}_v$ responds to flow pulsation to a much lesser extent than $\bar{\delta}$ and $\bar{\Delta}$. As shown in Figure 4.4a, $\bar{\delta}_v$ oscillates between a maximum which is 32% greater than the initial value and a minimum which is 7% less than the initial value. The effect of vapor layer oscillation can be seen in terms of Nusselt number variation in Figure 4.4b. Maximum Nu_* reaches peaks 7% greater than the initial value. Minimum Nu_* falls 32% lower than the initial value.

Although the oscillation of $\bar{\delta}_v$ increases for the higher pulse amplitude of $\varepsilon = 0.3$, the maximum decrease in vapor layer thickness is only 7%. The reason for subjecting the film boiling boundary layers to flow pulsation is ideally to break down the vapor layer or decrease its time-averaged thickness and, therefore, increase heat transfer. The small 7% decrease and the 32% increase in vapor layer thickness do not imply a vapor layer breakdown for the parametric condition investigated. Moreover, convective heat transfer is less effective at higher pulse amplitudes.

To explore the influence of radiation on boundary layer response, the cases presented in Figures 4.1, 4.3, and 4.4 were repeated for a radiation parameter of $wh_R/k_v = 10$. Thus, radiative transport is activated in the balance of thermal energy at the liquid-vapor interface given by equation 2.22. The instantaneous boundary layer response is normalized by the initial values of $\bar{\delta}_{v_0} = 0.006561428$, $\bar{\delta}_0 = 0.063421017$, and $\bar{\Delta}_0 = 0.057488483$. Responses for a pulse amplitude of $\varepsilon = 0.1$ are shown in Figure 4.5a. A comparison of Figure 4.1a, without radiation, and Figure 4.5a reveals that the amplitude of the boundary layer oscillation is greater for the case with radiation. The liquid thermal and velocity boundary layers, $\bar{\delta}$ and $\bar{\Delta}$, reach maximums at approximately 3.75 times their initial value. The minimum values of $\bar{\delta}$ and $\bar{\Delta}$ are maintained around 60% of their initial value. The vapor boundary layer $\bar{\delta}_v$ responds to a smaller extent with maximum peaks 15% greater than the initial value and minimum peaks dropping no lower than 5% below the original value. The effect of vapor layer oscillation on heat transfer is presented in terms of Nu^* in Figure 4.5b. Although Nu^* reaches maximum peaks 5% greater than the original value, minimum peaks are 15% below the initial value and time-averaged heat transfer decreases. The slight increase in the amplitude of oscillation of the vapor layer for the case with radiation as compared to the case with no radiation can be explained by looking at the initial boundary layer thicknesses. The increased heat transfer due to radiation results in more energy being transported to the liquid layer. Therefore, more liquid is vaporized and the vapor layer becomes thicker. A thicker vapor layer is expected to be more unstable than a thinner layer due to the inherent instability of a dense liquid layer overriding a less dense vapor layer. Therefore, the vapor layer becomes more

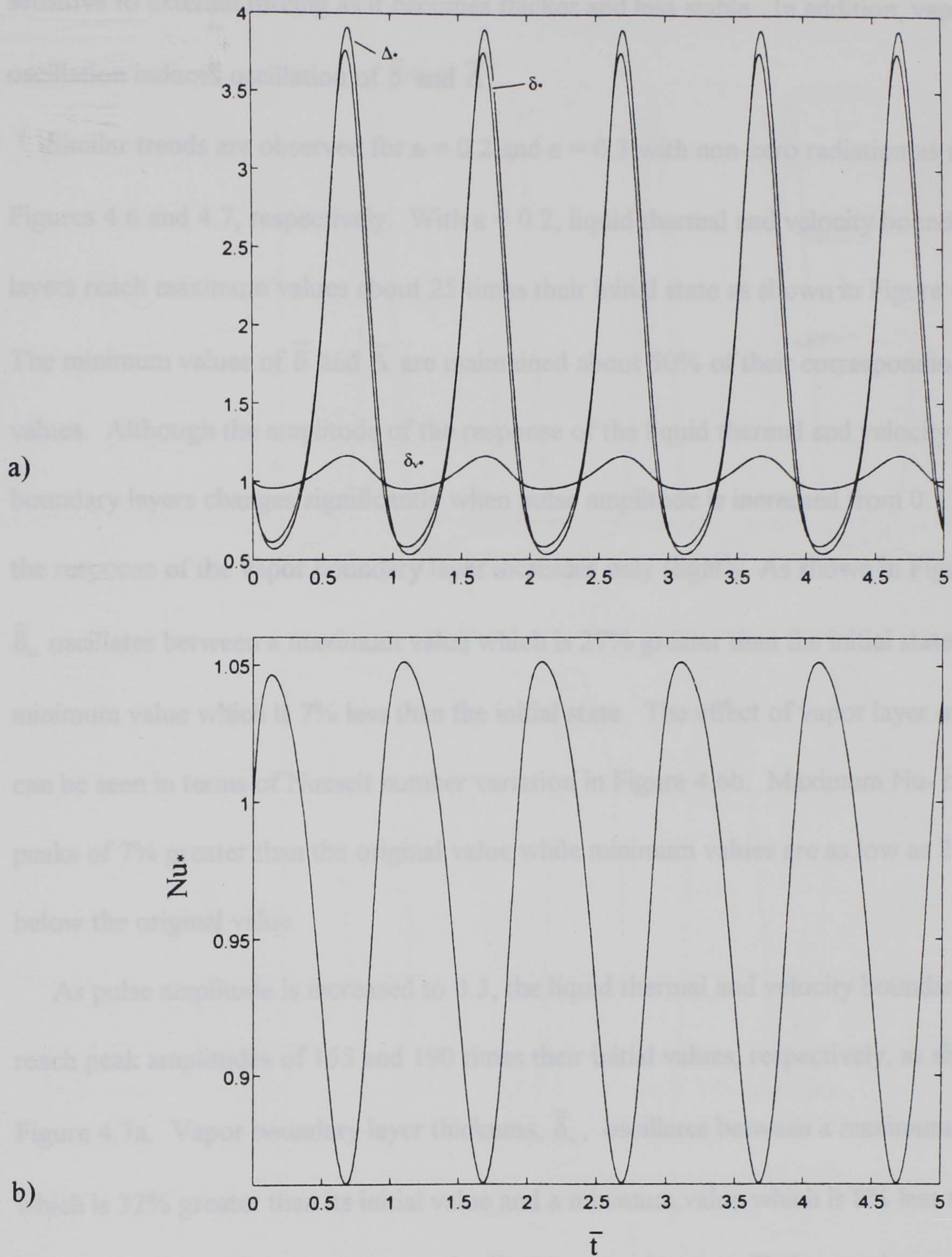


Figure 4.5. Response for sinusoidal flow pulsations: (a) normalized boundary layer thicknesses, (b) normalized Nusselt number with $Sr_w = 0.1667$, $\varepsilon = 0.1$, $\bar{v}_p = 1$, $Re_{wl} = 1700$, $Re_{ww} = 15$, $Pr_l = 4.0$, $Pr_v = 1.0$, $\mu_l/\mu_v = 20$, $\rho_l/\rho_v = 2200$, $\bar{\sigma}_s = 0.6$, $\beta = 0.03$, $Ja = 0.2$, $wh_R/k_v = 10$, $\bar{\delta}_{v0} = 0.006561428$, $\bar{\delta}_0 = 0.063421017$, and $\bar{\Delta}_0 = 0.057488483$.

sensitive to external forcing as it becomes thicker and less stable. In addition, vapor layer oscillation induces oscillation of $\bar{\delta}$ and $\bar{\Delta}$.

Similar trends are observed for $\varepsilon = 0.2$ and $\varepsilon = 0.3$ with non-zero radiation as shown in Figures 4.6 and 4.7, respectively. With $\varepsilon = 0.2$, liquid thermal and velocity boundary layers reach maximum values about 25 times their initial state as shown in Figure 4.6a. The minimum values of $\bar{\delta}$ and $\bar{\Delta}$ are maintained about 50% of their corresponding initial values. Although the amplitude of the response of the liquid thermal and velocity boundary layers changes significantly when pulse amplitude is increased from 0.1 to 0.2, the response of the vapor boundary layer increases only slightly. As shown in Figure 4.6a, $\bar{\delta}_v$ oscillates between a maximum value which is 27% greater than the initial state and a minimum value which is 7% less than the initial state. The effect of vapor layer oscillation can be seen in terms of Nusselt number variation in Figure 4.6b. Maximum Nu_* reaches peaks of 7% greater than the original value while minimum values are as low as 27% below the original value.

As pulse amplitude is increased to 0.3, the liquid thermal and velocity boundary layers reach peak amplitudes of 155 and 190 times their initial values, respectively, as shown in Figure 4.7a. Vapor boundary layer thickness, $\bar{\delta}_v$, oscillates between a maximum value which is 32% greater than its initial value and a minimum value which is 8% less than its initial value. The effect on heat transfer for this vapor layer oscillation can be seen in terms of Nusselt number variation in Figure 4.7b. Maximum Nu_* reaches peaks of 8% greater than the original starting value while minimum Nu_* falls to values 32% below the original starting value.

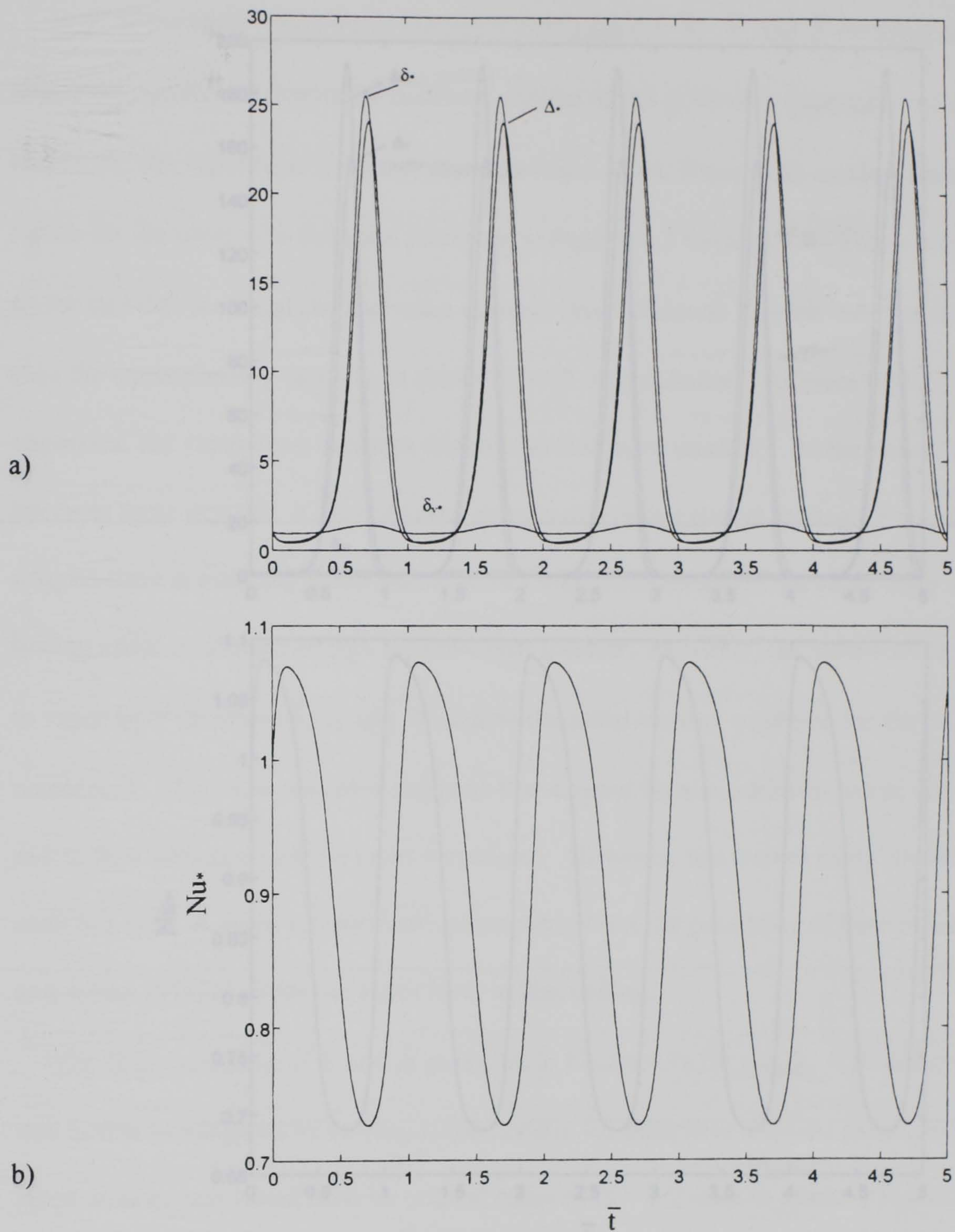


Figure 4.6. Response for sinusoidal flow pulsations: (a) normalized boundary layer thicknesses, (b) normalized Nusselt number with $Sr_w = 0.1667$, $\varepsilon = 0.2$, $\bar{v}_p = 1$, $Re_{wl} = 1700$, $Re_{ww} = 15$, $Pr_l = 4.0$, $Pr_v = 1.0$, $\mu_l/\mu_v = 20$, $\rho_l/\rho_v = 2200$, $\bar{\sigma}_s = 0.6$, $\beta = 0.03$, $Ja = 0.2$, $wh_R/k_v = 10$, $\bar{\delta}_{v0} = 0.006561428$, $\bar{\delta}_0 = 0.063421017$, and $\bar{\Delta}_0 = 0.057488483$.

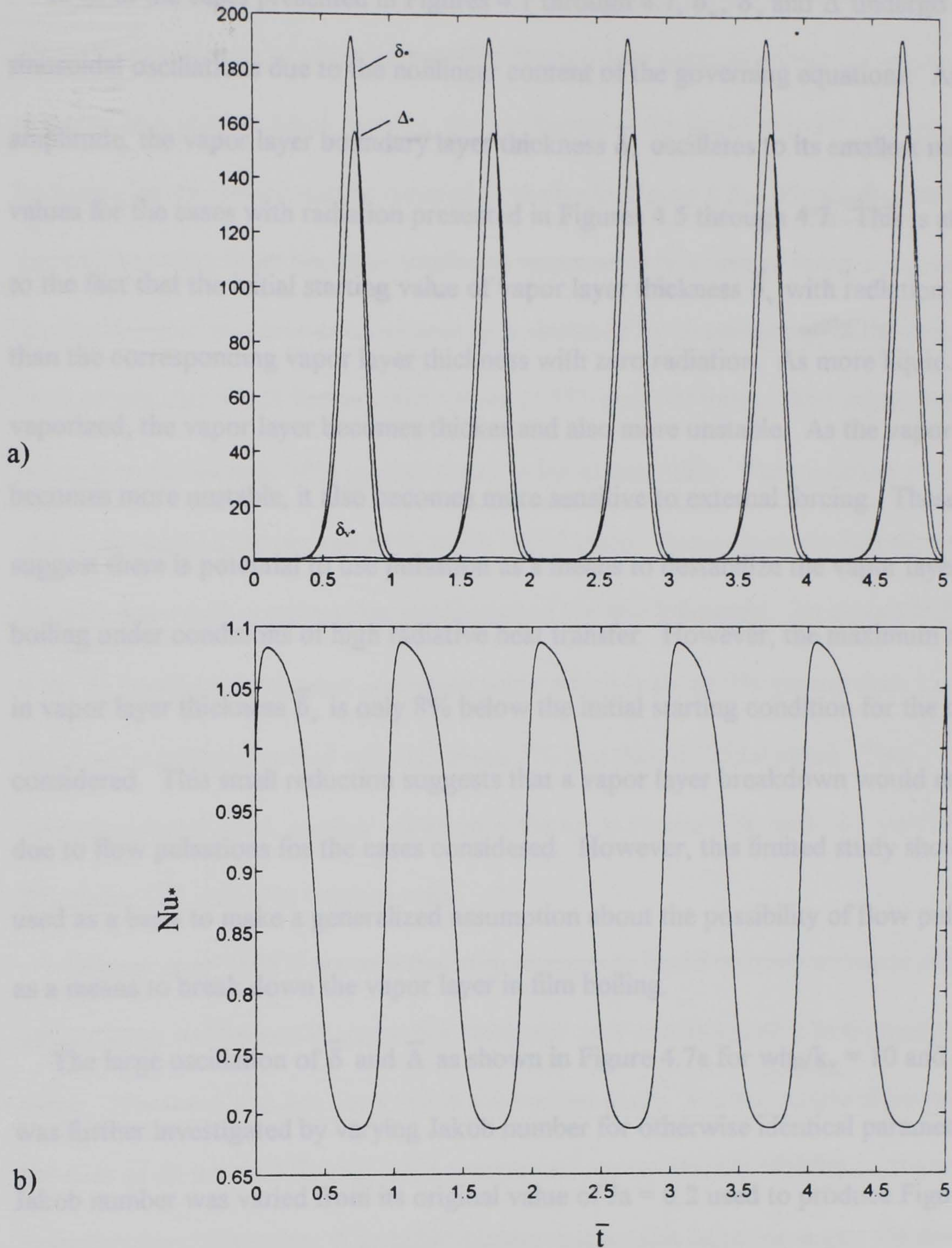


Figure 4.7. Response for sinusoidal flow pulsations: (a) normalized boundary layer thicknesses, (b) normalized Nusselt number with $Sr_w = 0.1667$, $\varepsilon = 0.3$, $\bar{v}_p = 1$, $Re_{wl} = 1700$, $Re_{ww} = 15$, $Pr_l = 4.0$, $Pr_v = 1.0$, $\mu_l/\mu_v = 20$, $\rho_l/\rho_v = 2200$, $\bar{\sigma}_s = 0.6$, $\beta = 0.03$, $Ja = 0.2$, $wh_R/k_v = 10$, $\bar{\delta}_{v0} = 0.006561428$, $\bar{\delta}_0 = 0.063421017$, and $\bar{\Delta}_0 = 0.057488483$.

In all of the cases presented in Figures 4.1 through 4.7, $\bar{\delta}_v$, $\bar{\delta}$, and $\bar{\Delta}$ undergo non-sinusoidal oscillations due to the nonlinear content of the governing equations. At each amplitude, the vapor layer boundary layer thickness $\bar{\delta}_v$ oscillates to its smallest minimum values for the cases with radiation presented in Figures 4.5 through 4.7. This is attributed to the fact that the initial starting value of vapor layer thickness $\bar{\delta}_v$ with radiation is greater than the corresponding vapor layer thickness with zero radiation. As more liquid is vaporized, the vapor layer becomes thicker and also more unstable. As the vapor layer becomes more unstable, it also becomes more sensitive to external forcing. These results suggest there is potential to use pulsation as a means to destabilize the vapor layer in film boiling under conditions of high radiative heat transfer. However, the maximum reduction in vapor layer thickness $\bar{\delta}_v$ is only 8% below the initial starting condition for the cases considered. This small reduction suggests that a vapor layer breakdown would not occur due to flow pulsations for the cases considered. However, this limited study should not be used as a basis to make a generalized assumption about the possibility of flow pulsations as a means to break down the vapor layer in film boiling.

The large oscillation of $\bar{\delta}$ and $\bar{\Delta}$ as shown in Figure 4.7a for $wh_R/k_v = 10$ and $\varepsilon = 0.3$ was further investigated by varying Jakob number for otherwise identical parameters. Jakob number was varied from its original value of $Ja = 0.2$ used to produce Figure 4.7 to a smaller value of $Ja = 0.02$. The initial values of $\bar{\delta}_{v0} = 0.006206590$, $\bar{\delta}_0 = 0.034341779$, and $\bar{\Delta}_0 = 0.027005552$ correspond to these parametric conditions. Jakob number is the ratio of maximum sensible energy absorbed by the vapor to the latent energy absorbed by the vapor during boiling. In many applications, the sensible energy is much less than the

latent energy and Ja has a small value. Therefore, smaller Ja correspond to larger energy absorption by change of phase and smaller temperature changes across the vapor. In response to a smaller Jakob number, the oscillation of the liquid thermal and velocity boundary layers is dramatically reduced as shown in Figure 4.8a. Physically, the liquid thermal boundary layer becomes smaller in response to less energy being conducted across the liquid-vapor interface as more energy is absorbed by phase change in the vapor layer. Peak amplitudes which had reached values of 155 and 190 times initial values were reduced to values only 30% greater than the initial condition. The minimum values of $\bar{\delta}$ and $\bar{\Delta}$ are maintained around 85% of the initial value. Oscillations are less asymmetrical for this case which suggests that nonlinearities are less influential. As shown in Figure 4.8a, $\bar{\delta}_v$ oscillates between a maximum value which is about 2% greater than its initial value and a minimum value which is about 2% less than its initial value. The corresponding Nusselt number variation is shown in Figure 4.8b with Nu_* varying within 2% above and below its original value.

Orozco et al. (1987) showed that step changes in liquid velocity or vapor superheat initiate large oscillations in vapor film thickness as it converges on a new steady state value. This trend was not observed in the current study. Rather, steady state values for the case of no external forcing were approached asymptotically without oscillations in boundary layer thickness. A possible explanation for this behavior is that the study of Orozco et al. (1987) neglects the effects of interfacial tension. Interfacial tension tends to stabilize the interface (Berenson, 1961) and would therefore dampen the oscillations observed by Orozco et al. (1987).

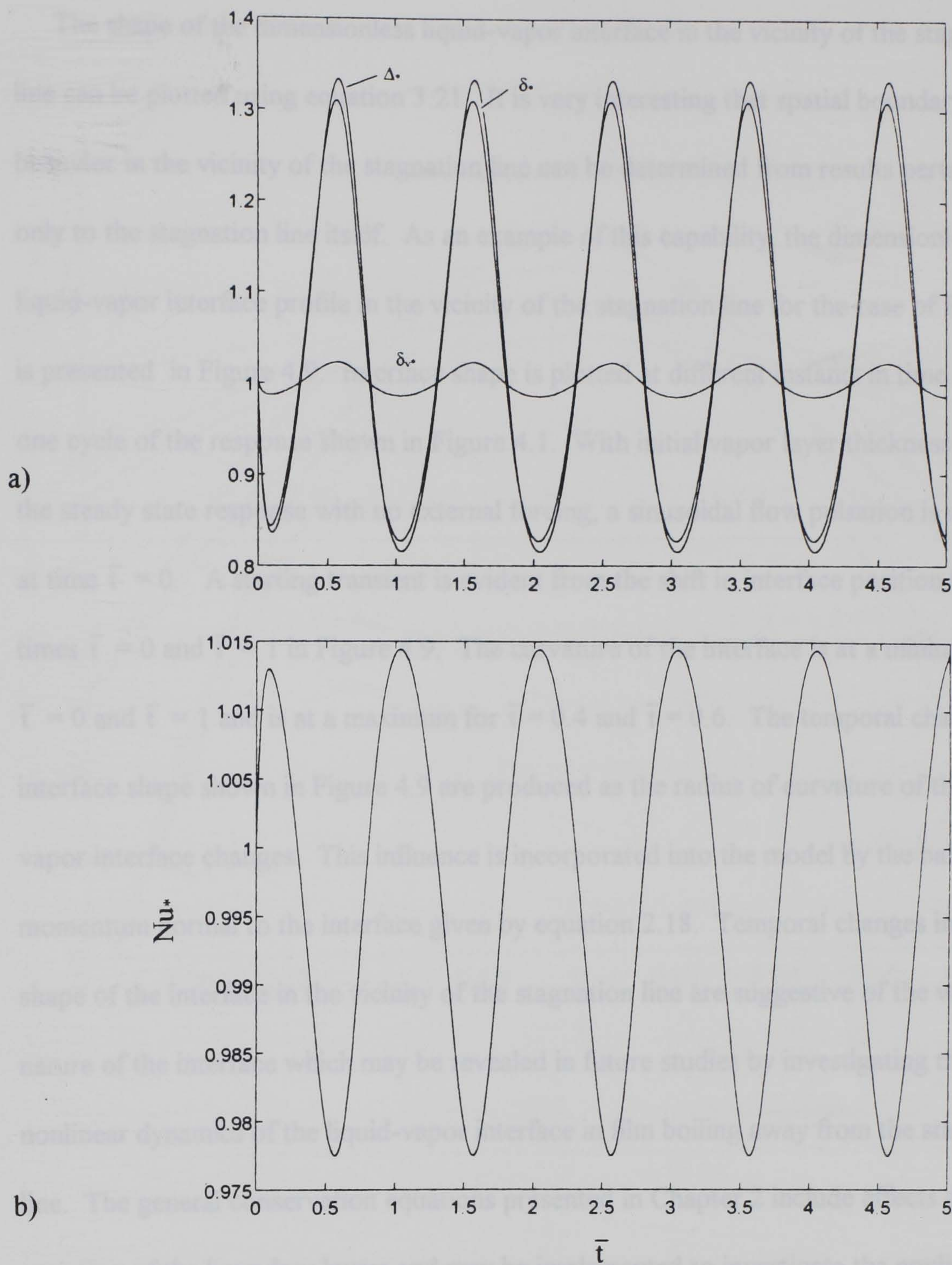


Figure 4.8. Response for sinusoidal flow pulsations: (a) normalized boundary layer thicknesses, (b) normalized Nusselt number with $Sr_w = 0.1667$, $\varepsilon = 0.3$, $\bar{v}_p = 1$, $Re_{wl} = 1700$, $Re_{ww} = 15$, $Pr_l = 4.0$, $Pr_v = 1.0$, $\mu_l/\mu_v = 20$, $\rho_l/\rho_v = 2200$, $\bar{\sigma}_s = 0.6$, $\beta = 0.03$, $Ja = 0.02$, $wh_R/k_v = 10$, $\bar{\delta}_{v0} = 0.006206590$, $\bar{\delta}_0 = 0.034341779$, and $\bar{\Delta}_0 = 0.027005552$.

The shape of the dimensionless liquid-vapor interface in the vicinity of the stagnation line can be plotted using equation 3.21. It is very interesting that spatial boundary layer behavior in the vicinity of the stagnation line can be determined from results pertaining only to the stagnation line itself. As an example of this capability, the dimensionless liquid-vapor interface profile in the vicinity of the stagnation line for the case of Figure 4.1 is presented in Figure 4.9. Interface shape is plotted at different instants in time during one cycle of the response shown in Figure 4.1. With initial vapor layer thickness given by the steady state response with no external forcing, a sinusoidal flow pulsation is imposed at time $\bar{t} = 0$. A starting transient is evident from the shift in interface position between times $\bar{t} = 0$ and $\bar{t} = 1$ in Figure 4.9. The curvature of the interface is at a minimum for $\bar{t} = 0$ and $\bar{t} = 1$ and is at a maximum for $\bar{t} = 0.4$ and $\bar{t} = 0.6$. The temporal changes in interface shape shown in Figure 4.9 are produced as the radius of curvature of the liquid-vapor interface changes. This influence is incorporated into the model by the balance of momentum normal to the interface given by equation 2.18. Temporal changes in the shape of the interface in the vicinity of the stagnation line are suggestive of the wavy nature of the interface which may be revealed in future studies by investigating the nonlinear dynamics of the liquid-vapor interface in film boiling away from the stagnation line. The general conservation equations presented in Chapter 2 include effects due spatial variation of the boundary layers and may be implemented to investigate the nonlinear dynamics of the liquid-vapor interface away from the stagnation line. Therefore, these equations have the potential to extend the curves presented in Figure 4.9.

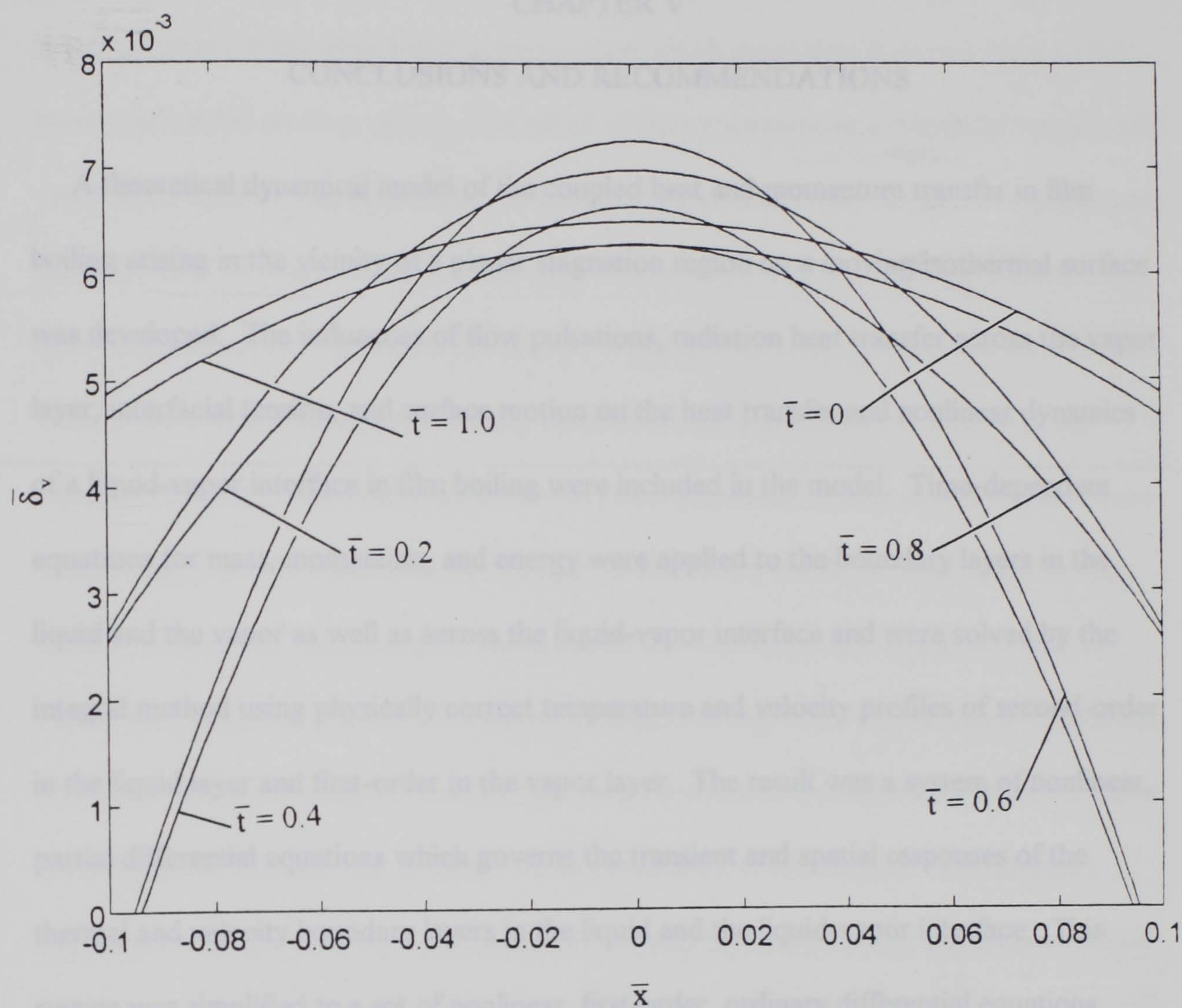


Figure 4.9. Dimensionless liquid-vapor interface shape in the vicinity of the stagnation line for sinusoidal flow pulsations with $Sr_w = 0.1667$, $\varepsilon = 0.1$, $\bar{v}_p = 1$, $Re_{wl} = 1700$, $Re_{ww} = 15$, $Pr_l = 4.0$, $Pr_v = 1.0$, $\mu_l/\mu_v = 20$, $\rho_l/\rho_v = 2200$, $\bar{\sigma}_s = 0.6$, $\beta = 0.03$, $Ja = 0.2$, $wh_R/k_v = 0$, $\bar{\delta}_{v,0} = 0.006500068$, $\bar{\delta}_0 = 0.057726632$, and $\bar{\Delta}_0 = 0.051433868$.

CHAPTER V

CONCLUSIONS AND RECOMMENDATIONS

A theoretical dynamical model of the coupled heat and momentum transfer in film boiling arising in the vicinity of a planar stagnation region on a moving isothermal surface was developed. The influences of flow pulsations, radiation heat transfer across the vapor layer, interfacial tension, and surface motion on the heat transfer and nonlinear dynamics of a liquid-vapor interface in film boiling were included in the model. Time-dependent equations for mass, momentum, and energy were applied to the boundary layers in the liquid and the vapor as well as across the liquid-vapor interface and were solved by the integral method using physically correct temperature and velocity profiles of second-order in the liquid layer and first-order in the vapor layer. The result was a system of nonlinear, partial differential equations which governs the transient and spatial responses of the thermal and velocity boundary layers in the liquid and the liquid-vapor interface. This system was simplified to a set of nonlinear, first-order, ordinary differential equations governing boundary layer response in the vicinity of the stagnation line with time as the sole dependent variable by recognizing symmetry in the dividing flow about the stagnation streamline.

Numerical solutions to the resulting system of ordinary differential equations were obtained by fourth- and fifth-order Runge-Kutta integration techniques for a sinusoidal variation in the flow velocity. Instantaneous boundary layer thicknesses and Nusselt numbers were calculated at the stagnation line. As expected, sinusoidal flow pulsations

were shown to produce non-sinusoidal oscillations in the boundary layer thicknesses due to the nonlinear content of the governing equations. Flow pulsations tended to increase boundary layers above their initial starting values much more than it caused them to fall below their initial starting values. The effect of flow pulsations and interfacial tension on vapor layer stability was considered. Decreasing interfacial tension was shown to increase the magnitude of boundary layer oscillation. Therefore, reducing interfacial tension may be a means to induce vapor layer instability. Several cases were compared both with and without radiation. The vapor boundary layer thickness was shown to oscillate to its smallest value with radiation present at each pulse amplitude. These results suggest there is potential to use flow pulsation as a means to destabilize the vapor layer in film boiling under conditions of high radiative heat transfer. However, the maximum reduction in vapor layer thickness was only 8% below its initial starting value for the cases considered. This small reduction suggests that a vapor layer breakdown would not occur for the cases considered. In addition, for all of the cases considered, time-averaged heat transfer decreased in response to flow pulsations. However, this limited study should not be used as a basis to make a generalized assumption about the possibility of using flow pulsations or altering interfacial tension as a means to break down the vapor layer or enhance heat transfer in film boiling. The results presented do suggest the need for further investigation by means of a full parametric study of the influences of flow pulsation, interfacial tension, and radiation on the temporal boundary layer response at the stagnation line.

Each case investigated in this study showed greater oscillations in the liquid boundary layers in response to flow pulsations than in the vapor boundary layer. This behavior may

result from the limiting assumption of a constant pressure in the vapor layer. In a physical system, the pressure in the vapor changes in response to changes in the pressure in the liquid. The assumption of a constant pressure in the vapor layer limits the applicability of the current model to lower pulse amplitudes. The vapor layer in this study cannot fully respond to higher pulse amplitudes because pressure variations in the vapor layer are not modeled. The current study could be improved and extended to include higher pulse amplitudes by incorporating the effects of pressure variations in the vapor layer in response to pressure fluctuations in the liquid layer. Allowing interfacial saturation temperature to vary in response vapor pressure variations through a simple thermodynamic relationship could also improve the model. In addition, property value estimates could be improved by referring interfacial properties such as interfacial tension to the temperature of the interface rather than to film temperature.

The shape of the liquid-vapor interface in the vicinity of the stagnation line was determined from results pertaining to the stagnation line. The curvature of the liquid-vapor interface in the vicinity of the stagnation line was shown to change temporally in response to flow pulsations. These temporal changes are suggestive of the wavy nature of the interface which may be revealed in future studies by investigating the nonlinear dynamics of the liquid vapor interface in film boiling away from the stagnation line. The conservation equations presented in this study before invoking the symmetry condition at the stagnation line include the effects of spatial variation away from the stagnation line. The results obtained for interface shape in the vicinity of the stagnation line may be extended away from the stagnation line by implementing these equations. It is

recommended that future studies extend the present model for boundary layer response and heat transfer in the vicinity of the stagnation line by implementing the conservation equations without invoking the symmetry condition at the stagnation line. Therefore, both spatial and temporal boundary layer responses away from the stagnation line could be investigated.

In a two-dimensional study, the radius of curvature of the liquid-vapor interface at a point is determined by modeling the interface as a plane curve. As discussed by Thomas and Finney (1938), when moving along a differentiable curve in the plane, the unit tangent vector T to the curve turns as the curve bends. The rate at which T turns is measured by the change in the angle ϕ that T makes with the unit vector i (Figure A-1). At each point P , the absolute value of $d\phi/ds$, stated in radians per unit length along the curve, is called the curvature κ at P . If $|d\phi/ds|$ is large, T turns sharply as it passes through P and the curvature at P is large. If $|d\phi/ds|$ is close to zero, T turns more slowly and the curvature at P is small. The circle of curvature at a point P on a plane curve where $\kappa \neq 0$ is the circle in the plane of the curve that

1. is tangent to the curve at P (has the same tangent that the curve has),
2. has the same curvature that the curve has at P , and
3. lies toward the concave or inner side of the curve (as in Figure A-2).

The radius of curvature ρ of the curve at P is the radius of the circle of curvature and is given by

$$\rho = 1/\kappa \quad (A.1)$$

By first calculating curvature and then taking its reciprocal, radius of curvature can be determined.

APPENDIX
RADIUS OF CURVATURE

In this two-dimensional study, the radius of curvature of the liquid-vapor interface at a point is determined by modeling the interface as a plane curve. As discussed by Thomas and Finney (1988), when moving along a differentiable curve in the plane, the unit tangent vector \mathbf{T} to the curve turns as the curve bends. The rate at which \mathbf{T} turns is measured by the change in the angle ϕ that \mathbf{T} makes with the unit vector \mathbf{i} (Figure A-1). At each point P , the absolute value of $d\phi/ds$, stated in radians per unit length along the curve, is called the curvature κ at P . If $|d\phi/ds|$ is large, \mathbf{T} turns sharply as it passes through P and the curvature at P is large. If $|d\phi/ds|$ is close to zero, \mathbf{T} turns more slowly and the curvature at P is small. The circle of curvature at a point P on a plane curve where $\kappa \neq 0$ is the circle in the plane of the curve that

1. is tangent to the curve at P (has the same tangent that the curve has);
2. has the same curvature that the curve has at P ; and
3. lies toward the concave or inner side of the curve (as in Figure A-2).

The radius of curvature ρ of the curve at P is the radius of the circle of curvature and is given by

$$\rho = 1 / \kappa. \tag{A.1}$$

By first calculating curvature and then taking its reciprocal, radius of curvature can be determined.

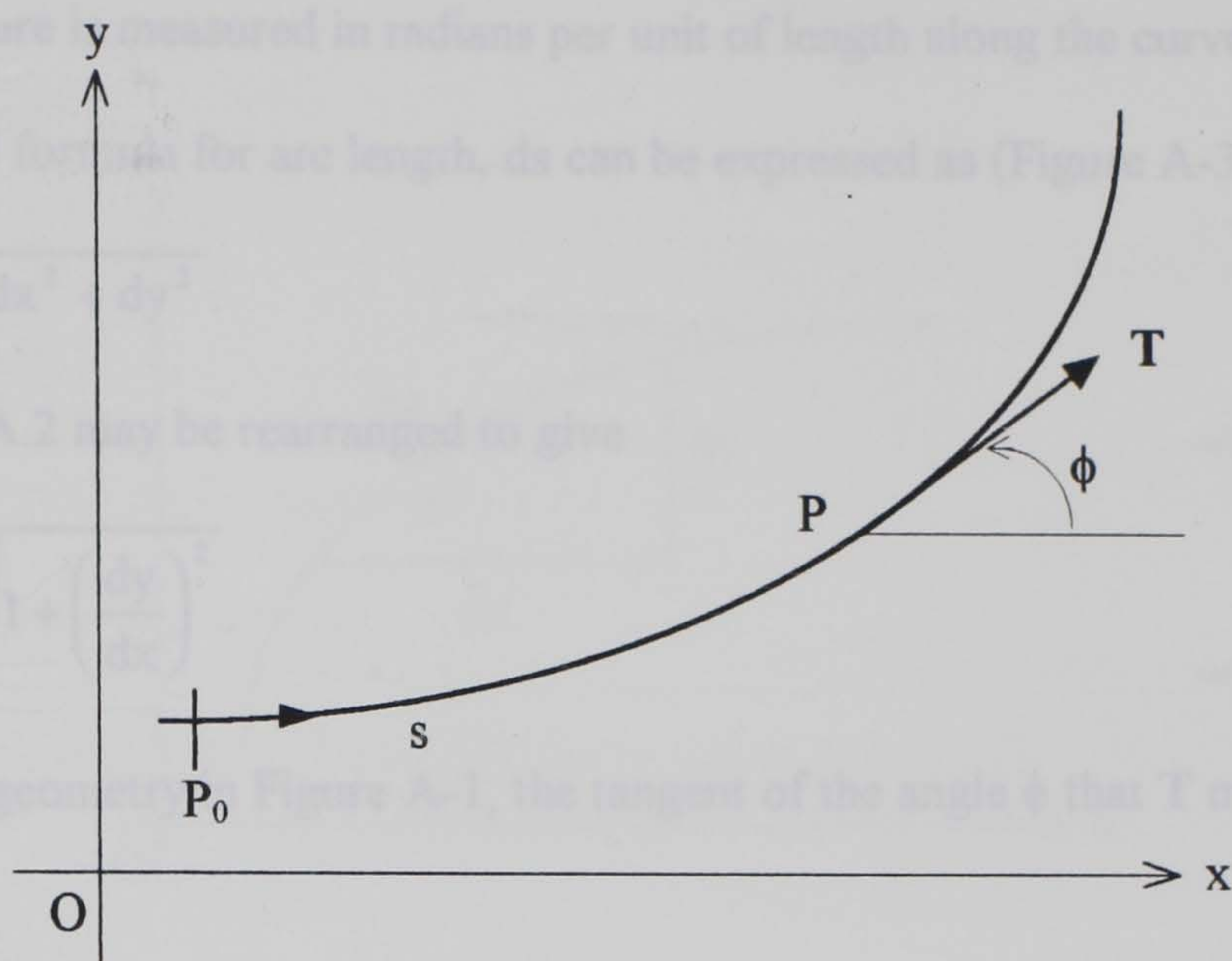


Figure A-1. Unit tangent vector \mathbf{T} and angle ϕ for the determination of curvature κ at point P .

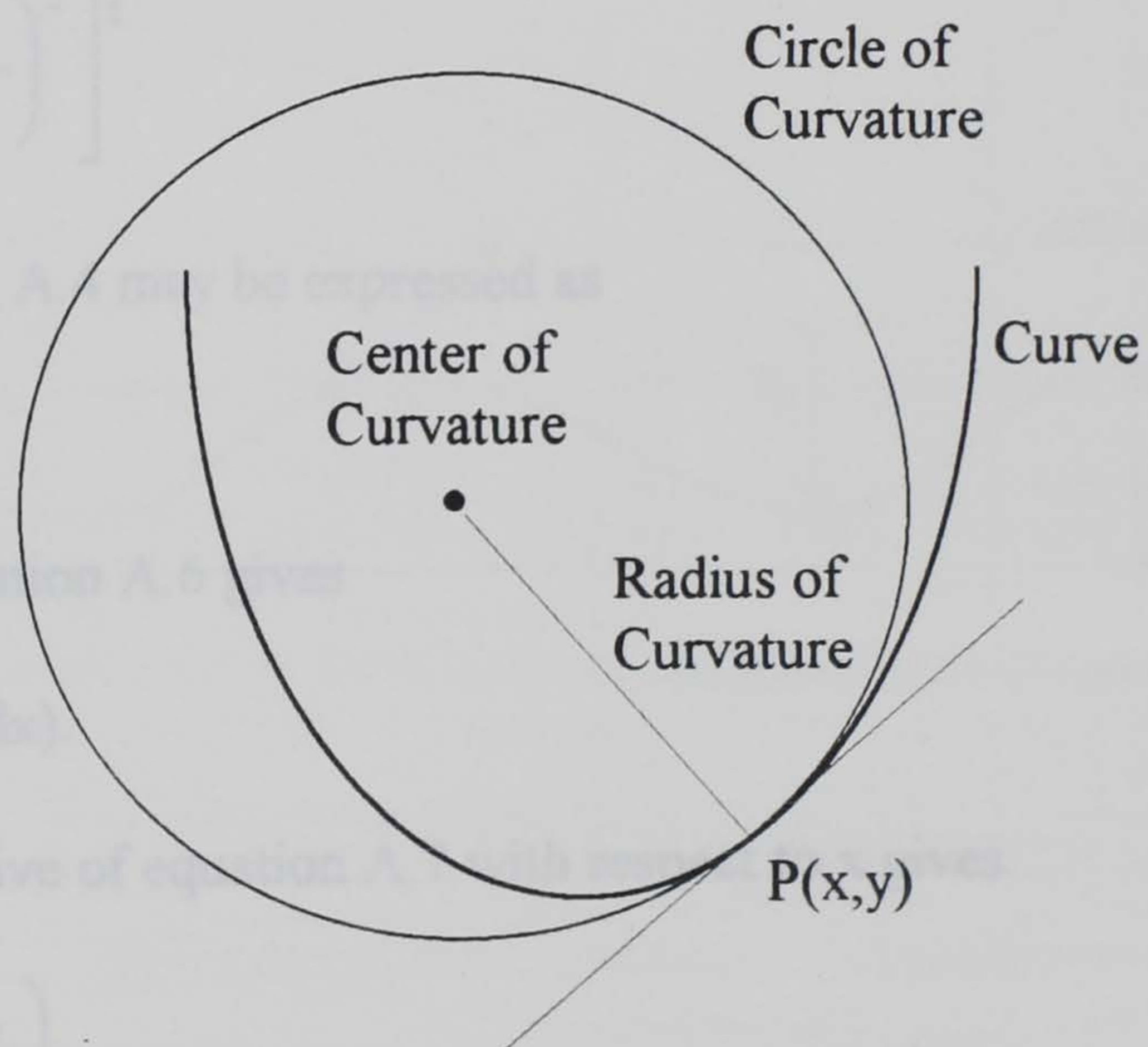


Figure A-2. Circle of curvature at $P(x,y)$ for determination of radius of curvature.

Curvature is measured in radians per unit of length along the curve. From the differential formula for arc length, ds can be expressed as (Figure A-3)

$$ds = \sqrt{dx^2 + dy^2} . \quad (\text{A.2})$$

Equation A.2 may be rearranged to give

$$\frac{ds}{dx} = \sqrt{1 + \left(\frac{dy}{dx}\right)^2} . \quad (\text{A.3})$$

From the geometry in Figure A-1, the tangent of the angle ϕ that \mathbf{T} makes with the unit vector \mathbf{i} is

$$\tan \phi = dy/dx. \quad (\text{A.4})$$

To determine the radius of curvature of the liquid-vapor interface at an instant of time, the interface is modeled as the plane curve $\delta_v(x)$ as shown in Figure A-4. Along the interface, dy is equivalent to $d\delta_v$. Making this substitution in equation A.3 gives

$$\frac{ds}{dx} = \left[1 + \left(\frac{d\delta_v}{dx}\right)^2 \right]^{\frac{1}{2}} . \quad (\text{A.5})$$

Similarly, equation A.4 may be expressed as

$$\tan \phi = d\delta_v / dx. \quad (\text{A.6})$$

Solving for ϕ , equation A.6 gives

$$\phi = \tan^{-1} (d\delta_v / dx). \quad (\text{A.7})$$

Taking the derivative of equation A.7 with respect to x gives

$$\frac{d\phi}{dx} = \frac{\frac{d}{dx} \left(\frac{d\delta_v}{dx} \right)}{1 + \left(\frac{d\delta_v}{dx}\right)^2} . \quad (\text{A.8})$$

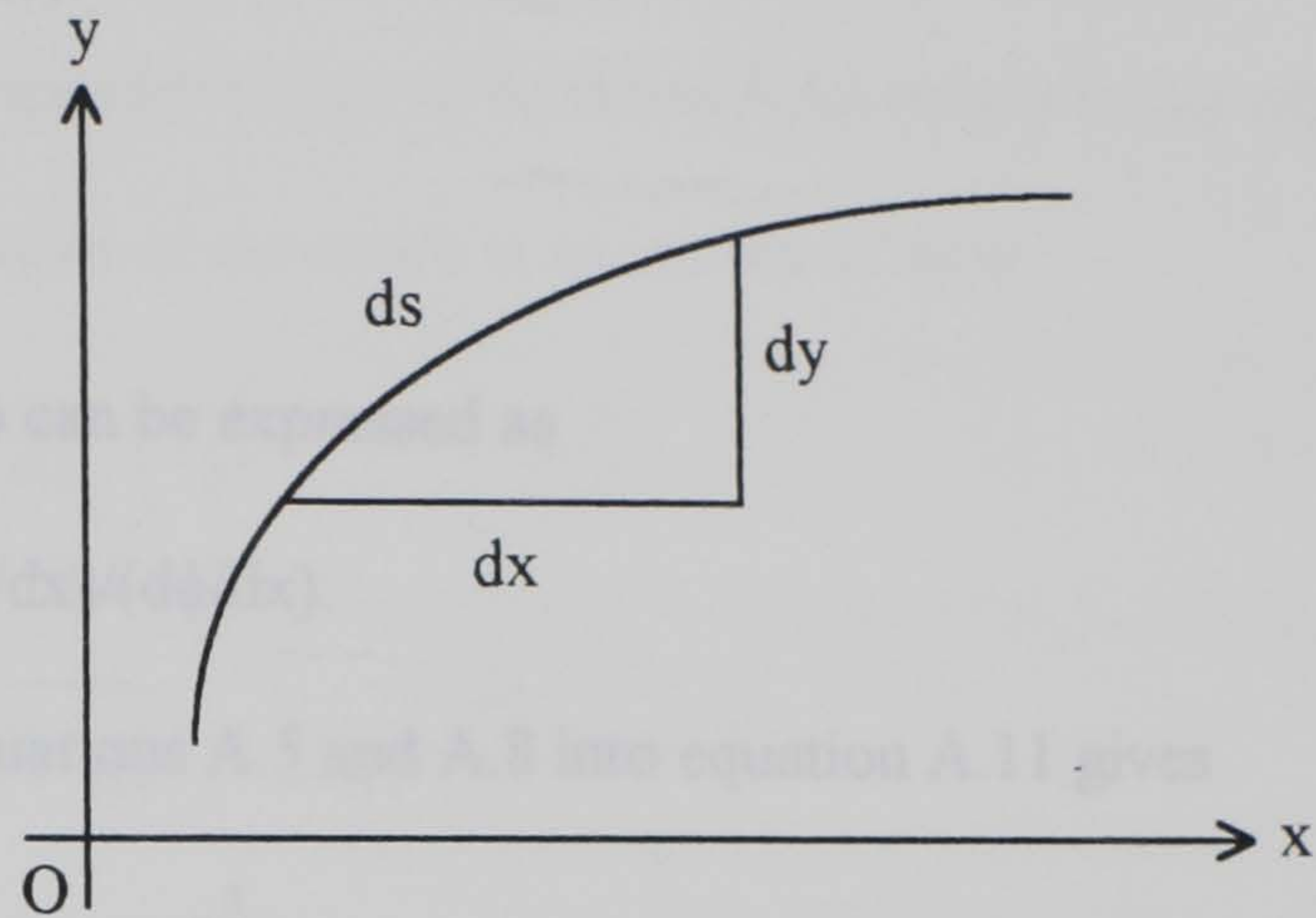


Figure A-3. A differential of arc length ds for the formulation of the relationship between ds , dx , and dy .

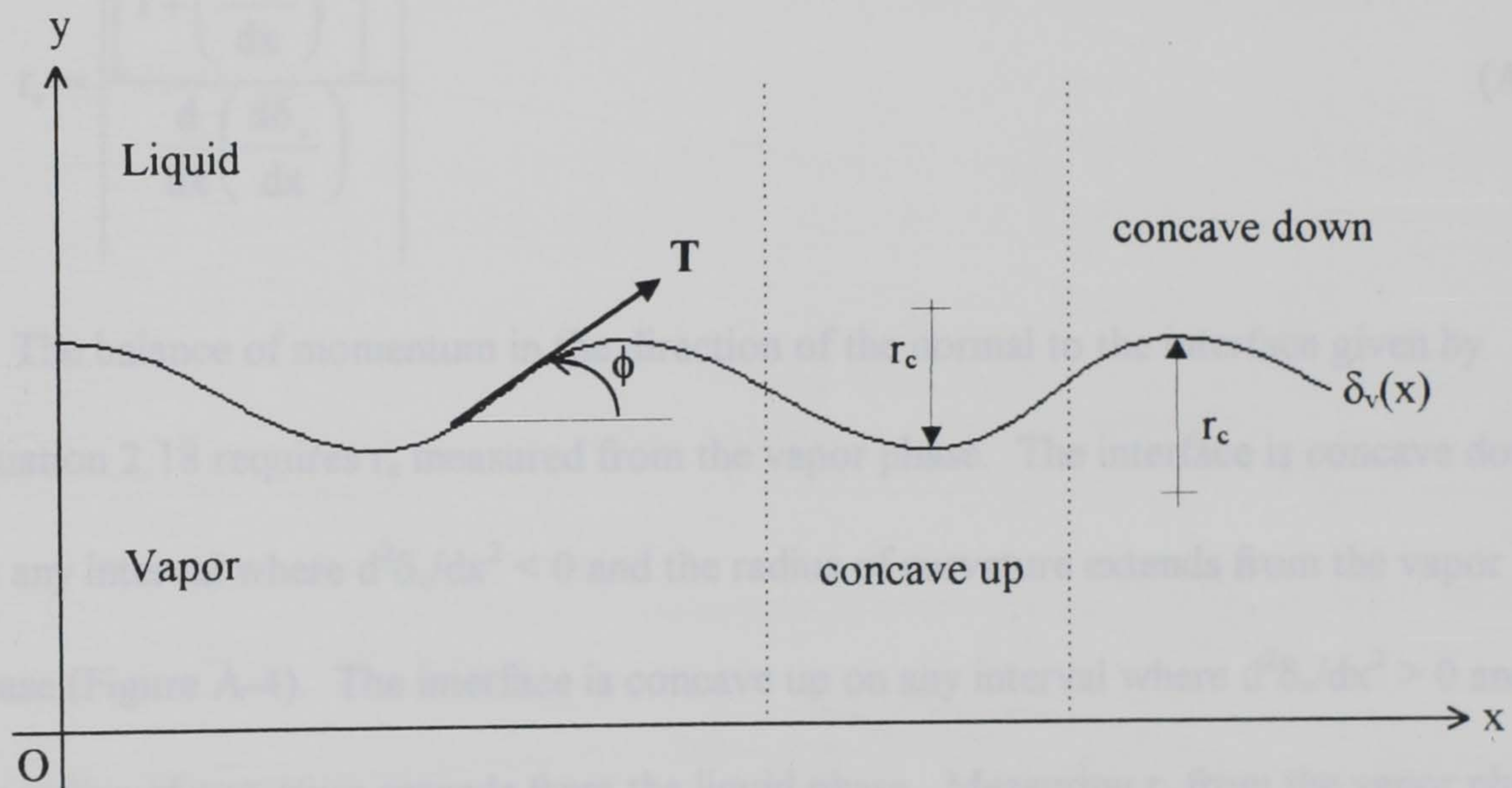


Figure A-4. The liquid-vapor interface modeled as the plane curve $\delta_v(x)$ at an instant in time.

Recall that κ measured from the vapor phase is positive,

$$\kappa = |d\phi/ds|. \quad \text{From the liquid phase is negative.} \quad (\text{A.9})$$

Therefore, the sign convention to equation A.13 results in the expression which was used

$$\rho = |ds/d\phi|. \quad \text{radius of curvature at an instant of time.} \quad (\text{A.10})$$

Note that $ds/d\phi$ can be expressed as

$$ds/d\phi = (ds/dx)/(d\phi/dx). \quad (\text{A.11})$$

Substituting equations A.5 and A.8 into equation A.11 gives

$$\frac{ds}{d\phi} = \frac{\left[1 + \left(\frac{d\delta_v}{dx}\right)^2\right]^{\frac{3}{2}}}{\frac{d}{dx}\left(\frac{d\delta_v}{dx}\right)}. \quad (\text{A.12})$$

Therefore, radius of curvature is related to the vapor layer thickness $\delta_v(x,t)$ by

$$r_c = \left| \frac{\left[1 + \left(\frac{d\delta_v}{dx}\right)^2\right]^{\frac{3}{2}}}{\frac{d}{dx}\left(\frac{d\delta_v}{dx}\right)} \right|. \quad (\text{A.13})$$

The balance of momentum in the direction of the normal to the interface given by equation 2.18 requires r_c measured from the vapor phase. The interface is concave down on any interval where $d^2\delta_v/dx^2 < 0$ and the radius of curvature extends from the vapor phase (Figure A-4). The interface is concave up on any interval where $d^2\delta_v/dx^2 > 0$ and the radius of curvature extends from the liquid phase. Measuring r_c from the vapor phase suggests the following sign convention:

- r_c extending from the vapor phase is positive,
- r_c extending from the liquid phase is negative.

Applying this sign convention to equation A.13 results in the expression which was used to determine radius of curvature at an instant of time.

$$r_c = \frac{\left[1 + \left(\frac{d\delta_v}{dx} \right)^2 \right]^{\frac{3}{2}}}{-\frac{d}{dx} \left(\frac{d\delta_v}{dx} \right)} \quad (\text{A.14})$$

REFERENCES CITED

1. Arpaci, V. S., and Larsen, P. S., 1984, Convection Heat Transfer, Prentice-Hall, Inc., Englewood Cliffs, NJ, pp. 141-143, 169-172, 182-187.
2. Berenson, P. J., 1961, "Film-Boiling Heat Transfer From a Horizontal Surface," ASME Journal of Heat Transfer, Vol. 83, pp. 351-358.
3. Boyd, J. P., 1989, Lecture Notes in Engineering: Chebyshev and Fourier Spectral Methods, Vol. 49, Springer-Verlag, Berlin.
4. Burelbach, J. P., Bankoff, S. G., and Davis, S. H., 1988, "Nonlinear stability of evaporating/condensing liquid films," Journal of Fluid Mechanics, Vol. 195, pp. 463-494.
5. Carey, V. P., 1992, Liquid-Vapor Phase-Change Phenomena, Hemisphere Publishing Corporation, Washington.
6. Cess, R. D., and Sparrow, E. M., 1961, "Film Boiling in a Forced-Convection Boundary Layer Flow," ASME Journal of Heat Transfer, Vol. 83, pp. 370-376.
7. Chang, K. H., and Witte, L. C., 1990, "Hydrodynamics of Film Boiling from a Cylinder in Crossflow," Journal of Thermophysics and Heat Transfer, Vol. 4, No. 3, pp. 393-396.
8. Chappidi, P. R., Gunnerson, F. S., and Pasamehmetoglu, K. O., 1991, "Film-Boiling Drag and Heat Transfer on a Flat Surface," Numerical Heat Transfer, Part A, Vol. 19, pp. 327-344.
9. Chappidi, P. R., Gunnerson, F. S., and Pasamehmetoglu, K. O., 1990, "A Simple Forced Convection Film Boiling Model," Int. Comm. Heat Mass Transfer, Vol. 17, pp. 259-270.
10. Collier, J. G., 1981, Convective Boiling and Condensation, 2nd ed., McGraw-Hill, New York, pp. 121-139.
11. Epstein, M., and Hauser, G. M., 1980, "Subcooled Forced-Convection Film Boiling in the Forward Stagnation Region of a Sphere or Cylinder," Int. J. Heat Mass Transfer, Vol. 23, pp. 199-189.
12. Evans, H. L., 1962, Int. J. Heat Mass Transfer, Vol. 5, pp. 35-57.

13. Fodemski, T. R., 1985, "The influence of liquid viscosity and system pressure on stagnation point vapor thickness during forced-convection film boiling," *Int. J. Heat Mass Transfer*, Vol. 28, No. 1, pp. 69-80.
14. Hansen, A. G., 1964, Similarity Analysis of Boundary Value Problems, Prentice-Hall, Englewood Cliffs, NJ.
15. Inada, S., Miyasaka, Y., and Izumi, R., 1981, "A Study of the Laminar Flow Heat Transfer Between a Two-Dimensional Water Jet and a Flat Surface with Constant Heat Flux," *Bulletin of the JSME*, Vol. 24, pp. 1803-1810.
16. Kuethe, A. M., and Schetzer, J. D., 1959, *Foundation of Aerodynamics*, John Wiley & Sons, New York.
17. Liu, Q. S., Shiotsu, M., and Sakurai, A., 1992, "A Correlation for Forced Convection Film Boiling Heat Transfer from a Horizontal Cylinder under Subcooled Conditions," *ASME HTD, Fundamentals of Subcooled Flow Boiling*, Vol. 217, pp. 21-32.
18. McGannon, H. E., ed., 1971, The Making, Shaping, and Treating of Steel, 9th ed., United States Steel Corp., Herbeck and Held, Pittsburgh.
19. Mladin, E. C., and Zumbrennen, D. A., 1995, "Dependence of Heat Transfer to a Pulsating Stagnation Flow on Pulse Characteristics," *Journal of Thermophysics and Heat Transfer*, Vol. 9, No. 1, pp. 181-192.
20. Mladin, E. C., and Zumbrennen, D. A., 1994, "Nonlinear Dynamics of Laminar Boundary Layers in Pulsatile Stagnation Flows," *Journal of Thermophysics and Heat Transfer*, Vol. 8, No. 3, pp. 514-523.
21. Moon, F. C., 1992, Chaotic and Fractal Dynamics, John Wiley & Sons, Inc., New York.
22. Orozco, J., and Dix, D., 1988, "Oscillation of a Liquid-Vapor Interface: Experimental Observations," *Int. Comm. Heat Transfer*, Vol. 15, pp. 719-729.
23. Orozco, J., and Stellman, R., 1988, "Oscillation of a Liquid-Vapor Interface During Flow Film Boiling," *Int. Comm. Heat Transfer*, Vol. 15, pp. 125-140.
24. Orozco, J., Stellman, R., and Poulikakos, D., 1987, "Dynamic Response of a Liquid-Vapor Interface During Flow Film Boiling From a Sphere," *ASME Journal of Heat Transfer*, Vol. 109, pp. 1051-1055.
25. Parker, T. S. and Chua, L. O., 1989, *Practical Numerical Algorithms for Chaotic Systems*, Springer-Verlag, New York, pp. 1-56.

26. Piggott, B. D. G., White, E. P., and Duffey, R. B., 1976, "Wetting Delay Due to Film and Transition Boiling on Hot Surfaces," *Nuclear Engineering and Design*, Vol. 36, pp. 169-181.
27. Ruch, M. A., and Holman, J. P., 1975, "Boiling Heat Transfer to a Freon-113 Jet Impinging Upward onto a Flat, Heated Surface," *Int. J. Heat Mass Transfer*, Vol. 18, pp. 51-60.
28. Schlichting, H., 1979, *Boundary-Layer Theory*, 7th Ed., McGraw-Hill, New York.
29. Sparrow, E. M., 1964, "The Effect of Radiation on Film Boiling Heat Transfer," *Int. J. Heat Mass Transfer*, Vol. 7, pp. 229-238.
30. Stevens, J. W., and Witte, L. C., 1973, "Destabilization of Vapor Film Boiling Around Spheres," *Int. J. Heat Mass Transfer*, Vol. 16, pp. 669-678.
31. Thomas, G. B., and Finney, R. L., 1988, *Calculus and Analytic Geometry*, Addison-Wesley Publishing Company, Reading, Massachusetts, pp. 331, 385, 818-820.
32. Walsh, S. K., and Wilson, S. D. R., 1979, "Boundary-Layer Flow in Forced-Convection Film-Boiling on a Wedge," *Int. J. Heat Mass Transfer*, Vol. 22, No. 4, pp. 569-574.
33. Zumbrunnen, D. A., 1992, "Transient Convective Heat Transfer in Planar Stagnation Flows with Time-Varying Surface Heat Flux and Temperature," *Journal of Heat Transfer*, Vol. 114, pp. 85-93.
34. Zumbrunnen, D. A., 1991, "Convective heat and mass transfer in the stagnation region of a planar jet impinging on a moving surface," *ASME Journal of Heat Transfer*, Vol. 113, pp. 563-570.
35. Zumbrunnen, D. A., Incropera, F. P., and Viskanta, R., 1992, "A laminar boundary layer model of heat transfer due to a nonuniform planar jet impinging on a moving plate," *Warme-und Stoffubertragung*, Vol. 27, pp. 311-319.
36. Zumbrunnen, D. A., Viskanta, R., Incropera, F. P., 1989, "The Effect of Surface Motion on Forced Convection Film Boiling Heat Transfer," *ASME Journal of Heat Transfer*, Vol. 111, pp. 760-766.

